ATOMIC-LEVEL MECHANISMS OF FAST RELAXATION IN METALLIC GLASSES

A Dissertation Presented for the
Doctor of Philosophy
Degree
The University of Tennessee, Knoxville

Leo W. Zella
December 2023

ACKNOWLEDGEMENTS

I am deeply appreciative of everyone who has helped me on this journey to getting a PhD. Through this journey there were many people whom I could rely on especially during the most difficult moments.

I am thankful for my advisor Takeshi Egami for always being so supportive and encouraging of my work. For being patient with me as I grew as a scientist and developed my skills, for teaching me the fundamentals of good science. I am confident these skills will be deeply important in my future career. I would also like to thank current and former members in the research group who always provided great discussions on research and gave important feedback including Wojciech Dmowski, Yuya Shinohara, Eva Zarkadoula, Hua Chengyun, Jaeyun Moon, Chae Woo Ryu, Hui Wang, Zengquan Wang, Yadu Sarathchandran and Rudra Bista. My thanks also go to my committee members, Yanfei Gao, David Keffer, Michael Ohl and Maik Lang for their time and feedback on my dissertation.

I am also thankful for David Keffer who was instrumental in developing important computation skills that I used throughout my dissertation work and for providing excellent and clear feedback on my research. My time with Michael Ohl in Germany at Forschungszentrum Jülich was instrumental in opening my eyes to areas beyond my narrow research subject and I am thankful for having the chance to work with him. I am also appreciative of Jaeyun Moon who taught me so much about producing high quality research and was an excellent colleague.

Finally for my family for always being there for me and supporting my dreams. Who inspired me and encouraged me to continue, I would not be here otherwise.

ABSTRACT

Glasses are ubiquitous in daily life and have unique properties which are a consequence of the underlying disordered structure. By understanding the fundamental processes that govern these properties, we can modify glasses for desired applications. Key to understanding the structure-dynamics relationship in glasses is the variety of relaxation processes that exist below the glass transition temperature. Though these relaxations are well characterized with macroscopic experimental techniques, the microscopic nature of these relaxations is difficult to elucidate with experimental tools due to the requirements of timescale and spatial resolution. There remain many questions regarding the microscopic nature of relaxation in glass including the role of defects, determination of subsets of atoms that cause the relaxations, the time/space correlations and how low energy activations occur in the potential energy landscape (PEL). To give new insight into these questions we use classical molecular dynamics (MD) to mimic experimental techniques of mechanical perturbation by sinusoidally shearing a model Cu65Zr35 metallic glass. We then uniquely combine this technique with the concept of atomic-level stresses to identify the viscoelastic character of each atom during a cycle of sinusoidal straining. Using results from these techniques, we examine the microscopic nature of relaxation phenomena below the glass transition temperature, examining the transient nature, temperature dependence of said transience and spatial correlation of mechanical loss. We demonstrate the surprising transient nature of relaxation, the spatial correlation of mechanical loss and the low energy barriers on the order of 1meV that represent the ripples in the bottom of the PEL. These new insights into the microscopic nature of relaxation get us closer to being able to tune the properties of glass reliant on relaxation phenomena.

TABLE OF CONTENTS

LIST OF FIGURES

CHAPTER ONE
INTRODUCTION

Glasses have been used for thousands of years with some of the earliest production of glasses as beads in Mesopotamia around 2500 B.C. [1]. Glasses represent a ubiquitous group of materials and are used in a wide variety of applications for structures, cookware, telecommunications, optics, and pharmaceuticals as a few examples. A glass to the layperson is defined by its hardness and opacity, however these are insufficient properties to define a glass, so we turn to the microscopic structural description. Glasses are defined by their amorphous atomic structure which lacks long-range ordering as in crystals, this disordered structure defines the unique properties that glasses have [2]. Glassy and disordered systems also present unique scientific problems such as understanding and predicting the glass transition [3,4] and the opaque relationship between structure and dynamics [5–7] which makes it difficult to determine what 'defects' might be in glass and predict mechanical properties of glass. Understanding these scientific problems would allow for clearer first principles methods for modifying properties of glasses and formulations of new glasses.

The most common way to form a glass is by cooling a liquid down through a point where the dynamics slow down such that the system reaches structural solidity. The dramatic slowdown of viscosity from liquid to glass may be seen in

Fig. 1.1 Viscosity for a variety of glass forming systems scaled according to the glass transition temperature [3].

, showing the over 10 orders of magnitude change in viscosity [3]. Unlike the process of crystallization, which is a first-order transition, the glass transition occurs by a massive dynamics slowdown that can be seen in the change of viscosity. To estimate the glass transition temperature, T_g, there are a variety of ways such as by viscosity, characteristic relaxation time or the volume-temperature relationship during cooling. What is of great curiosity is how little the underlying liquid structure changes during the process of solidification into a glass.

This lack of clear structural change is what complicates the understanding of the structure-property relationship in glasses. In crystalline systems structural defects such as point defects and grain boundaries can be easily identified and related to important properties. In

glassy systems each atom is in essentially a unique local environment that cannot be described by a simple periodic repetition, and this has made the unambiguous definition of structural defects very difficult.

The understanding of the structure-property relationships in glass can lead to general insights into other amorphous solids. Granular solids such as sand, beads or powders exhibit some similar mechanical dynamics as seen in glass such as the memory formation [8–11], and avalanche behavior [12–14], despite having a much different length scale. Glassy polymers exhibit many of the same relaxation phenomena as other covalent glasses such as the α relaxation [15] that corresponds to the glass transition, the β relaxation [16] that is typically linked with diffusion and deformation behavior. Because of the long chain structure of polymers there are intermolecular relaxations which add to the vast array of relaxation phenomena. It was this complexity of relaxation phenomena that motivated Johari and Goldstein to study simpler molecular glasses to characterize the secondary relaxations[17]. Therefore, studying a disordered system that has less structural complexity such as metallic glass can lead to deep insights into amorphous solids in general.

Metallic glasses have been developed relatively recently with the first glasses formed in the 1960's [18] and are formed from rapidly cooled metallic liquids. In comparison to other glasses and alloys they have a desirable combination of high fracture toughness and yield strength [19,20]. They also serve as excellent systems for studying the fundamentals of glassy systems due to their lack of intermolecular forces such as in amorphous polymers and lack of network forming ability such as in amorphous silicon. Metallic glasses have been relegated to niche uses due to a range of issues such as difficulty in processing [21], glass formability [2], limited plasticity [22–26] which results in catastrophic failure as fracture [19,27]. To tune the properties of metallic glasses and make them more suitable for industrial applications, we need to understand the relaxation modes that control these dynamics.

Role of relaxation processes in glasses

Glasses are out of equilibrium systems which have wide timescales of relaxation as demonstrated by the massive slowdown of dynamics during the glass transition [18].

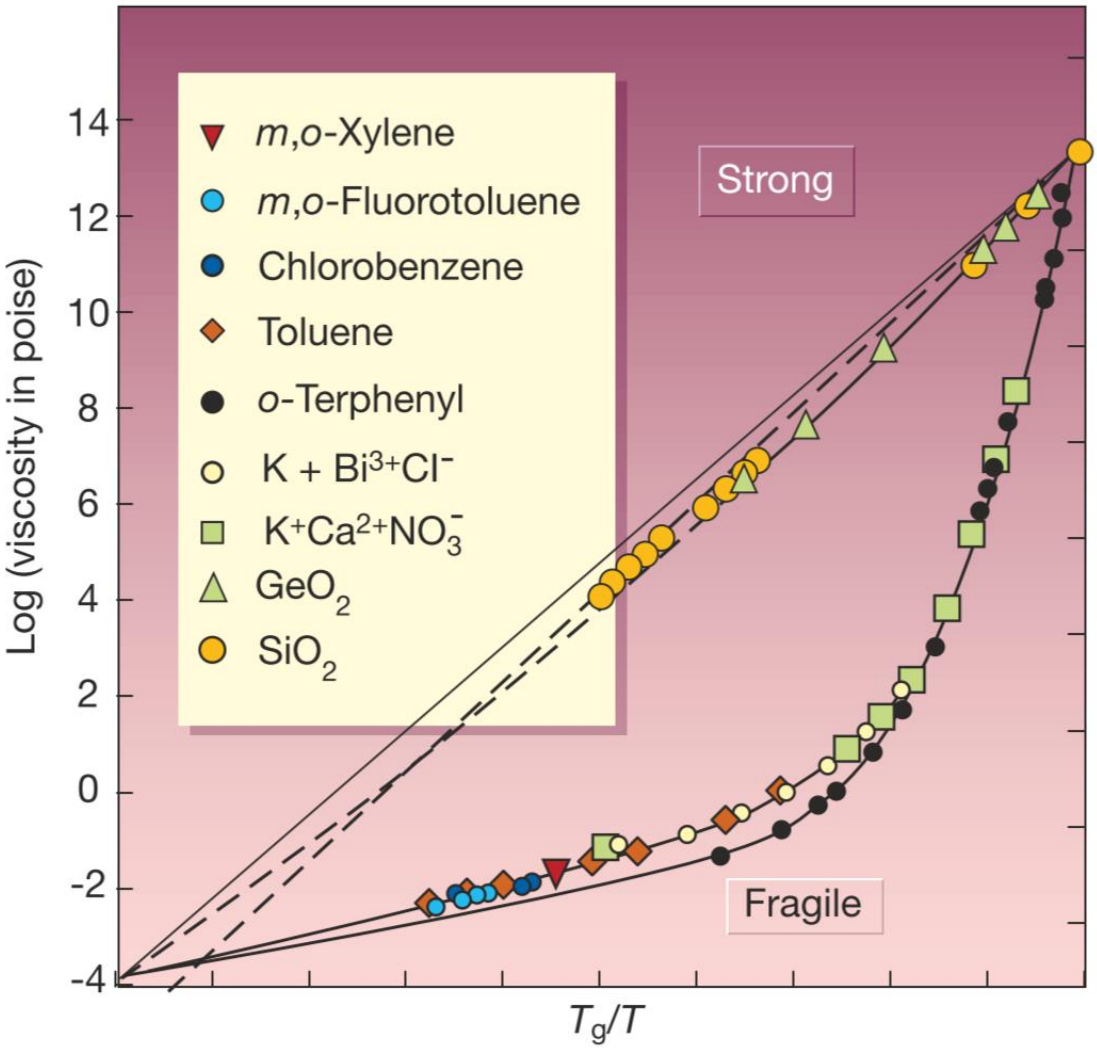

Fig. 1.1 Viscosity for a variety of glass forming systems scaled according to the glass transition temperature [3].

Dynamics such as deformation, diffusion, and aging/rejuvenation are all determined by the fundamental relaxation processes.

Dielectric spectroscopy, in which an alternating current is passed through the sample [19], reveals the vast timescales of relaxation in glass spanning over 20 orders of magnitude with changing temperature [20] as seen in Fig. 1.2. The main relaxation of interest has been the α relaxation [21] which is the 'primary' relaxation and controls the glass transition. However, below the glass transition temperature, T_g there are other important relaxations that control deformation and aging/rejuvenation.

In polymers a secondary relaxation has been characterized by both mechanical and dielectric means [22]. In simple molecular glasses the Johari-Goldstein β relaxation [23] represents one of the secondary relaxation modes characterized by dielectric spectroscopy. Since then, the β relaxation has been measured in many different disordered systems such as metallic glasses and high entropy alloys (HEAs) [20,24]. Phenomena such as aging, diffusion and deformation [25–29] have been linked to the β relaxation therefore understanding would allow for tuning of these properties.

In addition to the α and β relaxation, various low temperature relaxations have been discovered including the region of nearly constant loss (NCL) measured by Lunkenheimer et al. [19]. NCL lies between the β relaxation peak, and the region of excess low-frequency vibration modes known as the Boson peak [30,31]. This NCL relaxation has also been observed in many other disordered systems [32–34] which may mean it is a universal relaxation in glass just as α relaxation and β relaxation are. Despite the universality, there has not been much study of the origin of NCL. How does the NCL relaxation occur microscopically? What properties in glass does NCL control?

The origin of relaxations and deformations

What is the microscopic picture of how relaxations such as α, β or NCL occur? How cooperative are atoms in these relaxations? What is the relationship between structure and the relaxation in question? Answering these questions is of great importance for characterizing the underlying microscopic mechanisms of the fundamental relaxation phenomena.

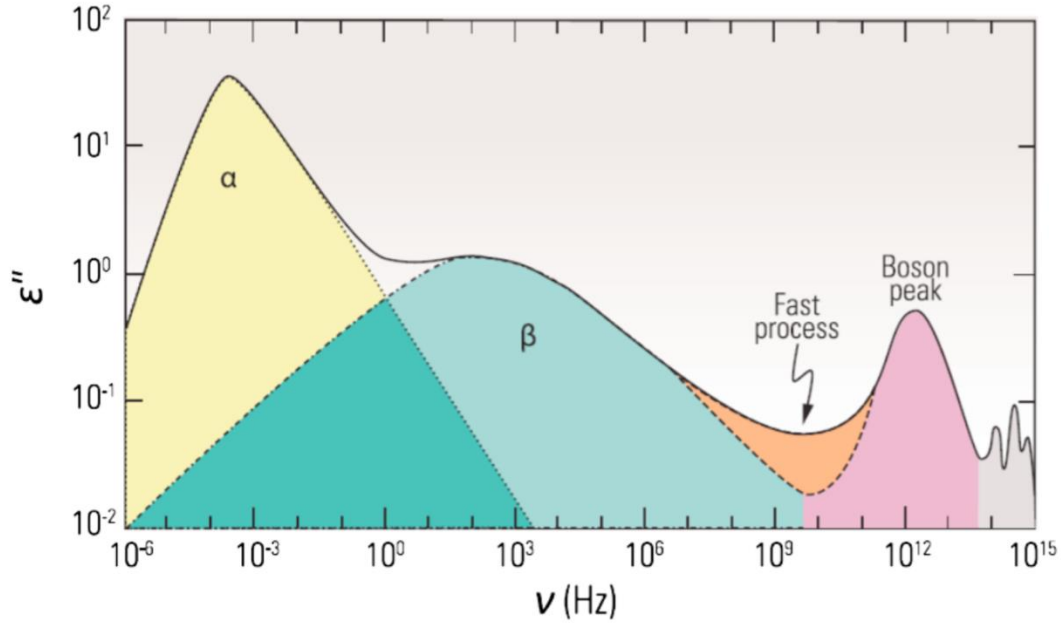

Fig. 1.2 Schematic of dielectric loss in glass forming systems with the most common relaxation behaviors labeled [28].

During relaxation, glass experiences a rearrangement of particles and thus passes through different free energy states.

All relaxations the system can experience may be described by the potential energy landscape (PEL) [29–31], which is a high dimensional space containing all possible configurations of the system and the corresponding free energies. An example PEL schematic is shown in Fig. 1.3.

This PEL is a landscape because 'traversal' across the landscape represents new spatial coordinates for all the atoms in the system, and summiting or descending the PEL represents the activation and relaxation phenomena respectively. While the PEL does contain all possible relaxation pathways, it is not easily accessible due to the $3N + 1$ (where N is number of atoms for the case of 3-dimensional system) dimensions of the configuration space. However, the PEL is still useful for interpretation of activation/relaxation events. α/β relaxations have been described in the PEL picture as moving the system across basins/valleys. Therefore, any thermal/mechanical perturbation that results in a rearrangement can be interpreted in this PEL picture. Thus, plastic deformations occur through activation and relaxation of relaxation processes that are determined by the underlying PEL.

Early attempts to understand the microscopic picture of deformation in metallic glasses were by Spaepen [32] who proposed a free-volume picture where atomic rearrangements occur by atoms moving into free volume voids. Argon [33] used bubble rafts to describe how groups of 'atoms' under a shear may as a group rearrange together and this work later inspired modern views on the mechanism of deformation as shear transformation zones (STZs) [34]. However, much is still not known about STZs such as what their size is, structural origin of STZs and their microscopic evolution [35,36].

Experimental techniques to understand deformation and relaxation range widely in their ability to differentiate timescale, length scale and evolution of said relaxation against temperature. Popular sinusoidal perturbation techniques such as dielectric loss spectroscopy and dynamic mechanical spectroscopy [37,38] are based on the principle of analyzing the susceptibility of systems and these susceptibilities are a resultant of the relaxation mechanism [38].

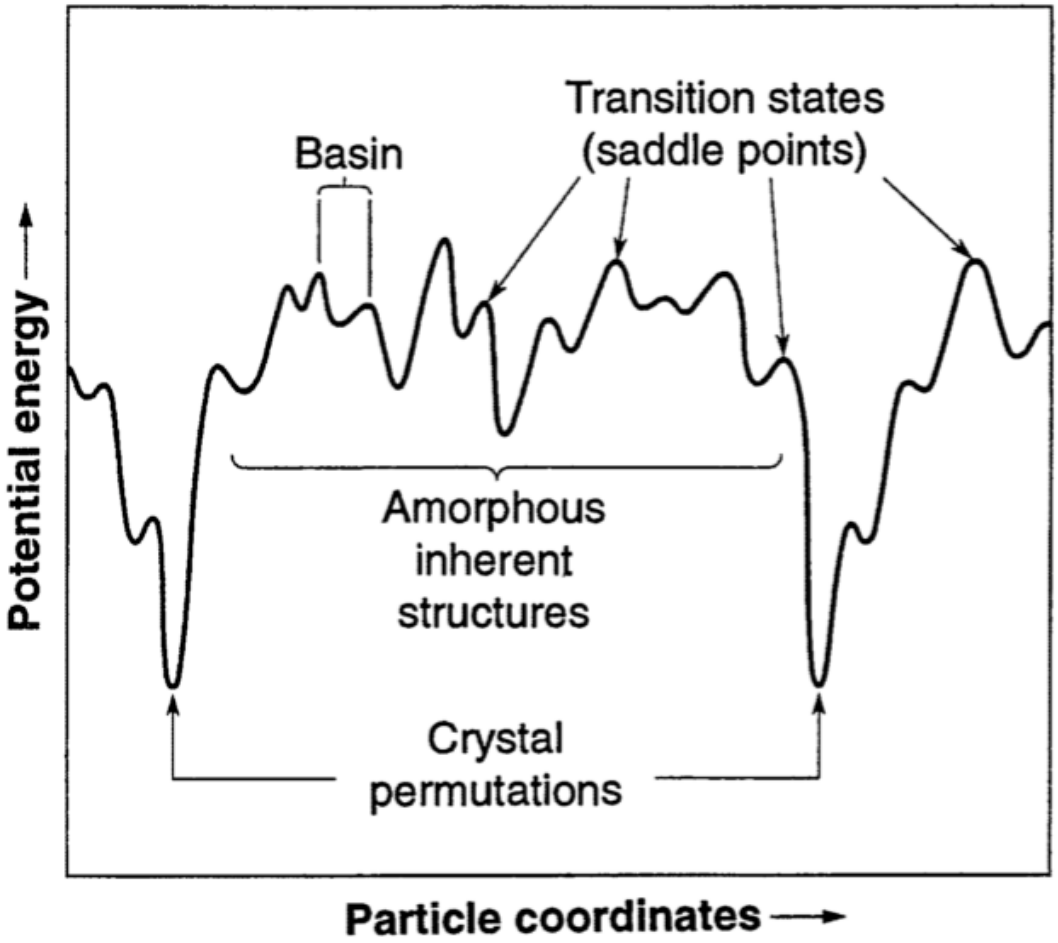

Fig. 1.3 Example cartoon of a PEL for an amorphous system. As the actual PEL is not possible to visualize, changes in overall system coordinates on the x-coordinate and the total potential energy of the system on the y-coordinate [39].

However, the drawback of these techniques is the lack of microscopic information, during mechanical or dielectric loss there is no ability to determine the microscopic motion or microscopic mechanism of these relaxations.

Therefore, other techniques may be used to examine the microscopic length scales such X-ray Photon Correlation Spectroscopy (XPCS) [40,41]. Still there are certain dynamics which are quite difficult to measure via experiments such as the string-like motions [42–44] proposed to be related to α relaxation and β relaxation. Some experimental techniques may excel at measuring a certain length scale but are not able to examine the needed timescale making fast relaxations [37] difficult to resolve. Even while these techniques can resolve relaxation time and length scale, the exact microscopic motions that result in the relaxation are not accessible.

Using simulation techniques such as classical molecular dynamics (MD) allows for examination of the exact trajectories and momenta of atoms during relaxation and deformation. This is how the microscopic mechanisms of relaxations and deformations may be studied in detail that is not possible in experiments. Simulation techniques have even been used to mimic experimental techniques of dynamical mechanical spectroscopy (DMS) to reproduce general features and temperature dependence of dynamic susceptibility in disordered systems [44–46]. Despite the advantage of precise trajectories and momentums in MD, the origins of relaxations such as α/β relaxation have been heavily debated [43,47–50]. One principal issue is how exactly to determine if atoms are involved in a relaxation or deformation. To determine this the timescale of dynamics of the atoms of interest may be linked to the relaxation time, or methods such as activation-relaxation technique (ART) [51–53] can be used to probe the various relaxations via searching the PEL. While these ART techniques may be used to examine the various activations and relaxations available to the system, it does not do so during dynamics so a big part of the puzzle of dynamic evolution of the relaxation remains missing. A different approach is to use set-to-point [54] techniques which were originally used to look at spatial correlations, these have been utilized to try to determine atoms involved and responsible for relaxations [45,55], during set-to-point sets of atoms are frozen or made to deform affinely and thus not contribute to mechanical loss. This approach interferes with local dynamics which makes determination of which atoms are causing the relaxation difficult. Because of the shortcomings of previous simulation works in identification and characterization of mechanical relaxation and the

considerable difficulty in examining the microscopic picture experimentally, there is need for new methods to make progress in understanding the origins of relaxation/deformation.

CHAPTER TWO SIMULATION METHODS FOR UNDERSTANDING RELAXATION

In this chapter we overview and detail the simulation methods used to understand relaxation and deformation in metallic glass. We overview the basics of classical molecular dynamics which is the main tool of choice for understanding relaxation processes in this work. We also discuss the method through which atoms that cause mechanical relaxation are identified.

Molecular dynamics

Molecular dynamics simulations are a computational technique where a set of defined particles are moved in time and space by an interatomic potential that is carefully chosen. The earliest classical molecular dynamics simulations in the late 1950's modeled hard sphere dynamics [56] and radiation damage [57]. Molecular dynamics simulations serve a crucial role of testing theory and unraveling atomistic mechanisms that would otherwise be difficult to observe experimentally.

In molecular dynamics there are a few simple steps to simulate the system. First, we initialize the parameters such as the positions of atoms, density, and temperature. Next, we proceed with the calculation of dynamics which runs in a loop where the forces on all particles are calculated, and the equations of motion are integrated over some timestep which in our case is on the order of femtoseconds. This loop is continued until the desired length of simulation is achieved. To do this we first define a set of vectors $\vec{r_i}$ which defines the 3-dimensional position vector for each atom i. From these vectors the forces on each particle are as follows:

$$\vec{f_i}(r) = \frac{dU(r)}{d\boldsymbol{r}} \qquad (1)$$

where $\vec{f_i}(r)$ is the force vector on atom i, $U(r)$ is the potential as a function of distance r and **r** is the position vector. In the case of this work, we utilize a many-body potential known as an embedded atom potential (EAM) [58]. After the force evaluation takes place the equations of motion are integrated to calculate the new positions of particles after the length of the simulation timestep. A common algorithm used is the Verlet algorithm which gives the new position as follows:

$$\vec{r}_i(t+\Delta t) \approx 2r(t) - r(t-\Delta t) + \frac{\vec{f}_i(t)}{m}\Delta t^2 \qquad (2)$$

Where Δt is the simulation timestep and m is the mass of the atom. In our case we use Large-scale Atomic/Molecular Massively Parallel Simulator (LAMMPS) [59] for all of our classical molecular dynamics simulations.

Simulation of glass

The simulation of glass requires some important considerations especially with the initial structure and preparation of the system. Glass is thermal history dependent and during the formation of real glasses the quench rate is a critical parameter in determining glass formability. Realistic cooling rates of metallic glasses may be in the range of $1 - 10^6\ K/s$ which is well beyond what is possible in molecular dynamics timescales. This creates a difficulty for those interested in simulating glass and getting results that are relevant to experimental observations. However, by examining the cooling rate trends we can determine how relevant the cooling rate is regarding the parameter of interest. Another approach is to explore the potential energy landscape to find new configurations [60] that would be beyond the timescale of standard molecular dynamics. Yet another approach is to use efficient Monte Carlo swap algorithms [49,61] to produce glasses with exceptional equilibration times.

The standard approach to form a glass by MD is by performing a melt and quench of the system where an initial crystal structure is melted at a high temperature and then equilibrated. After a sufficient equilibration at high temperature the system is quenched to the desired temperature that is somewhere below T_g, the glass transition temperature. In our simulation works this quench rate ranges from instantaneous to as slow as $10^{10}\ K/s$. The role of sufficient equilibration time for a formation of glass is demonstrated in Fig. 2.1 where a modified Johnson iron [62,63] is equilibrated for different times then quenched producing amorphous iron glasses with lower potential energies as a function of equilibration time.

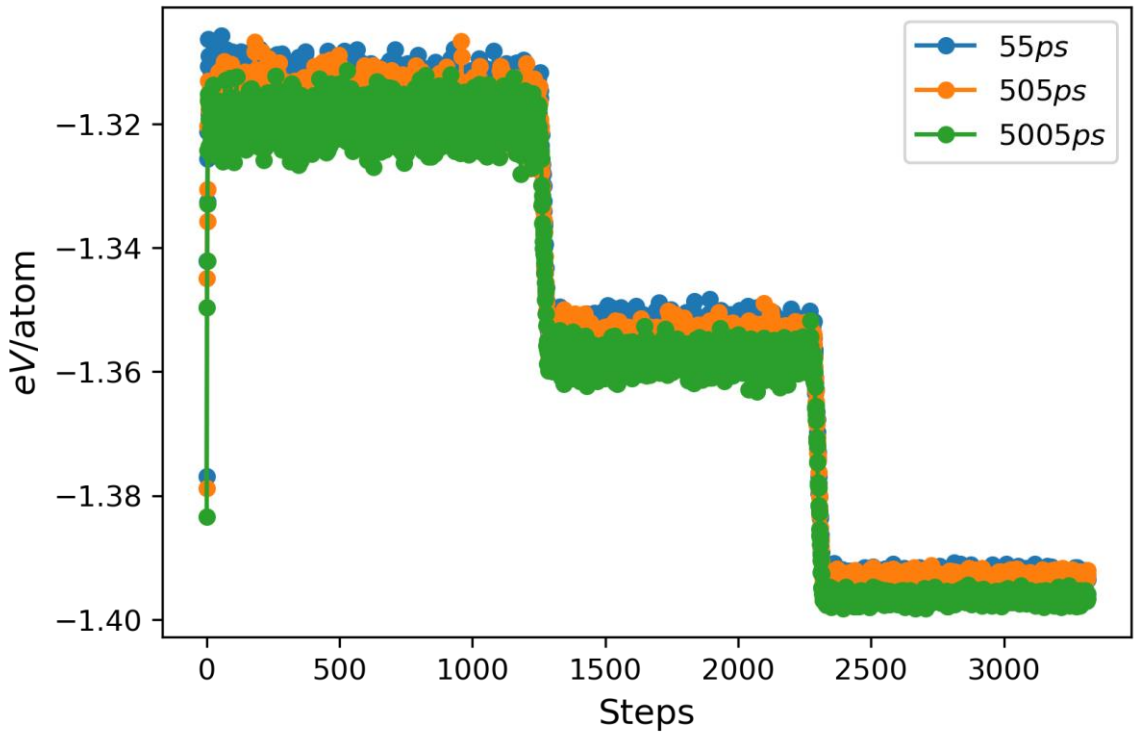

Fig. 2.1 Potential energy per atom of a modified Johnson iron system with 3 different equilibration times at high temperature.

During this quenching, it is important that the quench rate is sufficiently fast enough that the glass does not crystallize, and the verification of the glassy structure may be done by several methods. A useful measure of structure is the radial distribution function $g(r)$ which is a pair-correlation function that defines how likely a particle a distance r away may find another particle [64]. The radial distribution function may be defined as follows:

$$g(r) = \frac{r}{4\pi N^2} \sum_{\nu} \sum_{\mu} \delta(r - r_{\nu\mu}) \qquad (3)$$

where N is the number of atoms, $r_{\nu\mu}$ is the distance between atoms ν, μ and δ is the Dirac delta function. The radial distribution function is used widely to characterize the structure of materials and can be obtained by experiment and compared with simulation. Comparing $g(r)$ between glass and crystal readily shows the difference in the sharp peaks that exist for a crystal. This is shown in where $g(r)$ is plotted for amorphous iron and mostly BCC iron which was produced due to an insufficient cooling rate.

The choice of the system and potential to use for our simulation works was informed by the ability to compare our results with other literature and a potential that gives reasonable mechanical results for metallic glasses. Many metallic glasses of interest are multicomponent systems that are not possible to model with classical molecular dynamics because there is no suitable potential. Therefore, simpler metallic glass systems with less components are more available for molecular dynamics simulations. A simple two component $Cu - Zr$ metallic glass can be made experimentally [65,66] and there are two EAM potentials [5,67] which reproduce the pair-distribution function, densities and give reasonable glass transition temperatures. Particularly there is more work studying the $Cu_{65}Zr_{35}$ composition and when implementing the technique of molecular dynamics dynamic mechanical spectroscopy (MD-DMS) we wanted to reproduce literature results which utilized this same composition [46].

Molecular dynamics dynamic mechanical spectroscopy

In the study of mechanical properties of materials, a technique known as dynamic mechanical spectroscopy (DMS) is widely utilized for measuring the complex viscoelastic response of materials and for capturing the various relaxation phenomena of systems [38,68]. By applying a sinusoidal force to a material, the resulting sinusoidal strain may be captured and from the response amplitude σ_A and phase difference of the response, δ. This technique has been used to measure

various relaxation behaviors [47] especially in metallic glasses where dielectric spectroscopy cannot be used due to the lack of an electric dipole moment. This same experimental technique may be done in simulation, but rather an affine strain is applied, and this results in the applied force. This can be seen in which demonstrates a large shear strain of a $Cu - Zr$ glass. If the material is not completely elastic, there is a phase shift between the stress and strain which may be seen in Fig. 2.4 [46]. Therefore, in the case of a sinusoidal shear strain, $\varepsilon(t) = \varepsilon_A \sin(\omega t)$ where t is time, $\omega = 2\pi/T_\omega$ and ε_A is the amplitude of the applied strain. From this the complex shear modulus may be calculated, $G^* = G' + iG''$ with G' as the storage modulus which is the elastic energy stored during the straining and G'' as the loss modulus representing energy dissipation. Additionally, the storage and the loss modulus are related to the sinusoidal amplitude and strain by $G' = \sigma_A/\varepsilon_A \cos(\delta)$ and $G'' = \sigma_A/\varepsilon_A \sin(\delta)$.

Cohen et al. [45] demonstrated this simulation technique known as molecular dynamics dynamic mechanical spectroscopy (MD-DMS) by calculating the complex modulus under shear stress relating to the β relaxation peak and examining microscopic mechanisms involved in the relaxation. Since then MD-DMS has been used to study internal friction [46], low temperature relaxation [55,69] and the nature of the β relaxation [70,71]. While MD-DMS operates under the same principles as the experimental technique it mimics, there are significant differences in the length and timescale between experiment and simulation. Dynamic mechanical spectroscopy is not a microscopic technique, though there are other experimental setups that are similar in principal such as atomic force microscopy [72–74]. Because of the difference in length scale of phenomena the dynamics studied should be on a sufficiently small scale to be observed by molecular dynamics. Secondly DMS experiments usually apply the force at a frequency in the range of 10's of HZ and in simulation the frequency is more likely to be $10^9 - 10^{12}$ HZ. Given these two differences, the mechanical phenomena studied by simulation should be captured at the microscale and understanding of the timescale of the dynamics studied should fall within the range that is accessible by simulation.

Where previous MD-DMS works have had issues is identifying the group of atoms directly involved the mechanical relaxation / mechanical loss that occurs. To try to pinpoint which atoms are involved in mechanical relaxation, Wang et al. 'pinned' sets of atoms [54,75,76] which only let them deform affinely then measured how this impacted the subsequent G".

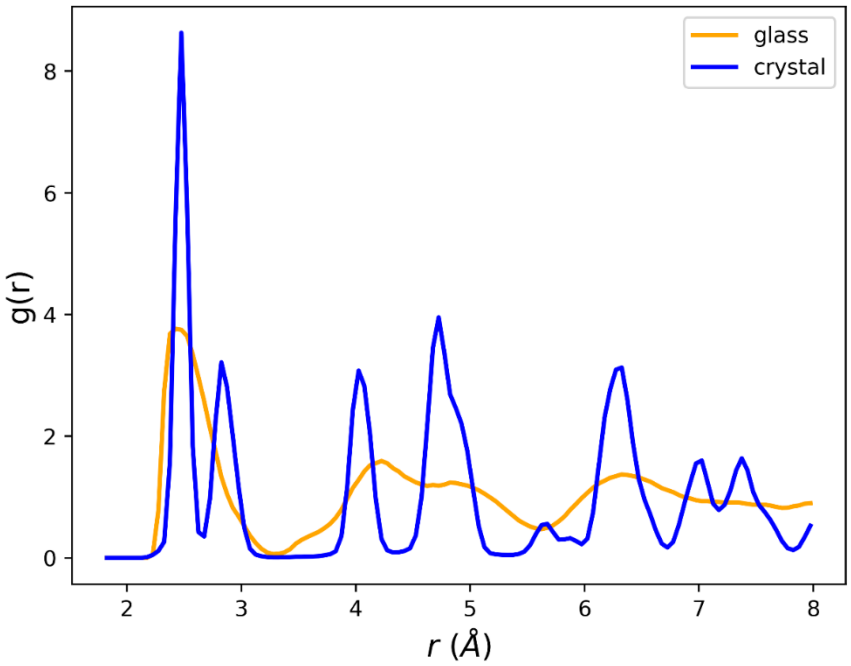

Fig. 2.2 Radial distribution function of a MD simulation of modified Johnson iron as a glass (orange) and a crystal (blue).

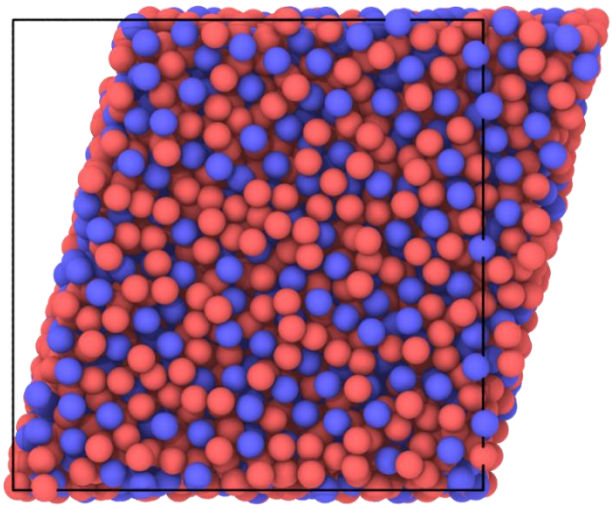

Fig. 2.3 $Cu_{65}Zr_{35}$ metallic glass in the middle of a sinusoidal strain cycle

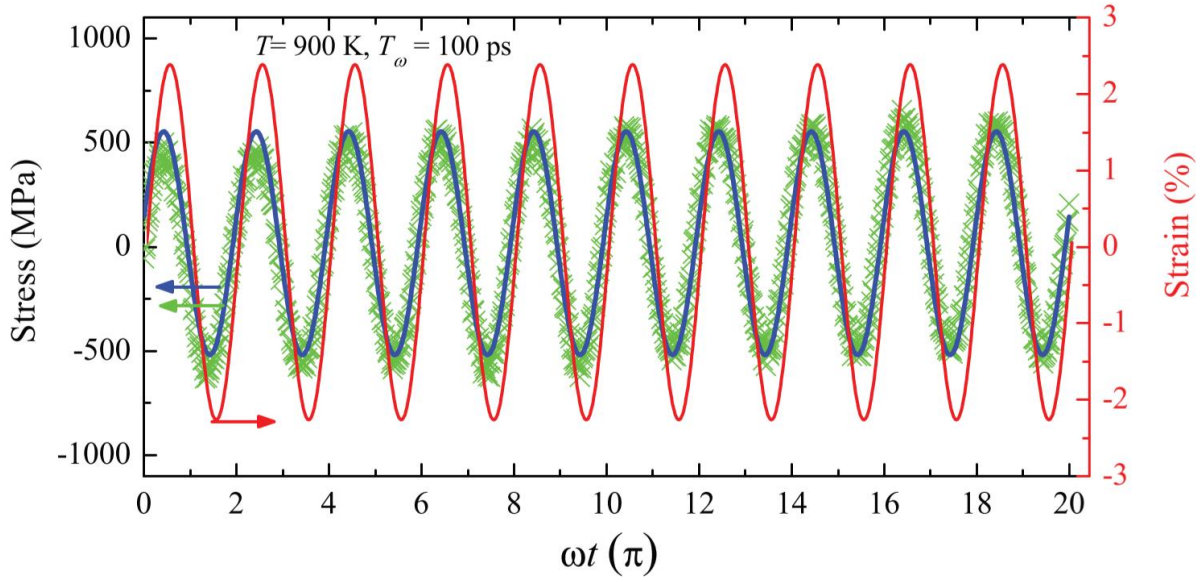

Fig. 2.4 Demonstration of phase shift difference between stress and strain during a shear strain, T = 900 K and T_ω= 100 ps [45].

However, by pinning these atoms we prevent cooperative motion which may have allowed sets of atoms to participate and cause relaxation and perhaps interfering with the dynamics in ways that are not predicted.

A different strategy is to observe dynamics such as non-affine displacement and match this temperature scaling with the phenomena of interest [46]. This is also useful but may be misleading, atoms involved in relaxations that are cooperative may have subtle atomic dynamics that only make sense in the context of a cooperative phenomenon and thus would be looked over. Therefore, being able to identify which atoms are directly involved in the mechanical loss of a cycle of straining would allow for new directions in understanding microscopic mechanisms. This is where we introduce the concept of atomic-level stress and thereby the identification of atoms participating in mechanical relaxation.

Atomic-level mechanical response

During the application of strain to a system, there is some macroscopic viscoelastic response. This may then be broken down into the atomic-level viscoelastic response during a cycle of straining. To do this we turn to the concept of atomic-level stress which is the first order response to strain [77,78]. This atomic-level stress is defined as a tensor which reflects the neighboring cage of atoms and includes both potential energy and kinetic energy components with the potential energy component generally dominating the term. We then write the atomic-level stress as follows:

$$\sigma_i^{ab} = \frac{1}{\Omega_i}\sum_j (f_{ij}^a r_{ij}^b + m_i v_i^a v_i^b) \qquad (4)$$

where *a* and *b* are Cartesian components, Ω_i is the atomic volume of atom *i*, f_{ij}^a is the two-body force between atoms *i* and *j*, r_{ij}^a is the *a* components of the distance vector, r_{ij}, between atoms *i* and *j*, and v_i^a is the *a* component of the velocity of atom *i*. Atomic-level volume is calculated by Voronoi tessellation [79]. Atomic-level stresses have been used to define topological instabilities based on the principle of local coordination number around some atom [80], by elastically straining some atomic site the local pressure can be calculated by atomic level stresses which gave a critical volume strain of 11% [81].

From this atomic-level stress we can decompose the system shear stress applied into the atomic-level components which may be written as $\sigma_{xy}(t) = \sum_i \sigma_{A,i} \sin(\omega t + \delta_i)$, where $\sigma_{xy}(t)$ is atomic-level shear stress. From this decomposition it is then possible to estimate the individual atomic-level viscoelastic response if the phase shift of an individual atom can be calculated. From this we get the atomic-level complex shear modulus is defined by $G^*_{atom} = G'_{atom} + iG''_{atom}$, and atomic-level phase shift by $\delta_{atom} = \arctan(G''_{atom}/G'_{atom})$.

Estimation of the phase shift of an individual atom can be complicated and depends on many factors including the magnitude of thermal fluctuations present. An example atomic-level shear response of an atom is show in Fig. 2.5, because of the thermal fluctuations in shear stress it is not immediately clear what the phase shift of the atom is, and the least-squares fit may not even be able to fit a response curve with reasonable error.

However, while in the time domain signal it might be quite difficult to extract the phase shift, it is much easier to move the data to the frequency domain because we know the frequency of the applied system strain and therefore what the frequency is of the atomic-level response. At low temperature the difference between atoms of different viscoelastic response is clear, we see in Fig. 2.6a representative elastic atom which follows the shear strain response closely. In contrast Fig. 2.8 Example of a 'lossy' atom at 0.1 K. It demonstrates shear stress 'breaks' during sinusoidal strain.

demonstrates a lossy atom with jumps in the shear stress, this clear response behavior is not easy to characterize at 300 K as seen in Fig. 2.5. To estimate the phase shift of an atom with thermal fluctuations, the Fourier transform is used to calculate the amplitude of the response of the atom to the applied strain. The atom in Fig. 2.5 represents the atomic-level shear stress response over one cycle of strain, using the Fourier transform the response is now in frequency space as shown in Fig. 2.8. From the complex space representation of the response after the Fourier transform, we may get both the amplitude and phase shift of the individual atom as seen in the diagram of complex plane representation of the atomic-level stress in Fig. 2.9.

The atomic-level phase shift, δ_{atom}, defined from the atomic-level stress response, ranges from $[-\pi, \pi]$ rather than $[0, \frac{\pi}{2}]$ because at the atomic level atoms can respond in the opposite direction of the strain. By applying a single cycle of shear strain, we can calculate the atomic-

level phase shift of all atoms. A characteristic distribution for a $Cu - Zr$ glass is shown in Fig. 2.10. We observe a roughly symmetrical distribution with a large peak centered around $\delta_{atom} \approx 0$ which represents the group of elastic atoms.

Using the atomic-level stress response to a cycle of straining we can estimate the relative magnitudes of atomic-level mechanical loss by the following equation: $G''_{atom} = {\sigma_{A,atom}}/{\varepsilon_{A,atom}} * \sin(\delta_{atom})$, where we make the assumption that all atoms are under a similar atomic-level strain (this assumption is a reasonable first approximation as the numerator dominates the equation for mechanical loss). This atomic-level mechanical loss can also be calculated in a different fashion by estimating the area of the stress-strain curve which corresponds to the mechanical loss. This stress-curve is shown for several different atoms in Fig. 2.11. We observe that most atoms follow a roughly linear stress-strain curve as seen in Fig. 2.11a where the slope may be used to estimate the atomic-level shear modulus. Other atoms have non-linear responses which then create an area in the curve as in Fig. 2.11b where the area is negative, thus there is an energy gain by that atom or Fig. 2.11d where the area is positive therefore considered a lossy atom. By computing the atomic-level loss for a set of atoms both ways we attempt to validate our atomic-level loss magnitude estimation as seen in Fig. 2.12, the ensemble of simulations was prepared with different velocity seeds and the mechanical loss calculations were performed at 300 K with a sinusoidal strain of $\varepsilon_A = 2.5$ % and a period of 100 ps. The strong correlation between the two methods adds more confidence in our estimation of lossy atoms that is used in later chapters.

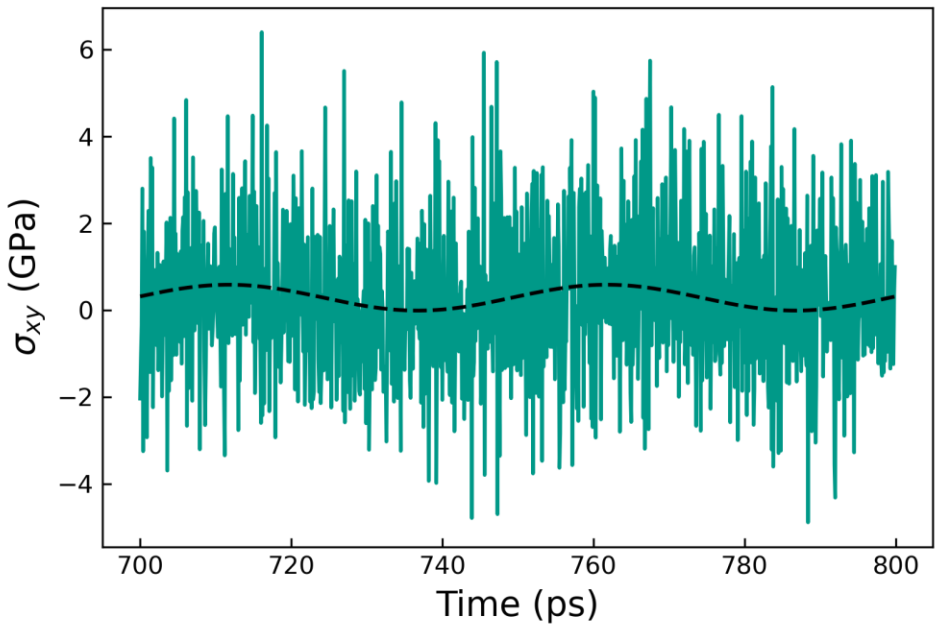

Fig. 2.5 Atomic-level shear stress response of an atom during 2 cycles of straining at 300 K.

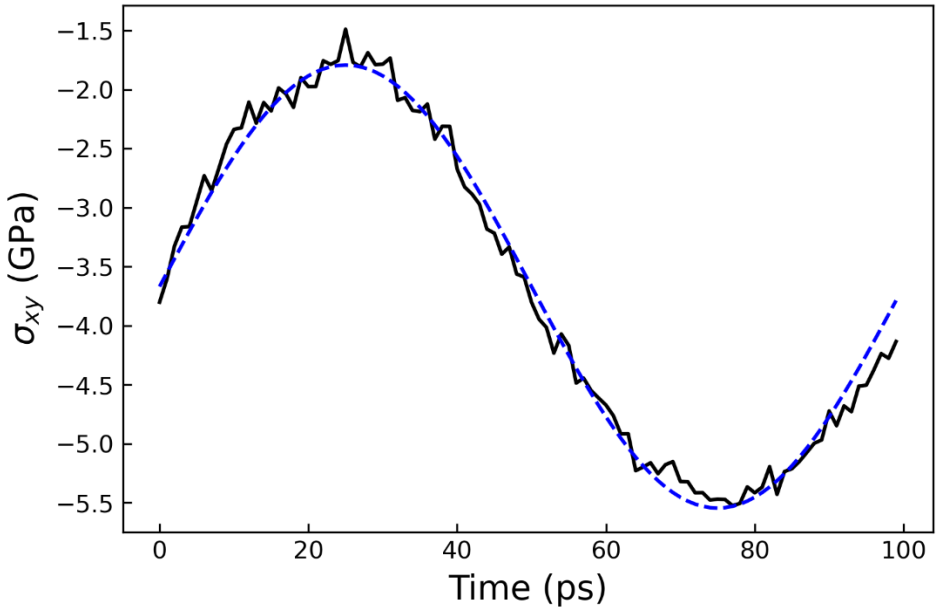

Fig. 2.6 Example of an elastic atom at 0.1 K. The sinusoidal shear stress response perfectly matches the applied strain.

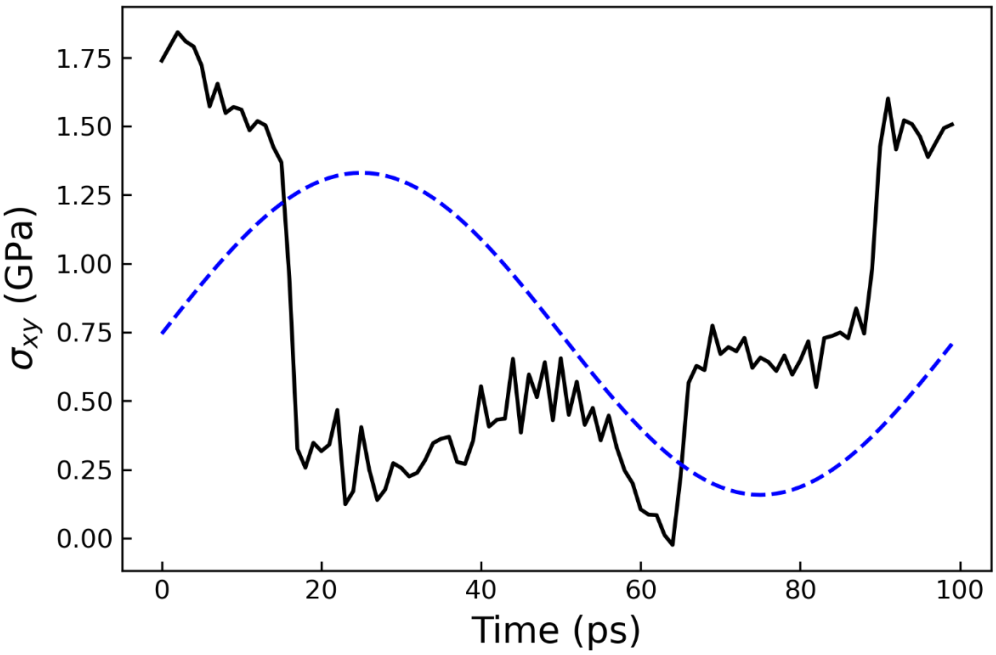

Fig. 2.8 Example of a 'lossy' atom at 0.1 K. It demonstrates shear stress 'breaks' during sinusoidal strain.

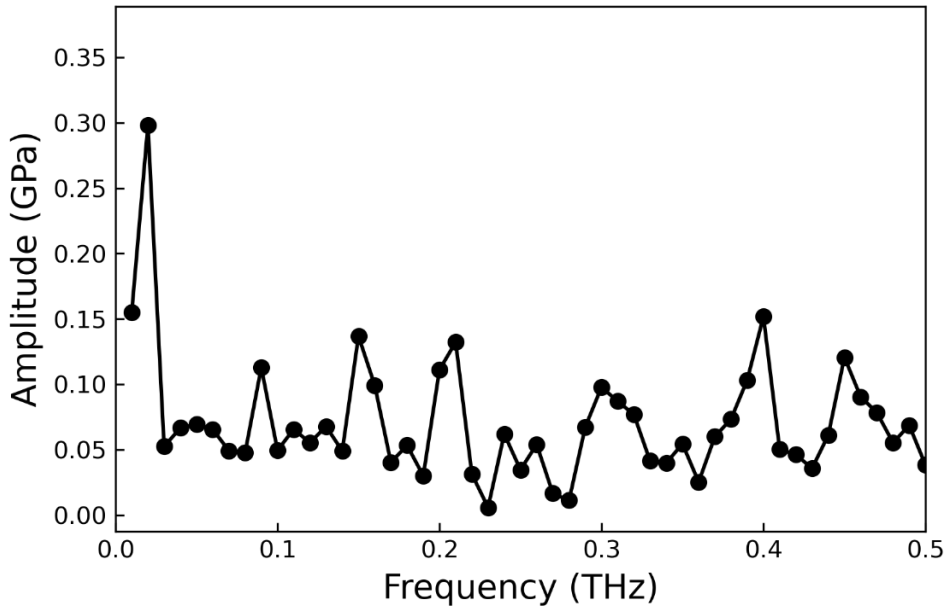

Fig. 2.7 Atomic-level shear response in frequency space from the atom shown in. The shear stress response signal of the atom is seen at 0.05 THz as a clear peak.

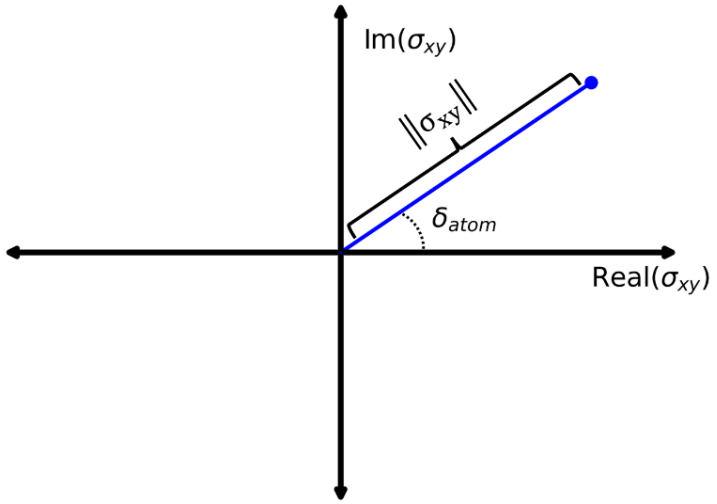

Fig. 2.9 Diagram showing the complex plane representation of the atomic-level shear stress response. By use of the Fourier transform we have a real and imaginary component and using these two components we can estimate the atomic-level phase shift

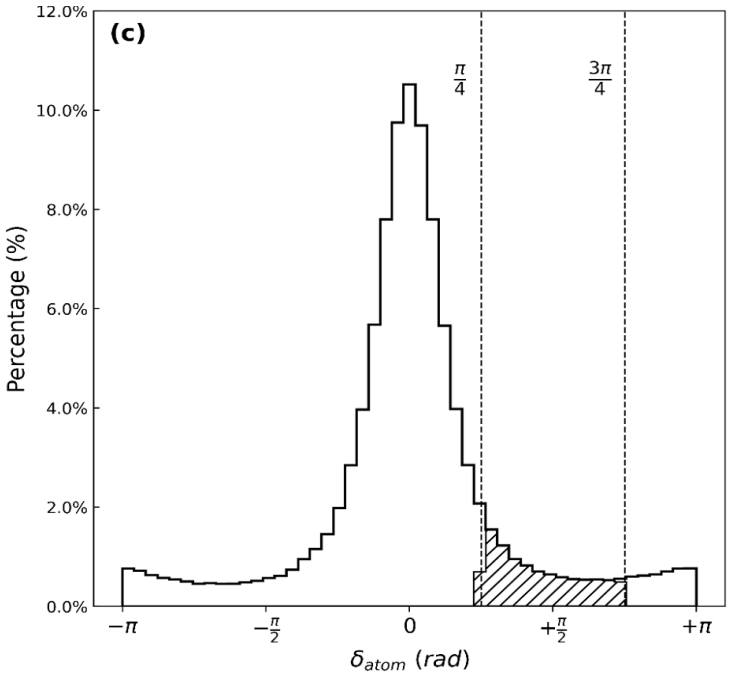

Fig. 2.10 Atomic-level phase shift distribution of a system of $Cu_{64.5}Zr_{35.5}$ metallic glass with 16,000 atoms. This is in response to a single cycle of shear strain. The cross-hatched region denotes the group of ‘lossy’ atoms during the strain cycle.

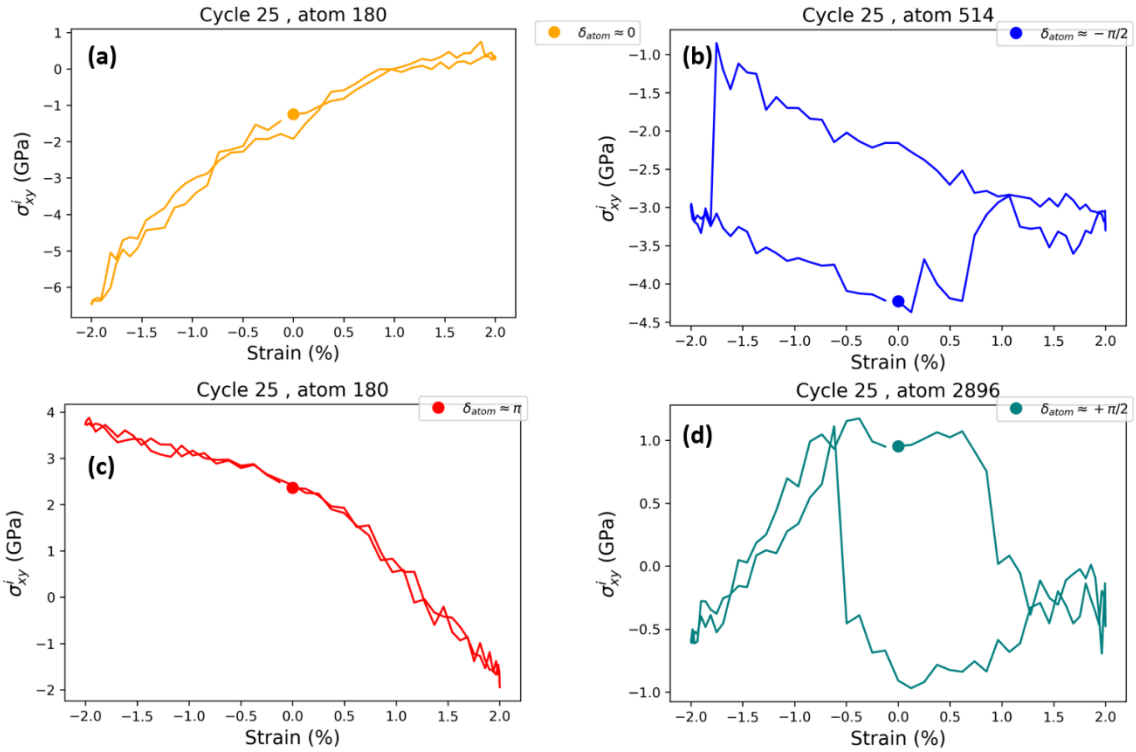

Fig. 2.11 Atomic-level shear stress response against strain for atoms with various δ_{atom} at 0.1 K. (a) Elastic atom with $\delta_{atom} \approx 0$ (b) Energy gaining atom with $\delta_{atom} \approx 0$ (c) Elastic atom with opposite response to strain $\delta_{atom} \approx \pi$ (d) Lossy atom with $\delta_{atom} \approx \frac{\pi}{2}$.

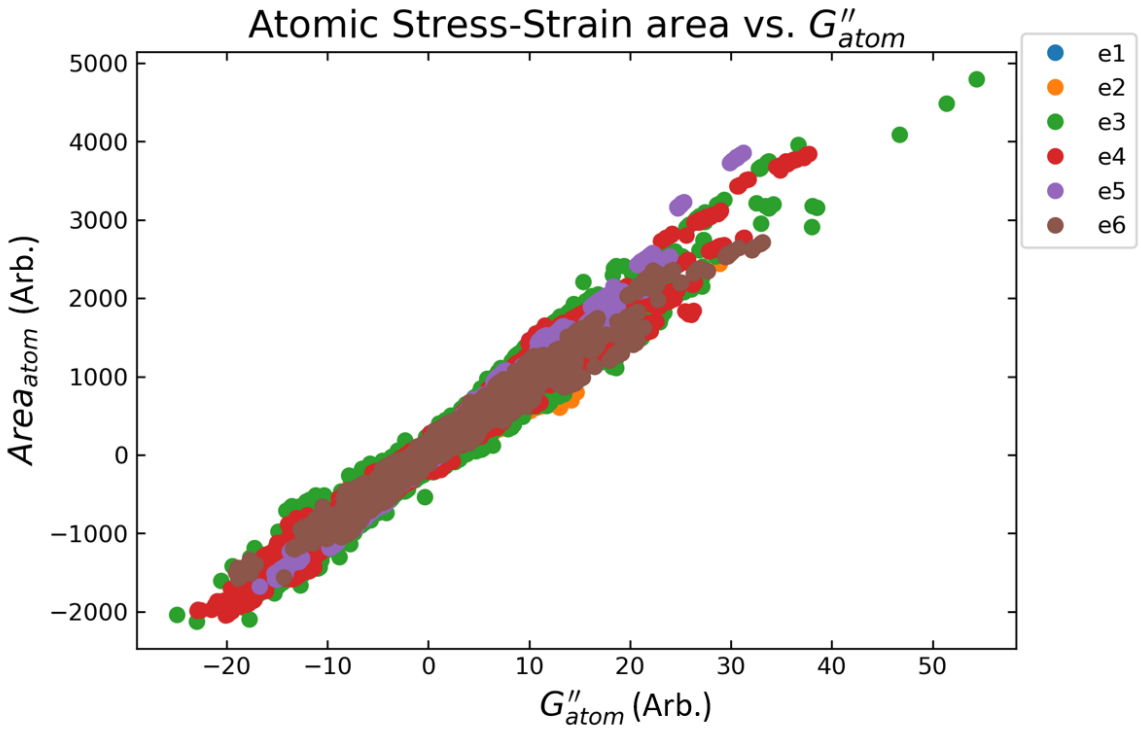

Fig. 2.12 Atomic-level loss for each atom calculated via two different methods for 6 different metallic glass systems with differing starting configurations during the liquid state. A clear correlation is shown between the two methods for estimating lossy magnitude. The units of loss for each atom are arbitrary.

CHAPTER THREE TRANSIENT NATURE OF FAST RELAXATION IN METALLIC GLASS

This chapter has been adapted from [82]:
L. Zella, J. Moon, D. Keffer, T. Egami, Transient nature of fast relaxation in metallic glass, Acta Materialia. 239 (2022) 118254. https://doi.org/10.1016/j.actamat.2022.118254.

Metallic glasses exhibit fast mechanical relaxations at temperatures well below the glass transition, one of which shows little variation with temperature known as nearly constant loss (NCL). Despite the important implications of this phenomenon to deformation, the origin of the relaxation is unclear. Through molecular dynamics simulations of a model metallic glass, $Cu_{64.5}Zr_{35.5}$, we implement molecular dynamics dynamical mechanical spectroscopy (MD-DMS) with system stress decomposed into atomic-level stresses to identify the group of atoms responsible for NCL. This work demonstrates that NCL relaxation is due to transient groups of atoms that revert to the typical atomic level viscoelastic behavior over picosecond timescales. They are homogenously distributed throughout the glass and have no outstanding features, rather than having defect-like local structure as previously reported.

Introduction

Identifying atomic origins of various dynamic processes is crucial in understanding mechanisms of various properties in amorphous solids, such as aging, relaxation, and deformation [83–87]. Metallic glasses are especially useful to study due to their simple close packed structures that are not dominated by local chemical bonds. The picture of relaxation processes in metallic glass has continued to evolve over time and now includes many processes including α relaxation [88], β relaxation [44,71,89], fast β relaxation [90,91], Boson peak dynamics [92], a low temperature relaxation peak (LTP) [93], and the subject of this paper, nearly constant loss (NCL) [28,37,94].

Dielectric loss measurements of glycerol and propylene carbonate by Lunkenheimer et al. [28] revealed “additional fast processes” between the boson peak and excess wing of the β relaxation, which is now characterized as nearly constant loss (NCL). NCL has been subsequently observed in numerous other disordered systems such as polymers, ionic conductors, and metallic glass

[37,94,95]. The transition from NCL to β relaxation has been measured by dynamical mechanical spectroscopy (DMS) and quasi-static tensile measurements in $La_{60}Ni_{15}Al_{25}$ bulk metallic glass (BMG) [37]. The same experiment measured the activation energy and found it to be roughly half that of the β relaxation. The hypothesized origin of NCL is thought to be rattling or fast caged dynamics which may be described by mode coupling theory (MCT) [94–97].

Since dielectric loss measurements and dynamical mechanical spectroscopy are macroscopic experimental techniques, it is not possible to identify the microscopic dynamics from these measurements alone. Classical molecular dynamics (MD) of $Cu_{65}Zr_{35}$ metallic glass investigated "fast processes", i.e. dynamics between boson peak and β relaxation which includes NCL, and identified a 40 GHz rattling mode that resulted in 'string-like' rearrangements of 2-3 neighboring atoms to the rattling center [98]**.** However, the amount of contribution of rattling type motion to NCL is undetermined as there has been no systematic measure of all dynamics related to the NCL relaxation. Additionally, the time dependence of atoms involved during the relaxation has not been resolved. Furthermore, the definition and precise characterization of rattling atoms are missing. Thus, despite these prior attempts to gain understanding of the NCL relaxation, the origin and mechanism of NCL are unclear.

In this work, we systematically identify the transient groups of atoms responsible for NCL using a standard molecular dynamics dynamical mechanical spectroscopy (MD-DMS) technique combined with atomic level stress calculations. Instead of focusing on specific dynamics such as rattling, we directly connect atoms causing mechanical loss to the relaxation mechanism. We show that the NCL relaxation sites are transient and spatially homogenous. We examine the correlation of NCL relaxation with atomic-level parameters often used in identifying defective sites, such as non-affine displacement, atomic-level stresses, atomic volume, and coordination number. We find no clear distinct features of atoms responsible for NCL, demonstrating the subtlety of the NCL mechanism.

Methods

Model Metallic Glass

Classical molecular dynamics simulations were performed using the Large-scale Atomic/Molecular Massively Parallel Simulator (LAMMPS) [99] with a timestep of 1 fs. Periodic boundary conditions were imposed. As a prototypical metallic glass, a $Cu_{64.5}Zr_{35.5}$ glass with 4000 atoms and cubic side lengths of 39.9 Å was made by a typical melt-quench method. The embedded atom method (EAM) potential was used to describe interatomic interactions [100]. First, the system was melted at 3000 K for 1 ns. It was then cooled down to 300 K with a cooling rate of 1 K ps^{-1} in the NVT ensemble. Equilibration was done at 300 K under NPT ensemble with zero pressure for 100 ps.

Molecular Dynamics Dynamical Mechanical Spectroscopy (MD-DMS)

By applying a sinusoidal strain to the system mimicking experimental DMS [38], the relaxation dynamics of the system is probed as in Ref. [101]. A sinusoidal shear strain was applied following $\epsilon(t) = \epsilon_A sin(\omega t)$ where t is time, $\omega = 2\pi/T_\omega$, with a maximum strain of $\epsilon_A = 1\%$ and a period of $T_\omega = 50$ ps. The system was in the linear elasticity regime throughout, this was verified by a set of simulations validating the linear stress-strain regime. In this paper, 30 cycles were done for a total production time of 1500 ps. We anticipate that our results are independent of system size and strain frequency as demonstrated by Yu et al. [46]. The complex shear modulus $G^* = G' + iG"$ describes the viscoelastic response of the system to the sinusoidal straining, with G' being the storage modulus representing elastic energy storage and $G"$ being the loss modulus representing energy dissipation. Additionally the storage and loss modulus are related to the sinusoidal amplitude and strain by $G' = {}^{\sigma_A}/_{\epsilon_A} \cos(\delta)$ and $G" = {}^{\sigma_A}/_{\epsilon_A} \sin(\delta)$, respectively, where σ_A is complex sinusoidal stress amplitude, ϵ_A is magnitude of strain, and δ is the phase shift between the strain and stress response. In this work, we will focus on the phase shift δ as it is related to the magnitude of loss modulus. To study the transient nature of the NCL relaxation, we divided the 1.5 ns simulation into 15 blocks of 100ps each in length and calculated the phase shift of the entire system of 4,000 atoms for each block.

Atomic-Level Stress Frequency Representation

To gain an atomic perspective on the origin of the NCL, we calculated atomic-level stresses, which represent the first order response of an atom to a strain [77,78]. By partitioning the system stress into individual atomic-level stress responses, we can describe the local stress environment of an atom. The pairwise atomic-level stress is given by:

$$\sigma_i^{ab} = \frac{1}{v_i}\sum_j f_{ij}^a r_{ij}^b + \frac{1}{2m_i} V_i^a V_i^b \quad (1)$$

where a and b are Cartesian components, v_i is the atomic-level volume of atom i, f_{ij}^a is the two-body force between atoms i and j, r_{ij}^a is the a component of the distance vector, $\boldsymbol{r_{ij}}$, between atoms i and j, and V_i^a is the a component of the velocity of atom i, $\boldsymbol{V_i}$. This calculation is done in LAMMPS with periodic boundary conditions [102]. At such a low temperature kinetic contribution is expected to be negligible. Because an EAM potential is used, the many-body forces are naturally included during force calculations in the pairwise atomic-level stress calculation. Comparison of the system stress to the sum of the atomic-level stresses in Fig. 3.1 validates the sufficiency of the pairwise atomic-level stress. Atomic-level volume is calculated by standard Voronoi tessellation [103].

By transforming the time dependent atomic-level stress response into frequency space by Fourier transform, we identify the atomic-level stress response amplitude and phase for each atom. While the Fourier transform is not the only way to identify atomic-level response amplitude and phase, it was found to be more accurate than cross-correlation or least squares fit. The individual complex atom shear modulus is defined by $G^*_{atom} = G'_{atom} + iG''_{atom}$, and atomic-level phase shift by $\delta_{atom} = \arctan(G''_{atom}/G'_{atom})$. In typical MD-DMS calculations the phase shift is limited to $[0, \frac{\pi}{2}]$. However, locally the response can be in an opposite direction to the strain. For this reason, we computed the atomic level phase shift from $[-\pi, \pi]$ and due to periodicity, the atoms with phase shift $-\pi$ and $+\pi$ are equivalent. The system stress response is thus partitioned amongst individual atoms and the system stress response sum is recovered by $\sigma_{xy}(t) = \sum_i \sigma_{A,i} \sin(\omega t + \delta_i)$ with $\sigma_{A,i}$ being the amplitude of atom, i, and δ_i is the phase shift of atom i.

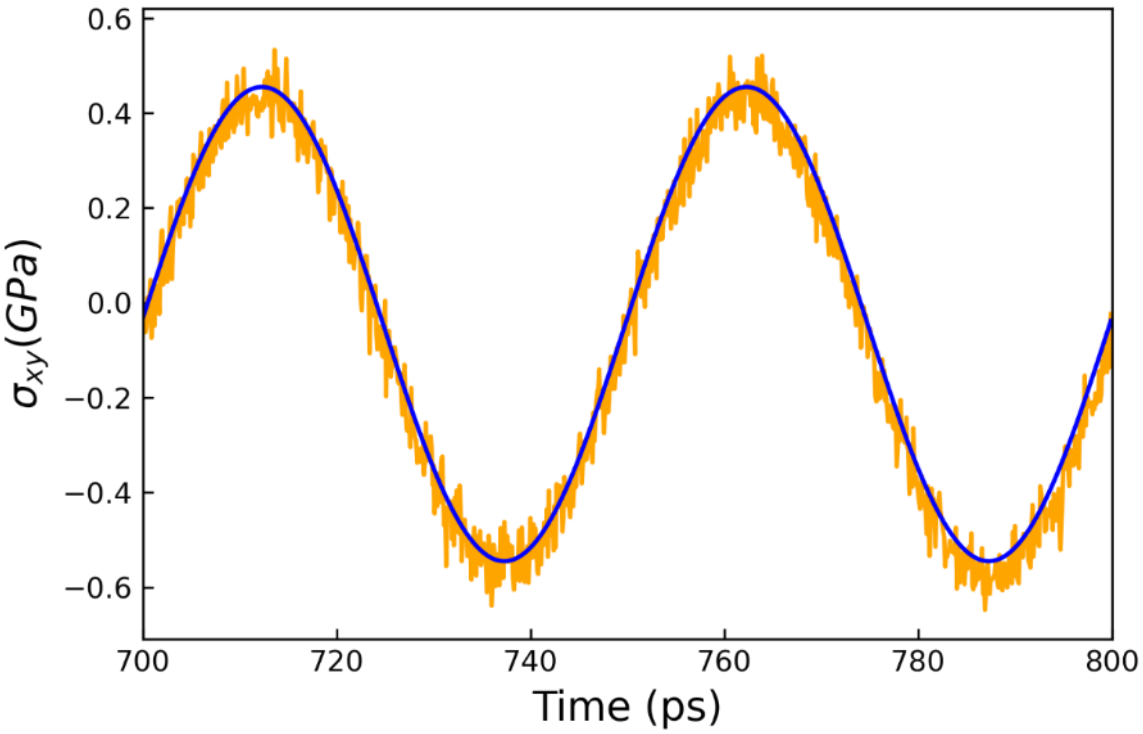

Fig. 3.1 Blue: System stress response. Orange: Sum of all atomic stress response with phase and amplitudes estimated by Fourier transform. The system stress response from the individual atom Fourier transform method is shown to be accurate in phase and amplitude when compared to system stress response.

The system stress response sum is shown to be accurate in phase and amplitude when reconstructed from sinusoidal atomic-level stress responses calculated by the Fourier transform as seen in Fig. 3.1.

To investigate a group of atoms that may be responsible for the loss modulus during sinusoidal straining, a partial stress which excludes the sinusoidal stress contributions from selected atoms is calculated. From this method new phase shifts, $\delta_{partial}$, and amplitudes, $\sigma_{A,partial}$, of the partial stress response are then found. If the partial stress has a smaller phase shift after excluding the atoms of interest, this means that the excluded set of atoms was contributing measurably to the overall phase shift and thus the loss modulus of the system. In this work, various groups of 5% of the atoms of the system total (200 atoms) were excluded to form the partial stresses. Error bars are calculated by the bootstrap method [104]**.**

Results

Atomic phase shift distribution and transient phase shift

The system stress as a function of time is shown in Fig. 3.2a in blue for a time range corresponding 6 cycles in the middle of production simulation of 1.5 ns. The overall stress response due to the oscillating strain is well fit by a sine function and has a small phase shift δ, in relation to the applied sine shown by a dashed curve in orange. In Fig. 3.2b, the atomic-level stress for a single representative atom is shown. The fluctuation around the best-fit sine function is much greater than that for the system, which was averaged over 4,000 atoms. However, the clear oscillatory nature is evident in the figure. Curves such as the one shown were computed for each atom. An example Fourier transform for an individual atom is shown in Fig. 3.2c. The largest peak at 0.02 THz corresponds to the principal response to the strain, whereas other components are thermal and mechanical noise.

The calculation of atomic-level phase shift and amplitude allows for insight into the atomic-level viscoelastic response.

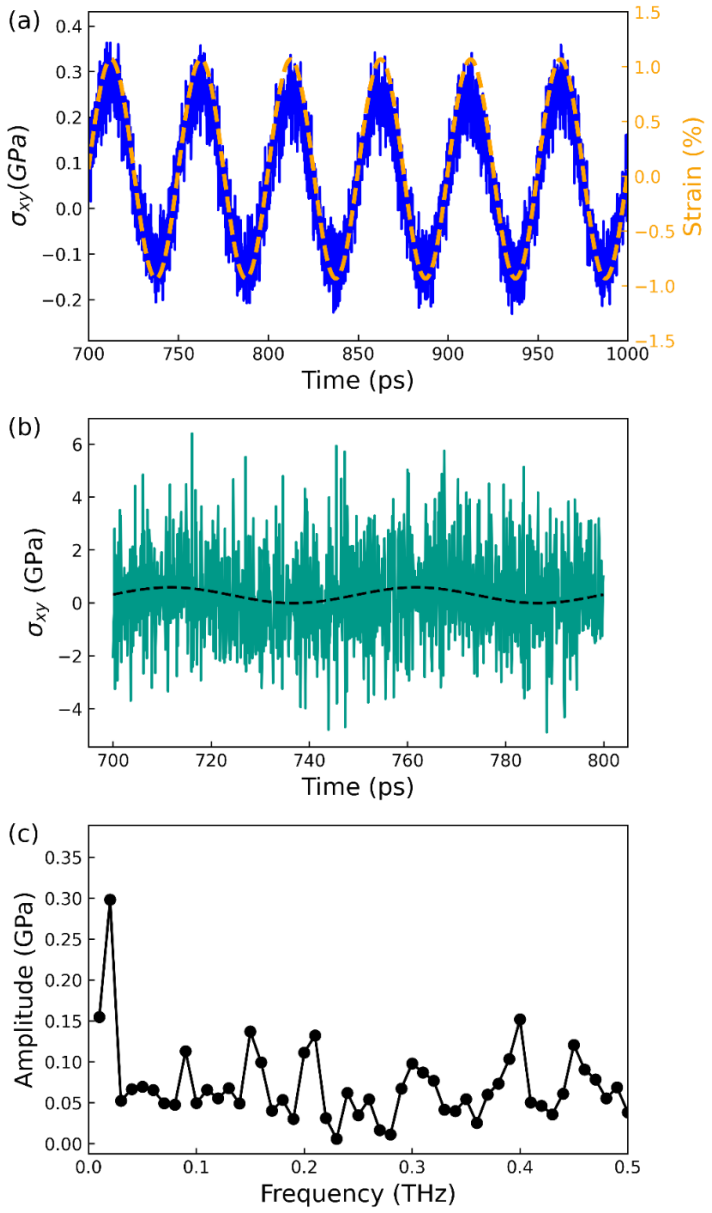

Fig. 3.2 Shear stress and strain over 6 cycles of sinusoidal straining (b) Atomic level shear stress (teal) of an individual atom with sinusoidal fit (black dashed) calculated by Fourier transform. (c) Atomic level shear stress amplitude vs. frequency from Fourier transform. The clear peak from the sinusoidal strain is seen at 0.02 THz.

Fig. 3.3a shows a representative distribution of atomic level phase shift for all atoms from 700 ps to 800 ps which covers two cycles in the middle of the production simulation and after possible effects of equilibration of initial sinusoidal strain. The atomic-level phase shifts have a wide distribution from $-\pi$ to π and reveal a complex atomic-level viscoelastic response that exists in glass. Based on analogy with the bulk experiment, a phase shift of $\delta_{atom} \approx 0$ corresponds to an elastic response and an atom with phase shift $\delta_{atom} \approx \frac{\pi}{2}$ would be lossy. The distribution of atomic-level phase shifts shows a peak in the elastic response ($\delta_{atom} \approx 0$) and with local maximum at $\delta_{atom} \approx -\pi, \pi$ and minima at $\delta_{atom} \approx -\frac{\pi}{2}, \frac{\pi}{2}$. Taking the partial stress and excluding 5% of the atoms from certain regions shows the role of each group of atoms on the phase shift and thus energy dissipation. These partial stress calculations centered at $\delta_{atom} = -\frac{\pi}{2}, 0, \frac{\pi}{2}, \pi, -\pi$ from the atomic phase distribution, shown in Fig. 3.3a with different colors. Seen in Fig. 3.3b are the calculated phases shifts from partial stress over the 15-time blocks of 100 ps arranged sequentially. It is clearly shown that the removal of 200 $\delta_{atom} \approx 0$ atoms, represented by orange crosses have little to no impact on the system phase shift as expected. These atoms are mostly elastic and contribute to the central peak in the distribution. On the opposite end, removal of 200 $\delta_{atom} \approx \frac{\pi}{2}$ atoms, depicted by green stars results in a significant reduction of the phase shift of the partial stress indicating their role in causing energy dissipation. The exclusion of the group of atoms with $\delta_{atom} \approx -\frac{\pi}{2}$ causes the partial stress phase shift to increase. The 'out of phase' atoms with $\delta_{atom} \approx \pi, -\pi$ have minimal impact on system phase shift. The group composed of 5% of atoms with phase shift around $\delta_{atom} \approx \frac{\pi}{2}$ has the greatest impact on reducing the partial stress phase shift and thus can be identified as the main contributors to NCL. A validation that the average phase of the most lossy atoms is $\delta_{atom} \approx \frac{\pi}{2}$ can be seen in Fig. 3.4. To confirm our results of phase shift reduction, the loss modulus was also calculated using the same groups of excluded atoms as seen in Fig. 3.3a. We see the same trends as in Fig. 3.3b, indicating that the phase shift is an accurate indicator of loss modulus.

Fig. 3.3 (a) Representative phase shift distribution of all atoms during 700-800 ps with shaded regions of interest that were examined. Nearly elastic atoms make up the central peak, the small populations of atoms at $\delta_{atom} \approx -\frac{\pi}{2}, \frac{\pi}{2}$ are shown to have a large impact on the viscoelastic response of the system (b) Partial phase shift from excluding differing groups of atoms by atom phase. Green stars: $\delta_{atom} \approx \frac{\pi}{2}$, Black circles: System phase shift with no reduction. Orange cross marker: $\delta_{atom} \approx 0$, Red diamond marker: $\delta_{atom} \approx -\pi, \pi$, Blue squares: $\delta_{atom} \approx -\frac{\pi}{2}$. Atoms around $\delta_{atom} \approx \frac{\pi}{2}$ clearly have the greatest contribution to phase shift when compared to the other three groups examined. (c) Loss modulus of respective groups after calculating partial phase shift. The same trend is observed as in the reduced phase shift indicating that using phase shift as a proxy for loss establishes the same trends in mechanical energy dissipation.

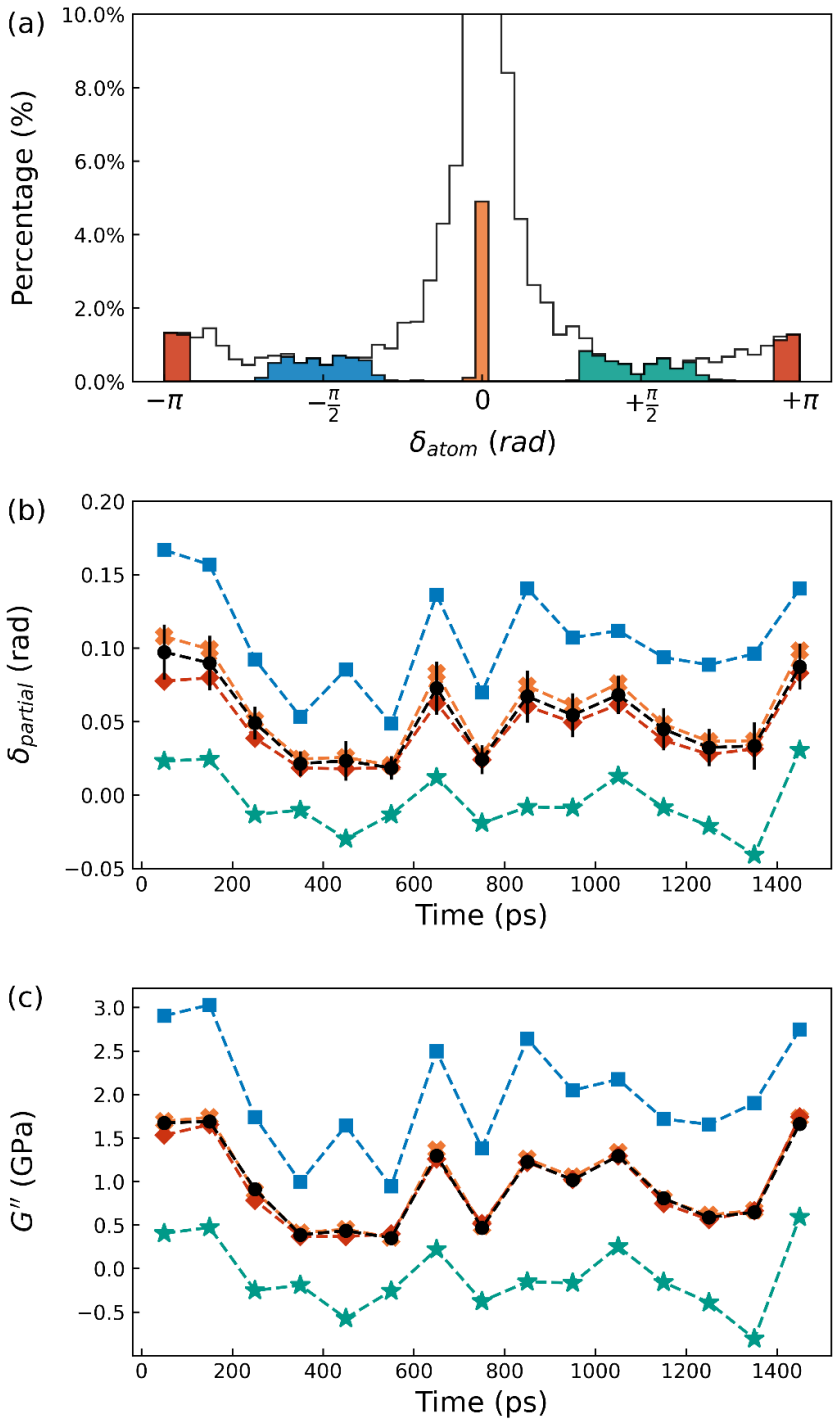

Fig. 3.3 continued

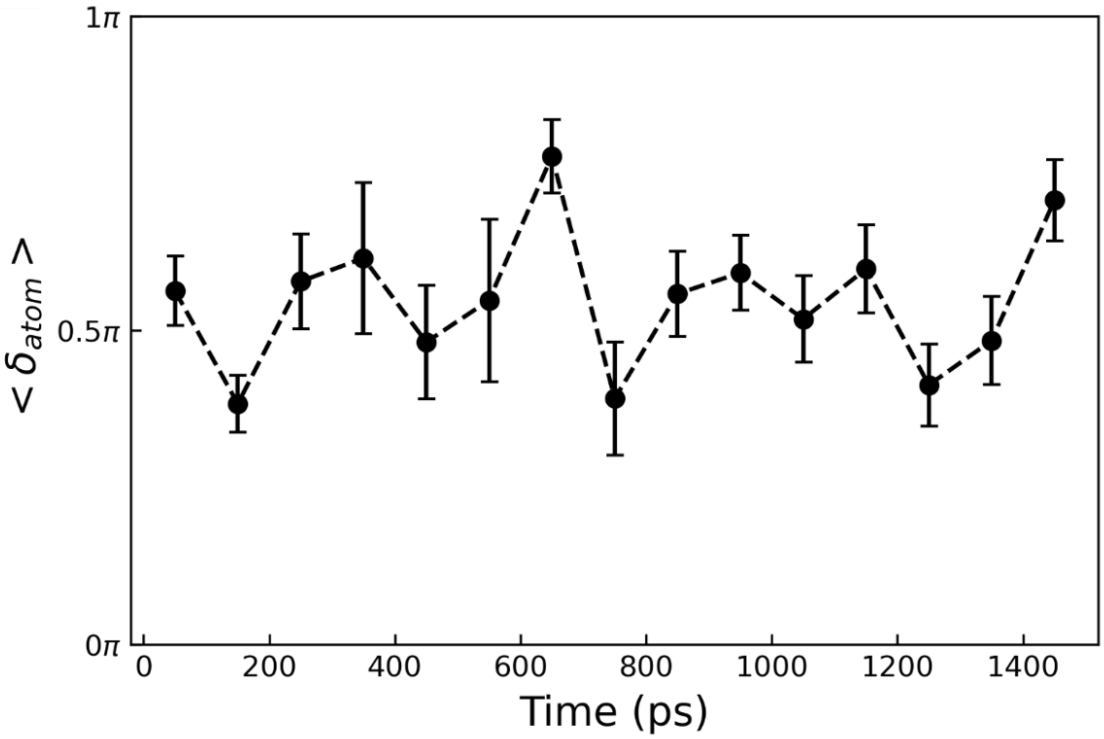

Fig. 3.4 Average phase shift of group of 200 atoms (5% of system) which when were excluded from atomic stress summation led to the largest decrease in the system phase shift. We demonstrate that atoms of the same approximate atomic-level phase shift are responsible across all cycles. Error represents standard deviation in atomic-level phase shift distribution of the 200 atoms selected.

We observe that loss modulus is effectively negligible when removing 200 $\delta_{atom} \approx \frac{\pi}{2}$ atoms, suggesting that we have successfully identified nearly all atoms responsible for nearly constant loss relaxation. These results further show that the atomic-level responses are strongly heterogeneous at any instant in time. Whereas a large portion of atoms show basically elastic response, a fraction of atoms behaves in a varied complex manner. The observed system-level energy dissipation results from contributions of individual atoms undergoing both energy loss and energy gain.

Transient Nature of Atomic Characteristics

We now examine the temporal behavior of atoms responsible for NCL relaxation. Fig. 3.5 shows how the nature of a group of atoms which had the initial phase shift, $\delta_{atom} \approx \frac{\pi}{2}$,evolves with time. As seen here atoms causing NCL during 700-800 ps have a distribution shown in Fig. 3.5a, but in the next 100 ps (Fig. 3.5b) they show widely distributed phase shifts, which resemble the system distribution except for a high phase group between $\delta_{atom} \approx [\frac{\pi}{2}, \pi]$. This rapid change of the phase distribution shows that after participating in NCL, lossy atoms have an atomic-level viscoelastic response distribution that represents a major change in viscoelastic response of the previously lossy atoms. Finally, these lossy atoms have their atomic-level phase shift δ_{atom} at the end of the simulation in Fig. 3.5c where the distribution still shows that these atoms are not principally involved in the loss. This may also be seen in Fig. 3.6 where the average phase distribution of the most lossy atoms is shown followed by the average phase distribution of the same group 2 cycles later. This surprising result shows that characterizing a single group of atoms at a fixed time as the origin of NCL relaxation is misleading and the transient nature is an important factor for considering the atomic-level mechanism of relaxation.

A spatial visualization of the atoms that cause NCL during 700-800 ps is seen in Fig. 3.7 as the blue atoms, this shows a spatial snapshot of the lossy atoms in the middle of the time block (2 cycles of straining) where the lossy atoms were identified. To look for obvious spatial correlations between lossy atoms, this same procedure was done for the next two cycles 800-900 ps and these lossy atoms are colored in red seen in Fig. 3.7. The visualization shows little overlap in the two groups of atoms causing the NCL relaxation.

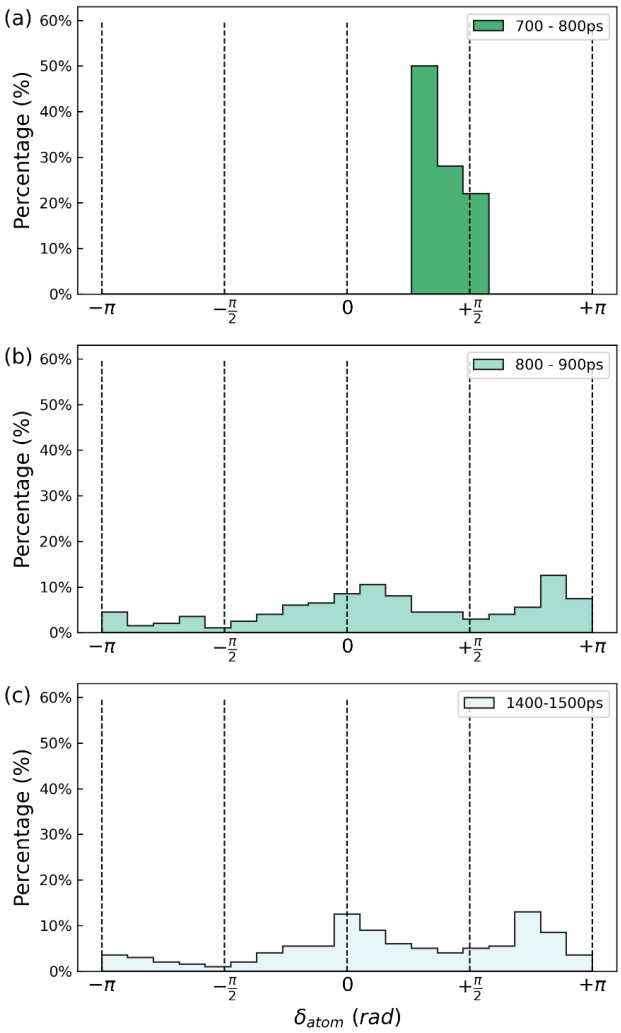

Fig. 3.5 The fast decay of the atomic phase distribution of NCL atoms from 700-800 ps. (a) Phase shift distribution of NCL causing atoms during 700ps-800ps. (b) Phase shift distribution of same set of atoms during 800ps-900 ps. (c) Phase shift distribution of same set of atoms in last 100 ps of simulation. Once NCL atoms are involved in a relaxation the distribution quickly decays to resemble representative phase shift distribution with a high phase group of atoms.

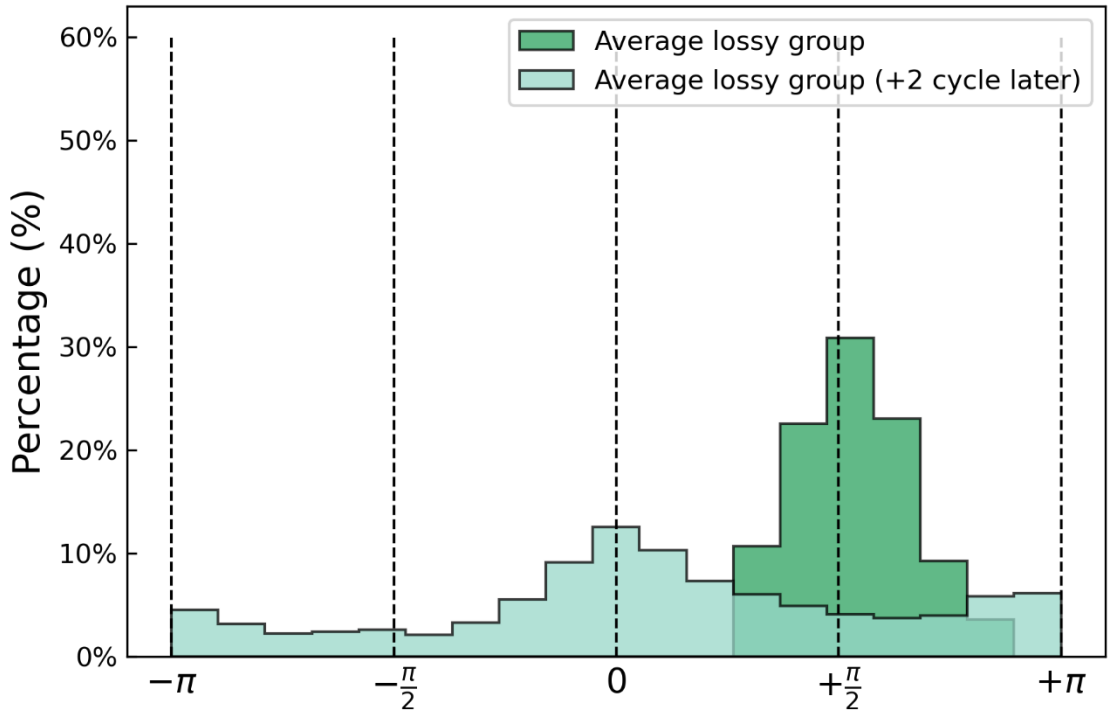

Fig. 3.6 Calculation of the averaged phase shift distribution of lossy atoms shows they have a drastically different phase, and most atoms no longer participate in the NCL relaxation. We show the phase shift distribution of the atoms causing the highest loss in dark green which is averaged. We calculated the phase shift of these same lossy atoms 2 cycles later and average them to produce the distribution in light green.

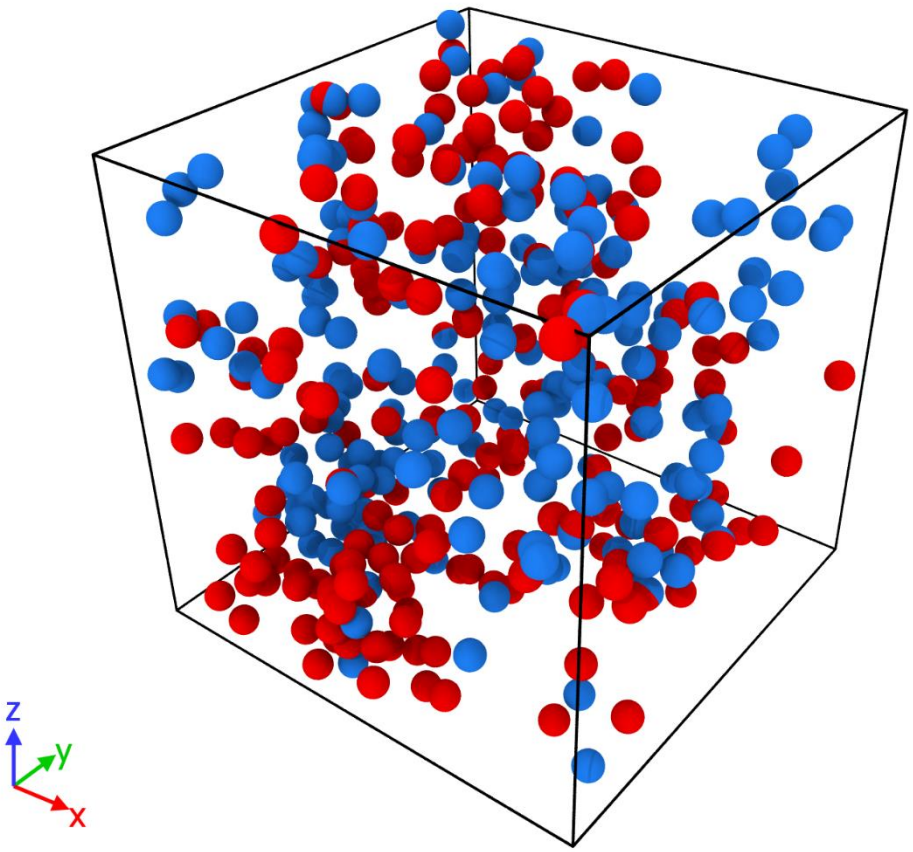

Fig. 3.7 Visualization of 200 atoms responsible for NCL mechanical loss from 2-time chunks (each time chunk has 2 cycles of sinusoidal straining). Blue: NCL causing atoms 700-800 ps. Red: NCL causing atom 800-900 ps. There is no obvious evidence of spatial aggregation but a homogenous distribution, additionally there are no obvious spatial correlations between the two time chunks.

The spatial distribution appears homogenous with no local aggregation as opposed to string-like distributions seen related to β relaxation [44,105]. There also does not appear to be a spatial correlation between regions of previous relaxation and subsequent atoms responsible for NCL. The spatial visualization confirms our results that the NCL relaxation evolves in time by involving different groups of atoms, this shows the stochastic nature of the atomic-level mechanism of NCL.

Subtle Nature of Nearly Constant Loss (NCL)

We performed further analysis to characterize the intrinsic nature of atoms responsible for NCL relaxation in terms of various factors which have been used in literature, including non-affine displacement, atomic-level shear stress, atomic-level volume, and coordination number. These results are summarized in Table 1**.** Non-affine displacements were calculated in between cycles during which no straining was occurring, in a similar fashion to Wang et. al [93] as the following equation; $u(\Delta t = t_p) = \|\vec{r}(t_0 + \Delta t) - \vec{r}(t_0)\|$ where t_p is the period of sinusoidal straining.

In a defect view, the NCL relaxation is caused by local regions of low density, high atomic-level stresses, or over/under coordination of neighbors. By calculating the averages and variances of atomic properties for the atoms causing NCL at the beginning and end of the time blocks and comparing to the system averages we attempt to ascertain if local property changes are related to NCL relaxation. We find that the atomic properties of the set of atoms causing NCL versus the system to show negligible differences which may be seen in Table 1.

Prior works investigating structural relaxation during sinusoidal straining have calculated non-affine mean squared displacement to determine mobility [93,106] and relate the mechanism of structural relaxation to the fastest non-affine atoms. We, therefore, calculated the non-affine displacements for every 100 ps which corresponds to 2 cycles of sinusoidal straining to understand the mobility of NCL causing atoms with $\delta_{atom} \approx \frac{\pi}{2}$. The results of the distribution are shown in Fig. 3.8 for all atoms in the system compared to atoms causing NCL relaxation. In the logarithmic scale on the y-axis, we can observe that NCL atoms have a tail of slightly larger non-affine displacements and overall have a broad distribution of non-affine displacements but on average are not more mobile as seen in the non-affine displacement value in Table 1.

Table 1 Variance and averages for σ_{xy}: atomic level stress shear,N_c: coordination number,v_i: atomic level volume. There are shown to be no substantive difference between NCL properties and system ensemble. Error calculated by block averaging.

	NCL Atom Group	System
$Var[\sigma_{xy}](GPa^2)$	12.04 ± 0.55	11.54 ± 0.06
$Var[N_c]$	1.59 ± 0.15	1.6 ± 0.0
$< N_c >$	11.24 ± 0.09	11.35 ± 0.0
$Var[V_{atom}](Å^6)$	3.28 ± 0.25	3.37 ± 0.01
$< V_{atom} > (Å^3)$	15.88 ± 0.13	15.89 ± 0.0
$< D(non-affine) > (Å)$	0.30 ± 0.17	0.28 ± 0.15

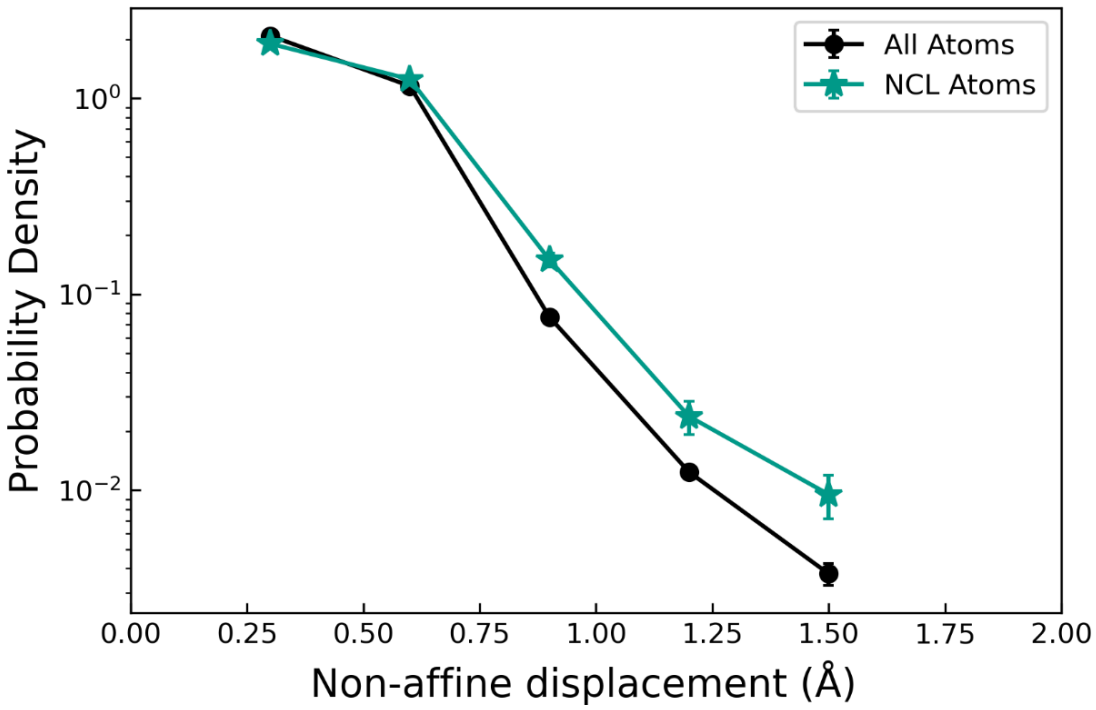

Fig. 3.8 Circles: Probability density of non-affine displacement for all atoms. Stars: Probability density of non-affine displacement for 200 atoms causing NCL averaged across all cycles. Atoms causing NCL mechanical loss have a wide range of displacements with slightly higher mobility on average. No evidence of preferred jumps or ranges of displacement is seen. Error bars calculated by standard deviation of distribution.

Discussion

Understanding the NCL relaxation is difficult due to lack of characteristic peak in temperature dependence. Because there are no direct experimental measurements of NCL relaxation length scale to shed light on the nature of the dynamics, simulations [98] and theory [94] are the only tools to provide insight into the atomic level dynamics of NCL. To identify atoms responsible for relaxation during MD-DMS, we calculated the DMS phase shift for each atom and identified the group of atoms with an atomic-level phase shift of $\delta_{atom} \approx \frac{\pi}{2}$ to be primarily responsible for NCL. On the other hand, the group of atoms at $\delta_{atom} \approx -\frac{\pi}{2}$ have a 'stabilizing' type effect in that their exclusion from partial stress resulted in an increase in the apparent mechanical loss. These atoms may have had stored energy prior to deformation and released the energy during deformation, thus resulting in negative phase shift. Atoms with no mechanical loss which are in the central peak of atomic phase shift in Fig. 3.3a account for roughly 80% of all atoms at any given time. The fraction of the atoms which have a high atomic-level phase shift representing inelastic response, is around 20% of all atoms and is consistent with measurements of liquid-like atoms measured by x-ray scattering [107].

Having identified the atoms causing NCL as those with an atomic-level phase shift of $\delta_{atom} \approx \frac{\pi}{2}$, we examined the nature of the atoms which show high levels of atomic-level energy dissipation. Whereas shear transformation zones (STZ) have been attributed to loosely packed regions [34] and loosely packed regions are also thought to be related to fast relaxation processes in $Cu_{65}Zr_{35}$ metallic glass [98], there are no differences in the distribution of atomic-level properties of the system vs. lossy atoms causing NCL. The lack of difference of atomic-level volumes suggests that NCL is also not due to local free volume fluctuations that have previously been related to structural relaxation [32,108] or due to local structural defects that can be calculated by atomic-level stress [30]. While we have looked at several structural indicators that may be linked to defects in the structure, the differences in lossy atoms from a structural point of view may be more subtle and thus not found by our measures.

The mean non-affine displacements measured as seen in Fig. 3.8 show the comparison between all atoms and atoms causing NCL which are only slightly more mobile. The low temperature peak (LTP) found in a metallic glass $Cu_{50}Zr_{50}$ system via MD-DMS technique was

linked to "reversible atoms (RAs)" with maximum non-affine displacements $u'_{max} \in [1\ \text{Å}, 2\ \text{Å})$ [93] and Yu et al. [46] related "faster atoms" to internal friction in a metallic glass $Cu_{65}Zr_{35}$ system where these "faster atoms" had displacements larger then $u* = {}^{r_0}/_{2} = 1.4$ Å; however, in our case no such groupings of mobility were found to be linked to the NCL relaxation**.** Additionally, there was no evidence that fast-moving atoms were solely responsible for NCL. These observations suggest a different mechanism for NCL relaxation compared to the proposed mechanism of β relaxation where string-like motion by a small proportion of highly mobile atoms causes structural relaxation [44].

An important characteristic of NCL is its transient nature. We found that after energy dissipation that is indicated by $\delta_{atom} \approx \frac{\pi}{2}$ these lossy atoms moved to having a prototypical viscoelastic response as shown by the rapid change as shown in Fig. 3.5. Our finding is consistent with the observation that after a deformation event, atoms lose their memory of the initial state [42]. Along the pathway of moving from a saddle point to a valley in the potential energy landscape for liquids and glasses, saddle states show universal melting behavior wiping out prior thermal history of atomic configurations [109]. Spatial visualization of lossy atoms in Fig. 3.7 shows a lack of spatial overlap demonstrating no obvious spatial correlation with previous regions of NCL relaxation demonstrating a stochastic behavior.

The set-to-point technique has been used in previous simulation works where certain atoms are made to deform affinely [54,93] in order to understand how these atoms participate in dynamics and relaxation. However, this technique interferes with local dynamics and thus may not be used to investigate transience of the atomic-level mechanism of relaxation. Our technique of measuring atomic level loss through the Fourier transform of the atomic-level stress thus represents a non-invasive method of directly identifying atoms responsible for mechanical loss and their atomic-level viscoelastic behavior before and after the energy dissipation. The NCL relaxation appears to be qualitatively and quantitatively different from known β relaxation mechanisms in terms of the atomic-level origin and relationship to local defects. However, the transient behavior observed in NCL has yet to be investigated regarding the β relaxation.

Conclusions

By utilizing the unique combination of atomic-level stress and MD-DMS, we directly identified the group of atoms responsible for the NCL relaxation and have revealed the surprising transient nature of the microscopic mechanism. The diverse atomic-level viscoelastic response identifies four groups of atoms that participate in the system viscoelastic response with one group primarily contributing to NCL relaxation. Our results demonstrate that NCL is due to a population of atoms with $\delta_{atom} \approx \frac{\pi}{2}$ which have been visualized and look to be homogenously in the simulation cell. After participating in NCL, the $\delta_{atom} \approx \frac{\pi}{2}$ atoms move to atomic-level viscoelastic responses that have an atomic-level phase shift distribution resembling the system distribution. This observation is supported by evidence of saddle state melting behavior wiping the thermal history shown in previous literature [109]. The atoms belonging to the $\delta_{atom} \approx \frac{\pi}{2}$ group, however, show no fundamental differences in local atomic parameters, such as atomic-level shear stress, coordination number, and atomic volume. This may indicate NCL does not occur at local structural defects, such as free volume fluctuations, but may be a stochastic event. If there is some subtle structural origin to mechanical loss it was not seen in our investigations. Whether these observations regarding the transience and structural origin at the atomic level of NCL also apply to other mechanical deformation events at higher temperatures, such as β relaxation, remains to be seen.

CHAPTER FOUR RIPPLES IN THE BOTTOM OF THE POTENTIAL ENERGY LANDSCAPE OF METALLIC GLASS

This chapter has been adapted from an under review submission:
L. Zella, J. Moon, T. Egami, Ripples in the Bottom of the Potential Energy Landscape of Metallic Glass, *under review*

In the absence of periodicity, the structure of glass is ill-defined, and many structural states are found at similar energy levels. However, little is known about how these states are connected to each other in the potential energy landscape. We simulate mechanical relaxation by molecular dynamics for a prototypical $Cu_{64.5}Zr_{35.5}$ metallic glass and follow the mechanical energy loss of each atom to track the change in the state. We find that the energy barriers separating these states are remarkably low, only of the order of 1 meV, implying that even quantum fluctuations can overcome these potential energy barriers. Our observation of small rough ripples in the bottom of the potential energy landscape puts many assumptions regarding the thermodynamic states of metallic glasses into question and suggests that metallic glasses are not totally frozen at the local atomic level.

Introduction

The relationship between structure and dynamics in disordered matters such as liquids and glasses are immensely difficult to characterize. Conceptually, at least, these complex states and dynamics can be described through the potential energy landscape (PEL) [3,29,30,110]. When a liquid is cooled without a phase change into a crystal, it falls into a local minimum in the PEL and becomes a glass, trapped in a non-equilibrium state. Given sufficient thermal and mechanical energies, transitions from this local minimum to a new local minimum occur through activation and relaxation processes over energy barriers. Classical depictions of the PEL focus on basins and metabasins within a basin, with the α-relaxation to connect different basins and the β-relaxation to connect metabasins. Within the metabasin glasses are assumed to be 'frozen'. However, recent simulation [111,112] and theory [113] suggest a more complex picture. The basins and metabasins in the PEL form a hierarchical structure, allowing for a greater diversity of activation-relaxation

phenomena. Since these features in the PEL play a crucial role in the structure-property relationship in disordered matters, it is important to characterize features of the basins in the PEL and how they are inter-connected.

These features within the basins should manifest as relaxation processes which can be probed mechanically. The α-relaxation and β-relaxation have been extensively studied using standard mechanical techniques such as dynamic mechanical spectroscopy (DMS) [38,114] and atomic force microscopy [72–74]. In addition, an early simulation work [115] suggested that metallic glasses undergo atomic-level plastic deformation even below the yield point. Because every atom in metallic glasses has a different local environment, when a macroscopic strain is applied across the system, there arise non-uniform strains at the atomic-level [116]. Such non-uniform strains could result in locally plastic behavior even in the apparently elastic regime. This prediction is now supported by a growing body of experimental works showing atomic-level local deformation upon loading and low energy mechanical relaxation in the form of microscopic rearrangements below the yield point [107,116,117], and also by simulation works demonstrating microscopic rearrangements in the apparently elastic regime [115,118–120].

To probe the microscopic plastic behavior, we utilize molecular dynamics dynamic mechanical spectroscopy (MD-DMS) on a prototypical $Cu_{64.5}Zr_{35.5}$ metallic glass (T_g = 700 K). We apply uniform sinusoidal shear strains with the maximum amplitude of $\epsilon_A = 1.0$ % and 2.5 % and a period of 100 ps at temperatures from 0.1 K to 300 K and decompose the stress into atomic-level stresses to observe the atomic response to a mechanical perturbation. We perform a cycle-to-cycle analysis to determine the atomic-level phase shift of the atomic-level shear stress compared to the macroscopic strain and evaluate the atomic-level energy loss due to atomic rearrangements. We find that above 100 K, most lossy atoms identified in one shear deformation cycle convert to non-lossy behavior in the next cycle, demonstrating high transience of local atomic structure participating in mechanical relaxation. In contrast, at cryogenic temperatures lossy atoms are largely reversible. From this temperature dependence, we find the activation energy for local structural change to be quite small, only on the order of $E_A \approx 1$ meV. Given that this activation-relaxation is well below α and β relaxation, we ascribe this to the small ripples in the bottom of the basin in the PEL. Such ripples were largely overlooked in earlier studies, but they may be related to the nearly constant loss observed at low temperatures [37,121]. Additionally, we

estimate the magnitude of quantum fluctuations using the vibrational density of states. The zero-point energy is far above the energy barriers of the ripple, implying that quantum fluctuations easily connect multiple subbasins. Our results suggest that the system moves easily within the PEL basin through quantum fluctuations and thermal excitations and challenges many assumptions regarding the thermodynamic states of metallic glasses.

Methods

Molecular dynamics simulation

Classical molecular dynamics simulations were performed using the Large-scale Atomic/Molecular Massively Parallel Simulator (LAMMPS) [59] with a timestep of 1 fs using a $Cu_{64.5}Zr_{35.5}$ metallic glass with 16,000 atoms and a density of 7.84 g/cm^3. Each low temperature glass was made by a typical melt-quench method with melting at 3000 K for 1 ns. Four different cooling rates were used: 100 K/ps, 1 K/ps, 0.1 K/ps and 0.01 K/ps. The embedded atom method (EAM) potential was used to describe interatomic interactions [100] and periodic boundary conditions were imposed. The relaxed system was then sinusoidally sheared following similar protocols in the literature [45,46] with a sinusoidal strain of $\varepsilon(t) = \varepsilon_A \sin(\omega t)$, where t is time, $\omega = 2\pi/T_\omega$, a period $T_\omega = 100$ ps and two different maximum strains of $\varepsilon_A = 2.5\%$ and $\varepsilon_A = 1.0\%$ to compare impact of strain magnitude. Before collecting data, 30 training/equilibration cycles were done followed by another 30 cycles for data collection.

Atomic-level loss and lossy fraction

To characterize atomic-level viscoelastic response and identify atoms responsible for mechanical loss, we used atomic-level stresses [122,123] to decompose the system response into atomic-level components [82]. Atomic-level stresses are calculated in LAMMPS as follows:

$$\sigma_i^{ab} = \frac{1}{\Omega_i}\sum_j \left(f_{ij}^a r_{ij}^b + m_i v_i^a v_i^b\right) \quad (1)$$

where a and b are Cartesian components, Ω_i is the atomic volume of atom i, f_{ij}^a is the two-body force between atoms i and j, r_{ij}^a is the a component of the distance vector, r_{ij}, between atoms i and

j, and v_i^a is the a component of the velocity of atom i. Atomic-level volume is calculated by standard Voronoi tessellation [79]. We identify atoms responsible for mechanical loss by the Fourier transform [124] of the time dependent atomic-level shear stress response seen in Fig. 4.1a and Fig. 4.1b. Each atom has a corresponding phase shift ranging from $[-\pi, +\pi]$ and a representative distribution of the system is seen in Fig. 4.1c. In a previous work [82] we showed atoms with $\delta_{atom} \approx \frac{\pi}{2}$ as responsible for mechanical loss and thus we define 'lossy' atoms in this work as $\delta_{atom} \in [\frac{\pi}{4}, \frac{3\pi}{4}]$ and are represented by the hatched region in Fig. 4.1c. The temperature scaling of our results is not sensitive to the choice of the boundaries as shown in Fig. 4.2.

The lossy fraction represents the fraction of atoms identified as lossy in some cycle n which remain lossy some cycle $n + m$ later. This is calculated as follows:

$$\langle f_{lossy}(n, n+m)\rangle = \langle \frac{N_{lossy,remain}(n,n+m)}{N_{lossy}(n)} \rangle \quad (2)$$

Zero-point energy calculation

We estimate the effective zero-point motion temperature from the vibrational density of states (vDOS) given by the Fourier transform of the velocity autocorrelation function by the following equation:

$$g(\omega) = \sum_{m=1}^{3N_{atom}} \delta(\omega - \omega_m) = \frac{1}{k_B T} \int_0^\infty \sum_{n=1}^{N_{atom}} m_n \langle v_n(t) \cdot v_n(0) \rangle e^{i\omega t} dt \quad (3)$$

where N_{atom} is the number of atoms, m_n is the mass of atom n, $v_n(t)$ is the velocity of atom n at some time t, thus the quantity $\langle v_n(t) \cdot v_n(0) \rangle$ represents the autocorrelation function for atom n [125–127]. For better statistics, vDOS calculations were done using 5 different initial velocity trajectories at 0.1 K. A plot of the vDOS is shown by Fig. 4.3. The effective temperature of the zero-point motion energy, T_{ZPE}, can then be approximated from the vibrational density of states by:

$$E_0 = \int \frac{1}{2} \hbar\omega \, g(\omega) d\omega = 3N_{atom} k_B T_{ZPE} \quad (4)$$

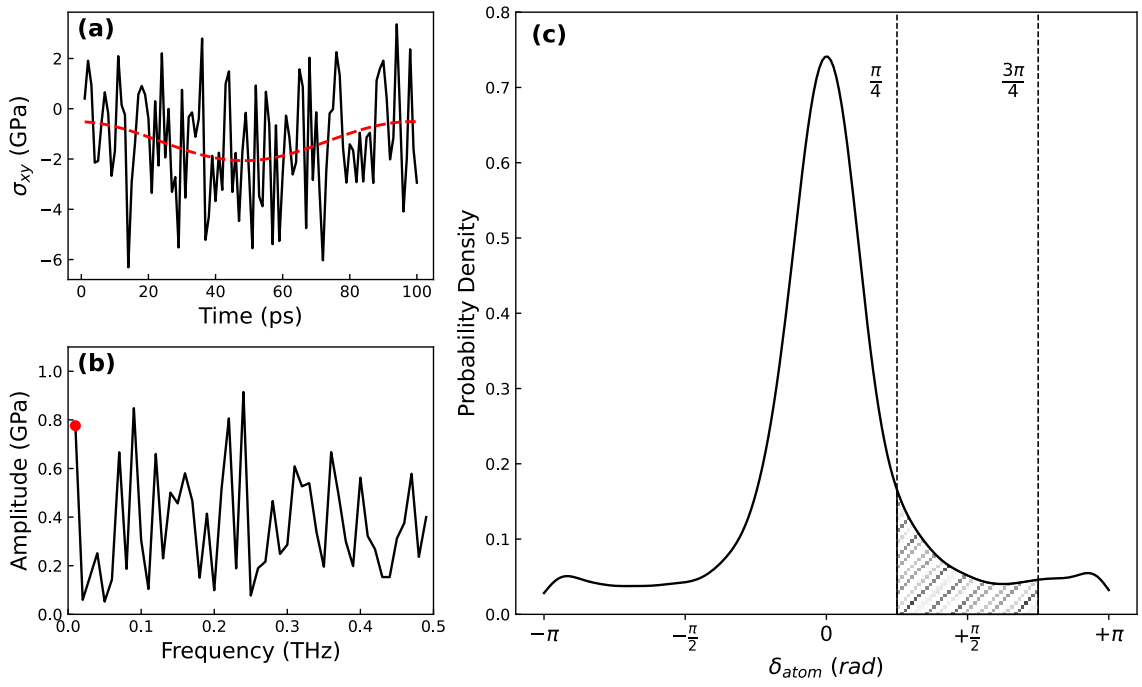

Fig. 4.1 Method for calculating atomic-level phase shift in frequency space and the resulting distribution of atomic-level phase shift at 300 K for the slowest cooling rate of 0.01 K/ps. (a) Atomic-level shear stress of a lossy atom with red dashed line representing amplitude and phase shift of atom calculated by Fourier transform. (b) Amplitude response in frequency representation of atomic-level shear stress with red data point representing the sinusoidal shearing frequency. (c) Atomic-level phase shift (δ_{atom}) distribution for all atoms from 1 cycle at 300 K. The hatched area within dashed lines indicates the bounds of the definition for lossy atoms.

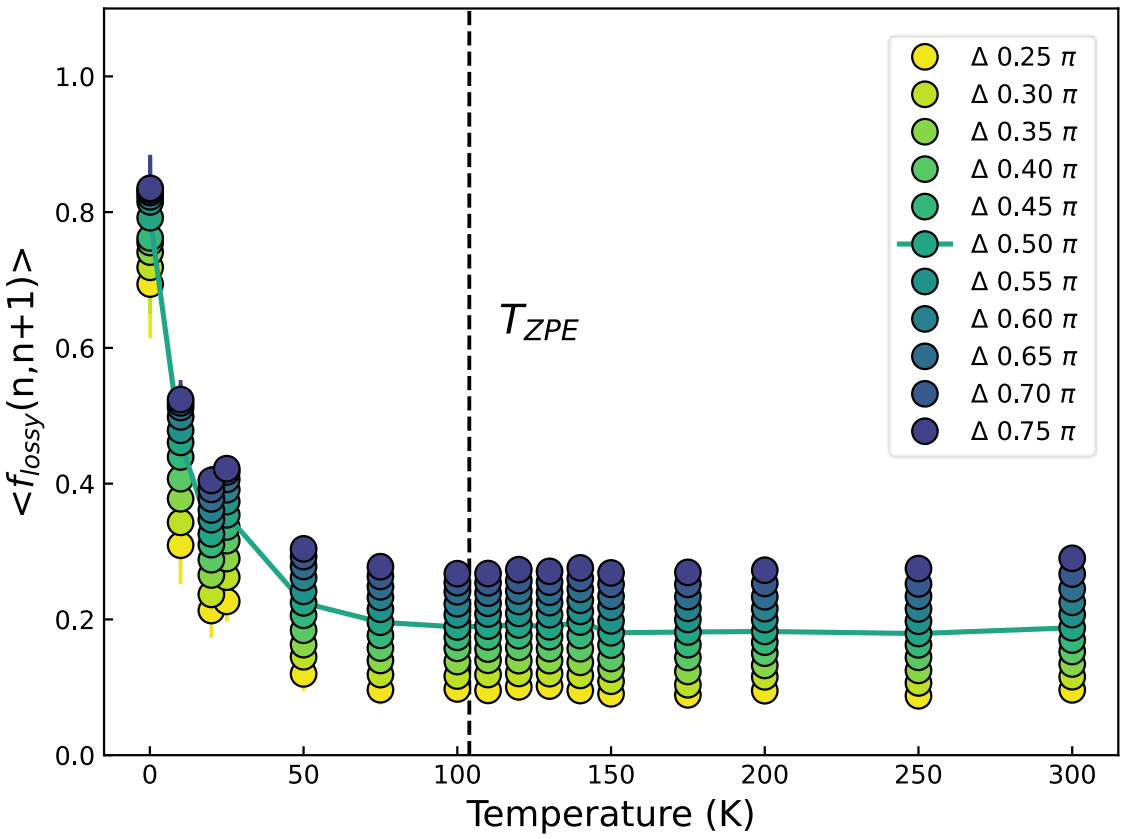

Fig. 4.2 Cycle-to-cycle transience for 0.01 K/ps with a variety of widths for the bounds that define lossy atoms. Solid line indicates the definition chosen for our work.

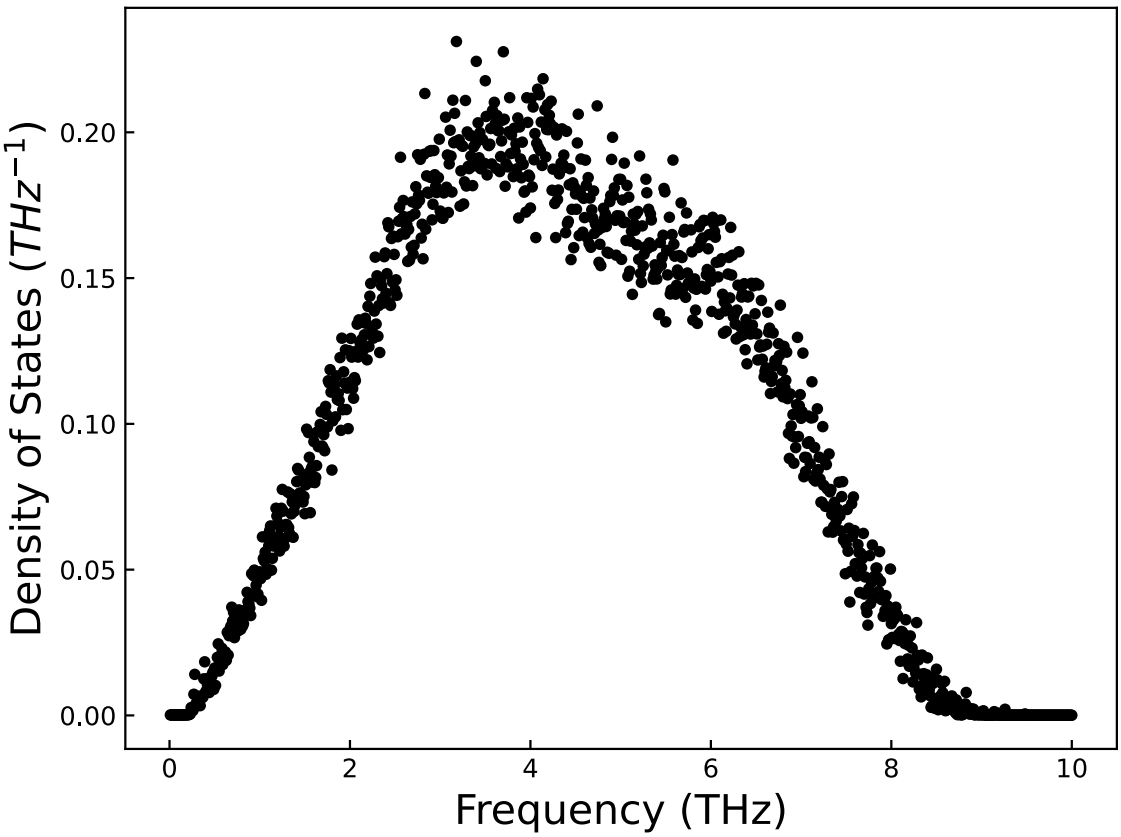

Fig. 4.3 Averaged vDOS from 5 different velocity trajectories with area normalized to 1.

Results

Lossy atom distribution

In an earlier study we have demonstrated that individual atomic-level shear stresses reveal the subset of atoms in the system responsible for the mechanical loss in a single cycle of shear strain [82]. From the atomic-level shear stress response in frequency space (Fig. 4.1a-b), we estimate individual atomic-level phase shift δ_{atom}, which corresponds to the atomic-level mechanical loss. The calculated δ_{atom} for all atoms over a single cycle of shear strain shows a symmetric distribution of atomic-level phase shift (Fig. 4.1c). We define atoms directly involved in the mechanical loss during the strain cycle by an atomic-level phase of $\delta_{atom} \in [\frac{\pi}{4}, \frac{3\pi}{4}]$. These lossy atoms are shown in the cross-hatched region in Fig. 4.1c. The identification of the phase of lossy atoms during mechanical loss was shown in a previous work [82].

By examining if atoms identified as lossy between a cycle (the cycle *n*) are still lossy in the subsequent cycle (the cycle *n* + 1) we can study how reversible the mechanical loss is. We find that the result strongly depends on temperature, but not much on cooling rate. We see that at cryogenic temperatures (0.1 K), the distribution of $\delta_{atom}(n+1)$ of lossy atoms as shown in Fig. 4.4, remains centered around $\delta_{atom} \approx \frac{\pi}{2}$, indicating most lossy atoms remain lossy. Thus, at this temperature lossy atoms mostly remain lossy. However, the distribution of $\delta_{atom}(n+1)$ changes dramatically with a relatively small increase in temperature, with the main peak at $\delta_{atom} \approx \frac{\pi}{2}$ decreasing rapidly and creating a distribution more akin to those of the whole system, centered around $\delta_{atom} \approx 0$, as seen in Fig. 4.1c. This rapid change represents a change from mostly reversible mechanical loss at very low temperatures to irreversible/transient mechanical loss at elevated temperatures. Above about 50 K atoms, identified as lossy, are more likely to be part of the elastic peak at $\delta_{atom} \approx 0$ in the next cycle. Comparing these temperature dependent trends across multiple cooling rates represented in Fig. 4.4a – d. shows minimal differences over the four decades of cooling rates used.

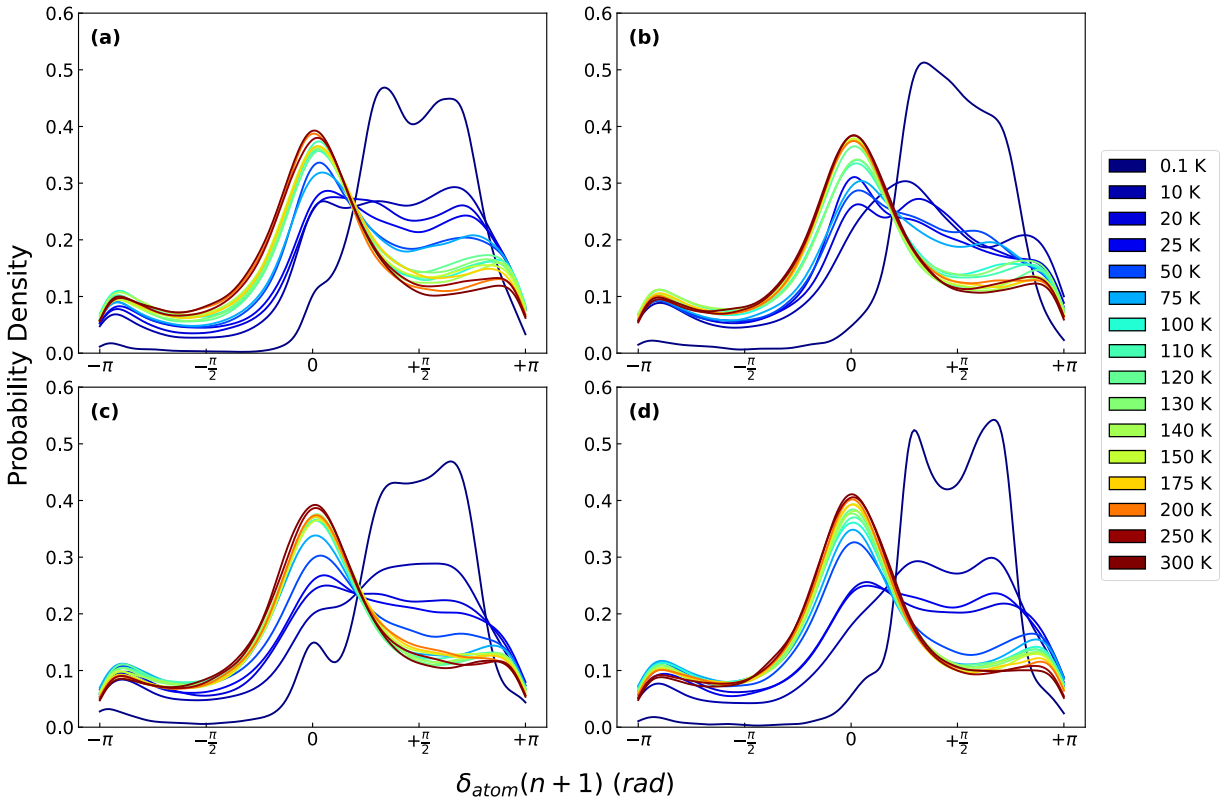

Fig. 4.4 Lossy atom phase shift distribution after 1 cycle after initial identification of lossy atoms at the strain of 2.5%. It is shown that at low temperatures, the mechanical relaxation is mostly reversible with lossy atoms remaining lossy (that is with $\delta_{atom} \approx \pi/2$). As temperature increases, the distribution more closely resembles that of the distribution of all atoms for all cooling rates at (a) 100 K/ps, (b) 1 K/ps, (c) 0.1 K/ps, and (d) 0.01 K/ps.

Temperature dependence of lossy fraction

To understand the evolution of lossy atoms over many cycles, we calculate the fraction of lossy atoms which remain lossy after identification as $\langle f_{lossy}(n, n+m)\rangle$ (see Eq. 2 in Methods section). The calculation of the fraction of lossy atoms that remain lossy for up to 9 cycles later and across a variety of temperatures and cooling rates is shown in Fig. 4.5. The $\langle f_{lossy}\rangle$ fraction starts at 1 for $m = 0$, that is the cycle when lossy atoms were identified. After the cycle where the lossy atoms are identified, there is a large drop in the fraction with increasing temperature. Interestingly this does not decay much as a function of number of cycles later ($m = 2 - 9$), apart from the highest cooling rate which shows a slight decay in intermediate temperatures (10 K − 75 K) seen in Fig. 4.5a.

For all cooling rates, $\langle f_{lossy}\rangle$ at 0.1 K remains high at around 0.7 even up to 9 cycles later, indicating lossy atoms remain largely lossy in a highly reversible, non-transient manner. Remarkably, the $\langle f_{lossy}\rangle$ fraction is rapidly reduced by the increase in temperature until reaching a plateau of $\langle f_{lossy}\rangle \approx 0.2$ at around 100 K. This represents a characteristic change in mechanical loss from highly reversible and non-transient at low cryogenic temperatures to highly transient at temperatures above 100 K. In order to study the role of strain magnitude, we plot the $\langle f_{lossy}(n, n+1)\rangle$ for just one cycle after identification at a shear strain of $\epsilon_A = 2.5$ % and $\epsilon_A = 1$ %, both of which are in the elastic regime macroscopically as shown in Fig. 4.6. The plot of $\langle f_{lossy}(n, n+1)\rangle$ in Fig. 4.7. clearly shows the same massive decrease in the lossy fraction as a function of temperature for both strain magnitudes. Interestingly, for the lower strain magnitude, we observe that the temperature dependent transition to the plateau occurs at a lower temperature. To further confirm if the large drop in lossy fraction was mostly after the first cycle, we also calculated $\langle f_{lossy}(n, n+9)\rangle$, that is the fraction of lossy atoms that remained lossy 9 cycles later seen in Fig. 4.8 which largely demonstrates the same trend.

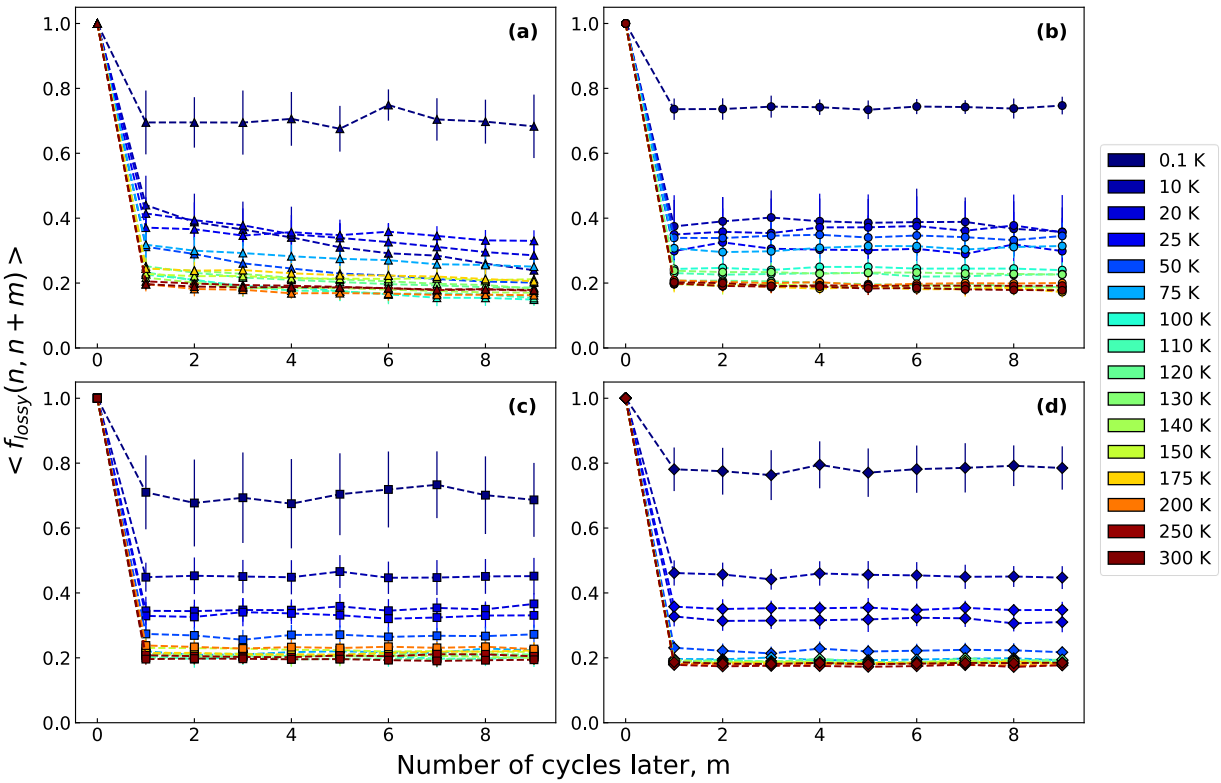

Fig. 4.5 The average fraction of lossy that remain lossy using a strain of 2.5 %, $\langle f_{lossy}(n, n+m)\rangle$, where m is the number of cycles later from cycle of identification n. Data is averaged from 20 cycles with error bars representing the standard deviation. This is done for a variety of cooling rates at (a) 100 K/ps, (b) 1 K/ps, (c) 0.1 K/ps, and (d) 0.01 K/ps.

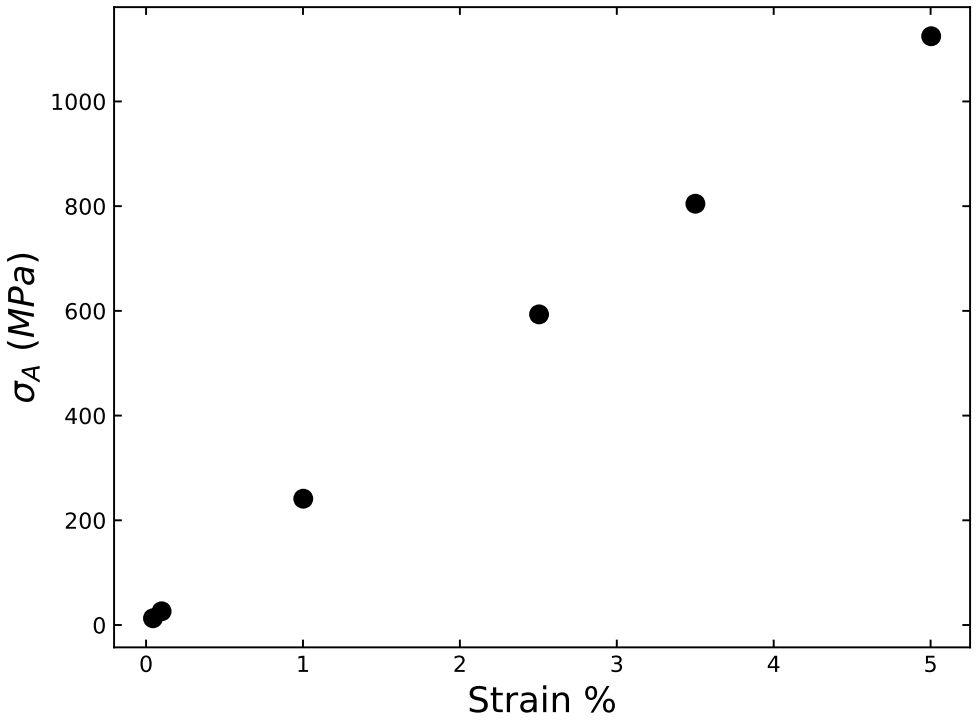

Fig. 4.6 Shear strain magnitude vs. shear stress response. Figure shows the linear stress-strain region.

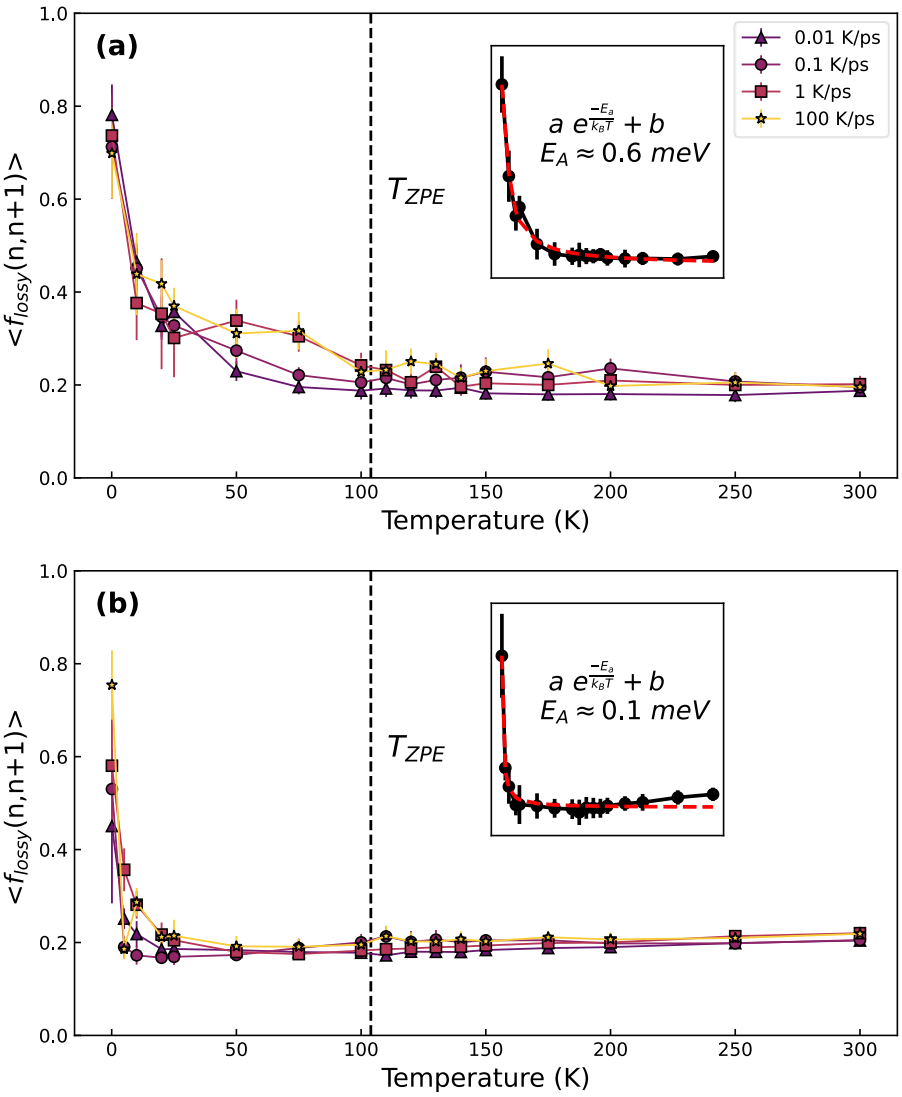

Fig. 4.7 Lossy fraction $\langle f_{lossy}(n, n+m)\rangle$ for various cooling rates demonstrating the rapid transition from mostly reversible to mostly irreversible mechanical loss using (a) $m = 1$ (one cycle later) at the strain of 2.5% with inset figure showing exponential fit and (b) $m = 1$ (one cycle later) at the strain of 1%. For both strains, a rapid transition from low transience where lossy atoms mostly remain lossy to high transience is shown with emerging plateau at high temperatures. The dashed line represents the effective zero-point energy temperature which is in the region of high transience. Inset figure show exponential fit to the slowest cooled system of 0.01 K/ps and gives the calculated activation energy.

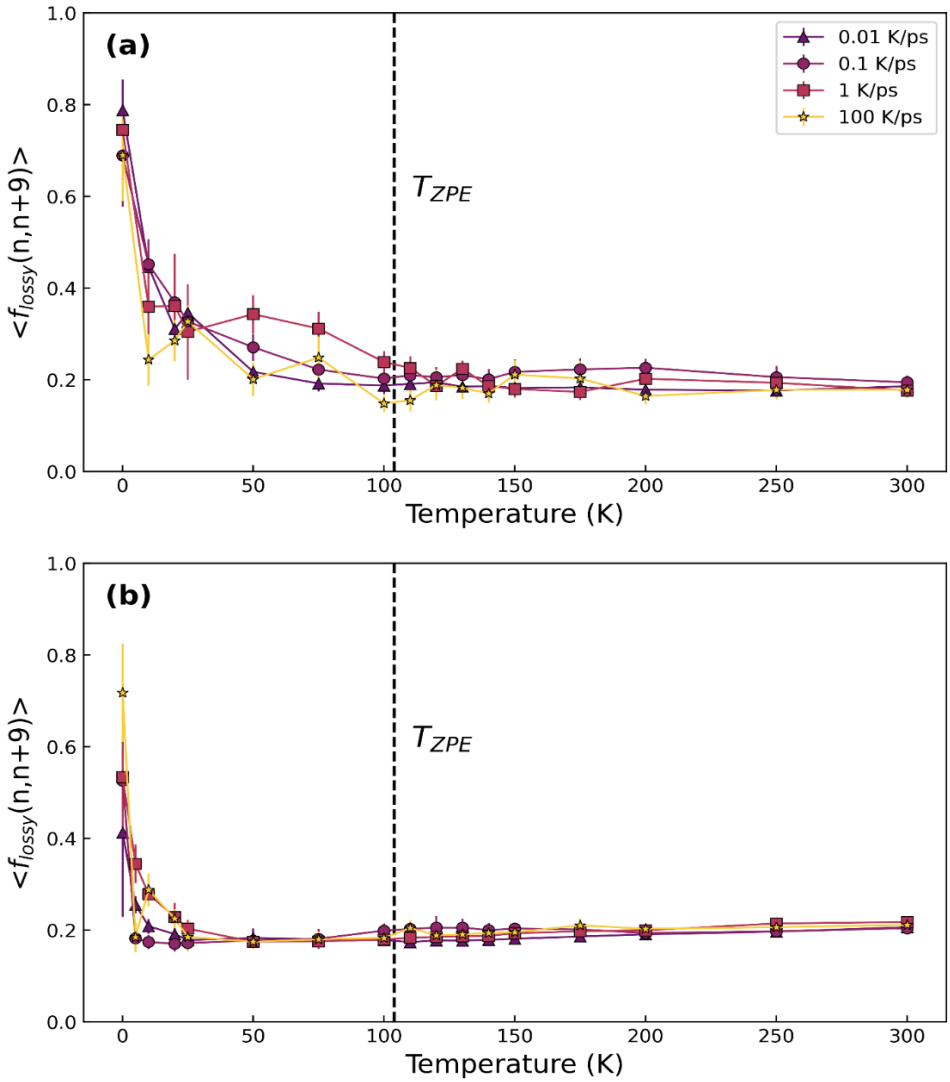

Fig. 4.8 Lossy fraction $\langle f_{lossy}(n, n+m)\rangle$ for various cooling rates using $m = 9$ (nine cycles later) at a strain of (a) 2.5% and (b) 1%. For both comparisons a rapid transition from low transience where lossy atoms mostly remain lossy to high transience is shown with plateau emerging earlier for the 1% results. The dashed line represents the effective zero-point energy temperature which is in the region of high transience.

To characterize the temperature dependence of the lossy fraction, we fit an exponential function as $\langle f_{lossy}(n, n+1)\rangle \approx ae^{-\frac{E_A}{k_B T}} + b$ to calculate the activation energy of the atomic rearrangements related to the change in mechanical loss. We find an activation energy of $\mathrm{E_A} \approx$ 0.6 meV at $\epsilon_A = 2.5$ % and $\mathrm{E_A} \approx 0.1$ meV at a strain of $\epsilon_A = 1$ %, with fit seen in the inset Fig. 4.7a-b for the slowest cooling rate. These activation energies are significantly smaller than the typical β relaxation in metallic glasses which is more on the order of 1 eV [47,50]. From the use of two different strain magnitudes, we observe a similar rapid change from reversible to mostly irreversible and transient mechanical relaxation for two different strain magnitudes.

As this rapid change in mechanical loss happens at low temperatures with such low activation energies, one wonders if quantum mechanical zero-point fluctuation is sufficient to overcome such small barriers. Utilizing the vibrational density of states (vDOS) of the system calculated at 0.1 K we estimate effective temperature of the zero-point motion, T_{ZPE} to be ~104 K and is indicated in Fig. 4.7 as the dashed vertical line. For both strain magnitudes, T_{ZPE} is large enough to be in the region of low mechanical reversibility. This implies that zero-point fluctuation is enough to overcome these ripples in the PEL, and the reversible loss will not occur in reality.

Discussion

The transition we observe in the $\langle f_{lossy}(n, n+1)\rangle$ fraction as a function of temperature shows that only at very low temperatures and in classical simulation mechanical relaxation occurs within mostly the same groups of atoms and thus is highly reversible. At higher temperatures or if the quantum effect is included, mechanical relaxation occurs through new groups of lossy atoms each cycle, thus characterized as irreversible. As thermal energy increases, so does the accessible relaxation processes in the PEL, this leads to transience which is consistent with the view of the PEL describing the 'valleys' of the PEL not as smooth, but rough [113,128]. The complex, fractal-like nature of the PEL basin was shown by Liu et al. [112] where an external shear to an atomistic simulation of a $Cu - Zr$ metallic glass created tortuous pathways for low-barrier activations in the PEL. The possibility of local rearrangements even deep in the glassy state is further supported by the freezing of medium range order but not of short range order in various metallic glasses [129].

It is interesting to note that the 'roughness' of the PEL allows for dynamics that are of lower energy [130,131] than α and β relaxations. This changes our view on the nature of mechanical loss; it is mostly stochastic and not reversible as is often assumed. By using two different strain magnitudes which have two different activation energies of around $\mathrm{E_A} \approx 0.6$ meV and $\mathrm{E_A} \approx 0.1$ meV, we are probing different parts of the PEL. If we assume that the activation energy is equal to the elastic energy due to the applied strain, $E_A \approx (GV/2)\varepsilon_A^2$, where *G* is shear modulus, *V* is the local volume of the object and ε_A is external shear amplitude, we find $V \approx 12$ Å^2, which is comparable to the atomic volume. Thus, this activation is achieved by the motion of a single atom. This is consistent with the observation that about 20% of atoms are liquid-like, and can easily be activated [81]. In Fig. 4.1a. the population of the lossy atoms with $\delta_{atom} \in [\frac{\pi}{4}, \frac{3\pi}{4}]$ is ~10%. After the first cycle it stays at about 20% from the second cycle at temperatures above 50K. This small increase must be a consequence of rejuvenation induced by cyclic deformation. During a deformation event, when the system reaches the saddle point in the PEL the configurational temperature is so high that locally a glass turns into a liquid [132]. When the system relaxes from the saddle point to the final state the process occurs quickly, in the timescale of 1 ps or less, so that locally liquid is rapidly quenched to a glass. This rapid local cooling results in a state with high fictive temperature, resulting in rejuvenation [133].

Conclusion

Plastic behavior in disordered solids has been extensively studied using athermal quasistatic simulations (AQS) [134,135]. In AQS, small strain steps are applied to glasses at 0 K followed by potential minimization moving the system to a local minimum in the PEL, mimicking the slow timescales of experiments. During these strain steps there will occasionally be plastic rearrangements which have been linked to 'defects' in the structure [136–138]. While the concept of defects has been successful in crystals [139], our result suggests that identifying defects in a static structure may be misleading in glasses. Classical AQS simulations do not include any thermal and quantum effects on atomic rearrangements. Therefore, the effectiveness of AQS simulations in glasses is in doubt without assessing these effects.

The nature of these local rearrangements in our work was shown to change drastically in character from reversible to mostly irreversible. Some of the reversible mechanical relaxation

observed in AQS works [9,140,141] may not be realistic in metallic glasses due to the mechanical and thermal coupling causing stochastic and irreversible behavior shown in this work. This stochastic process we observe is not entirely surprising given that activation relaxation technique (ART) simulations have shown that the β relaxation process is stochastic because of the local 'melting' at the saddle point [132] decoupling the activation and relaxation of deformations [133]. This rejuvenation is evident in the percentage of lossy atoms that remain lossy. From Fig. 4.1 the population of lossy atoms with $\delta_{atom} \in [\frac{\pi}{4}, \frac{3\pi}{4}]$ is ~10% at 300 K, with a relatively weak cooling rate dependence as seen in Fig. 4.9. After participating in relaxation roughly 20% of lossy atoms remain lossy, this increase above the system viscoelastic response is attributed to local 'melting' during which the configurational temperature is so high that locally glass turns into a liquid [132]. However, even at 0 K, quantum fluctuations may overcome the activation energy barrier to cause these rearrangements. Because the characteristic temperature T_{ZPE} is within the region of high transience as seen in Fig. 4.7, experimental works done may experience the high transience mechanical relaxation rather than a mostly reversible relaxation even at cryogenic temperatures.

Metallic glasses having a transient mechanical relaxation in this timescale is consistent with the observations that periodic loading below the yielding transition can relax or rejuvenate the system [142–144] and it has been used in other works studying internal friction and relaxation [46,55]. It also explains why cooling rates have a small impact on the magnitude and temperature dependence of transient behavior. Faster cooling rates lead to higher overall potential energies, but much of these initial differences were eliminated by the mechanical training protocol of 30 cycles seen in Fig. 4.10 and do not affect our results.

In summary, our results demonstrate the complex nature of the underlying PEL in metallic glass which fundamentally determines the relaxation dynamics of the system. The activation energies observed here are much smaller in magnitude in comparison to those for the α and β relaxations, the local structure of glass is not static, but is fluctuating, even at room temperature. Our results corroborate the experimental studies of low energy mechanical relaxation [116,117] and simulation and theory works showing the fractal nature of the PEL [112,113]. However, our results call into question many of the assumptions made about the nature of metallic glass and challenge the relevance of structural defects and the validity of AQS simulations.

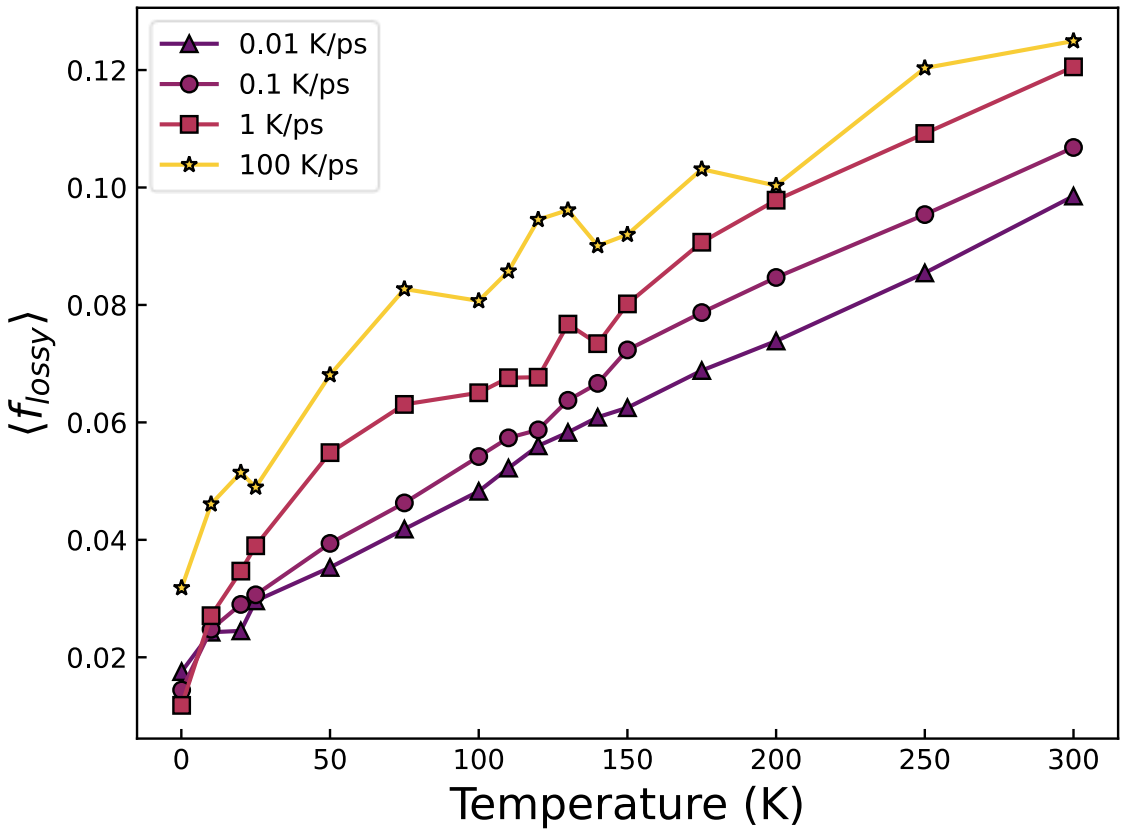

Fig. 4.9 Fraction of lossy atoms vs. temperature for various cooling rates. There is a weak temperature and cooling rate dependence.

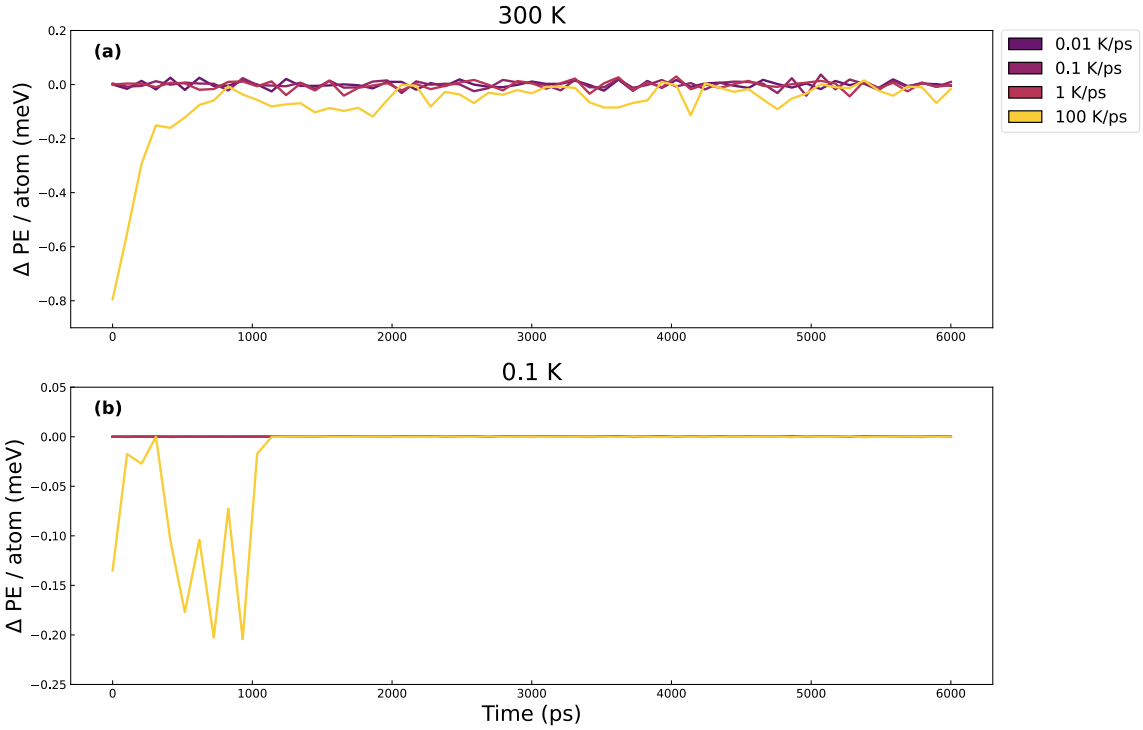

Fig. 4.10 Potential energy of system under mechanical straining for 60 cycles (6000 ps) of sinusoidal straining. First, 30 cycles are the training/equilibration cycles, and the last 30 cycles are for the data collection. Average potential energy change per atom for all four cooling rates at (a) 300 K and (b) 0.1 K.

CHAPTER FIVE MICROSCOPIC NATURE OF FAST RELAXATION IN METALLIC GLASS

The microscopic nature of the fast relaxation in metallic glasses known as nearly constant loss (NCL) is not well understood. While other relaxations such as the α and β relaxation have had more study of their microscopic mechanisms and spatial correlations, NCL, despite being found in many disordered systems, has been the subject of much less attention. Using a simulation technique of applying a sinusoidal shear in the linear elasticity regime, we probe the mechanical relaxations in a model $Cu_{65}Zr_{35}$ metallic glass to study this fast mechanical relaxation. By studying the features of this mechanical response at low temperatures to remove the thermal fluctuations, we demonstrate the role of jumps in the atomic-level shear stress response. We also find that lossy atoms act collectively to cause breaks in shear stress in this temperature regime. Calculations at 300 K reveal the fast decay of the spatial correlation that extends out to the first and second nearest neighbors of lossy atoms. These results further characterize the microscopic nature of NCL.

Introduction

The fundamental relaxation phenomena that exist in metallic glass such as the α [88,145], β [17,48,114,146,147] and other fast relaxations [55,90,98,121] are fundamental to important properties such as ductility, diffusion and mechanical loss. Through understanding of the microscopic mechanisms of how these relaxation phenomena occur, it would be possible to tune these important properties. In particular the fast relaxation phenomena that has been measured in metallic glasses known as nearly constant loss (NCL) [37,95,121], does not have a detailed picture of its microscopic mechanism of relaxation, despite it being more accessible than β relaxation by having an activation energy that is roughly half that of the E_β.

The β relaxation, in this case referring to the 'slow' β as opposed to the 'fast' β relaxation predicted by mode coupling theory (MCT) [97,148,149], is found in a wide variety of amorphous solids. The microscopic nature of how the β relaxation occurs in unresolved, but there are proposed mechanisms such as string-like motions of atoms found in classical molecular dynamics simulations that were connected to the strength of the β relaxation peak [71]. These

string-like motions occur by jumps of atoms to the next nearest neighbor shell which is followed by another atom taking the formers position, thus it is correlated in time. However these strings occur at a quite a low density and have yet to be observed experimentally. Cohen et al. [45] demonstrated the cooperativity of β relaxation by using MD simulations in which a small proportion of particles are pinned [54] and forced to deform affinely during sinusoidal shearing. The works mentioned before demonstrate how MD simulations may be used to investigate and understand the microscopic mechanisms of fundamental relaxations.

In the case of NCL there is not nearly as large of a literature regarding the microscopic nature of the relaxation. Palomino Rico et al. studied a $Cu_{65}Zr_{35}$ metallic glass via MD and examined the rattling motions that were ascribed to the relaxation. The spatial correlation between rattling clusters was estimated to be ~2.5 nm, however, spatial extent of the rattling regions was not explicitly calculated. Most works measuring NCL are experimental and are using some type of sinusoidal probe technique such as dielectric spectroscopy or dynamic mechanical analysis (DMA), neither of which can determine the length scales of the microscopic relaxation except through the interpretation of results through theory.

Utilizing MD simulations during which a $Cu_{65}Zr_{35}$ model metallic glass is sinusoidally shear strained, we identify lossy atoms using atomic-level stresses to decompose the system stress. This is done at two different temperatures, 300 K and 0.1 K, to clearly observe the microscopic mechanism of mechanical behavior by reducing thermal fluctuations. At the low temperature we observe the collective nature of the mechanical relaxation by studying groups of lossy atoms and their atomic-level shear stress response. By examining the role of large shear stress fluctuations and jumps, we conclude that these jumps in atomic-level shear stress are part of the mechanism through which mechanical loss occurs. At 300 K we calculate the spatial correlations of mechanical loss using the partial pair-distribution function and the distinct van Hove function to observe the evolution in time and space of these lossy atoms. From these results we conclude that NCL is collective, occurs via shear-stress breaks on the 1-2 ps timescale, is spatially correlated to the extent of the second set of nearest neighbors and the spatial correlation has a fast decay after one additional cycle of sinusoidal shear.

Methods

Molecular dynamics simulation

Classical molecular dynamics simulations were performed using the Large-scale Atomic/Molecular Massively Parallel Simulator (LAMMPS) [59] with a timestep of 1 fs using a $Cu_{64.5}Zr_{35.5}$ metallic glass with 16,000 atoms and a density of 7.84 g/cm^3. Each low temperature glass was made by a typical melt-quench method with melting at 3000 K for 1 ns. The system was cooled at a rate of 1 K/ps. The embedded atom method (EAM) potential was used to describe interatomic interactions [100] and periodic boundary conditions were imposed. The relaxed system was then sinusoidally sheared following similar protocols in the literature [45,46] with a sinusoidal strain of $\varepsilon(t) = \varepsilon_A \sin(\omega t)$, where t is time, $\omega = 2\pi/T_\omega$, a period $T_\omega = 100$ ps and a strain amplitude of $\varepsilon_A = 2.5\%$. Two temperatures were used to study mechanical loss behavior, 300 K and 0.1 K to study the atomic response with minimal thermal fluctuations. Before collecting data, 30 training/equilibration cycles were done followed by another 30 cycles for data collection.

Identification of lossy atom response and loss magnitude

Lossy atoms have been identified in this work according to the procedure outlined in Chapter Four and in Chapter Two. This involves calculations of the atomic-level shear stress of each atom during a cycle of sinusoidal shear, follow-ed by utilization of the Fourier transform to identify each atoms phase shift which correspond to the mechanical loss of the atom. For calculations at 300 K the definition was chosen such that lossy atoms are defined by the phase shift boundary as $\delta_{atom} \in [\frac{\pi}{4}, \frac{3\pi}{4}]$. At the lower temperature of 0.1 K the population of lossy atoms was much smaller, so the groups that were examined instead consisted of 50 atoms, this was done for both for the groups of atoms around $\delta_{atom} \approx -\frac{\pi}{2}$ and atoms with $\delta_{atom} \approx +\frac{\pi}{2}$.

To estimate the changes in magnitude of mechanical loss of an atom, we estimate the loss as outlined in Chapter Two giving the following equation, $G''_{atom} = (\sigma_{A,atom}/\varepsilon_{A,atom}) \sin(\delta_{atom})$. Again, under the assumption that $\varepsilon_{A,atom} \sim \varepsilon_A$ which gives us our approximation and ranking of mechanical loss magnitude for individual atoms. This is the calculation that allows us to estimate how removing a large atomic-level shear stress jump may impact the mechanical loss of the atom.

Spatial correlations of lossy atoms

To calculate the spatial correlation of atoms identified as lossy at 300 K, the partial pair-distribution function (PDF) was used to study the two-body correlations between atoms identified as lossy to themselves and to the system. Calculating the partial PDF for only lossy atoms as

$$\mathrm{g}(r)_{\mathrm{lossy-lossy}} = \frac{1}{4\pi \mathrm{N}_{\mathrm{lossy}} \rho_{lossy} r^2} \sum_{\mathrm{i,j}} \langle \delta(r - |\boldsymbol{r_i} - \boldsymbol{r_j}|) \rangle \quad (1)$$

With the atom indexes *i, j* over the lossy atoms identified in the cycle, $\boldsymbol{r}_i$ is the position of the *i*th atom, N_{lossy} is the number of lossy atoms in the system and ρ_{lossy} is the average number density of lossy atoms. The averaging, $\langle \cdots \rangle$ represents the averaged structure in between the cycles of straining, thus representing 30 structure snapshots. To understand both the temporal and structural correlations, this calculation was done with lossy atoms from cycle of identification *n* to a future cycle *n* + *m* up to 9 cycles later. This is essentially the distinct van Hove function [150] calculated as follows

$$G(r,t)_{\mathrm{d,lossy-lossy}} = \frac{1}{4\pi \mathrm{N}_{\mathrm{lossy}} \rho_{lossy} r^2} \sum_{\mathrm{i \neq j}} \langle \delta(r + r_j(0) - r_i(t) \rangle \quad (2)$$

The distinct part of the van Hove function gives the cross-correlation between lossy atoms and lossy atoms in future cycles. The times *t* are chosen such that they are calculated in between cycles of straining which occur with a period of 100 ps.

Results

Low temperature atomic-level shear response

To understand the atomic-level mechanisms of mechanical relaxation during sinusoidal shear we investigate the low temperature fluctuations from the mean atomic-level shear response for atoms with a $\delta_{atom} \approx \frac{\pi}{2}$ and $\delta_{atom} \approx -\frac{\pi}{2}$ are shown in Fig. 5.1.

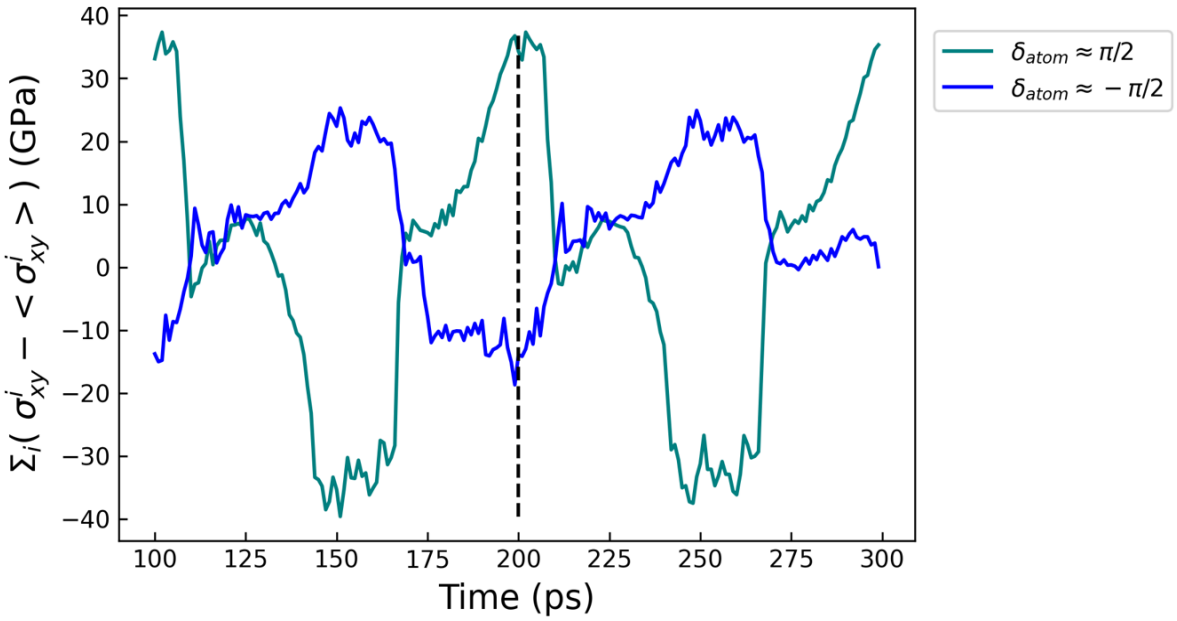

Fig. 5.1 The atomic-level shear stress deviation from the mean summed up for lossy atoms and for those gaining energy. This is over two cycles of sinusoidal strain with the dashed vertical line indicating the end of the first cycle.

To observe the stress fluctuations from the mean we take the difference in atomic-level shear response of each atom with respect to the average shear stress during a cycle as $\sigma_{xy}^{i} - \langle \sigma_{xy}^{i} \rangle$, where i is the atom index and $\langle \cdots \rangle$ is the time average over one cycle. Summing up over 50 atoms from each group we can observe the collective response of atoms causing mechanical loss and gaining energy during the sinusoidal straining. The response of the two groups is often correlated with each other in that large increases in stress for the lossy group typically correspond with opposite stress response in the energy gaining group. The lossy group also is seen to have the largest magnitude of stress before the cycle starts and ends with a similar amount of stress. These lossy atoms retrace the same shear stress response over the two cycles and this behavior was found to persist for later cycles. When examining the behavior of the atoms in Fig. 5.1, there are times at which lossy atoms are seen to exhibit a more sinusoidal response such as at the beginning of the cycle from 110 ps – 140 ps, it is interrupted by several sharp 'breaks' in shear stress at 110 ps and 150 ps.

To understand just how cooperative these stress breaks are for the group of lossy atoms, we calculate the sum of the derivative of the shear stress response as, $\sum_i (\frac{d\sigma_{xy}^{i}}{dt} - \langle \frac{d\sigma_{xy}^{i}}{dt} \rangle)$ and as before $\langle \cdots \rangle$ represents the time average over 1 cycle. This sum is seen in Fig. 5.2 where the response over 8 cycles is plotted. We observe very large jumps in the sum compared to the average fluctuations. Often within an individual cycles which is 100 ps long, there are two jumps, one that is positive and one that is negative. This represents the groups of lossy atoms cooperatively experiencing a large deviation in that atomic-level shear stress. To further investigate how the atomic-level shear stress changes for atoms that are energy gaining versus energy lossy, we calculate $\frac{d\sigma_{xy}}{dt}$ where dt = 1 ps over all cycles and plot the distribution shown in Fig. 5.3. To represent the rare large fluctuations, we use a semi-log plot and with the response of all other atoms besides those with a $\delta_{atom} \approx +\frac{\pi}{2}, -\frac{\pi}{2}$ labeled as 'system'. We observe that lossy atoms with $\delta_{atom} \approx \frac{\pi}{2}$ are more likely to have rare large fluctuations that are larger than roughly 2 GPa in magnitude. It is interesting that the same cannot be said for energy gaining atoms whose phase is $\delta_{atom} \approx -\frac{\pi}{2}$ which have a distribution that is quite similar to the system distribution.

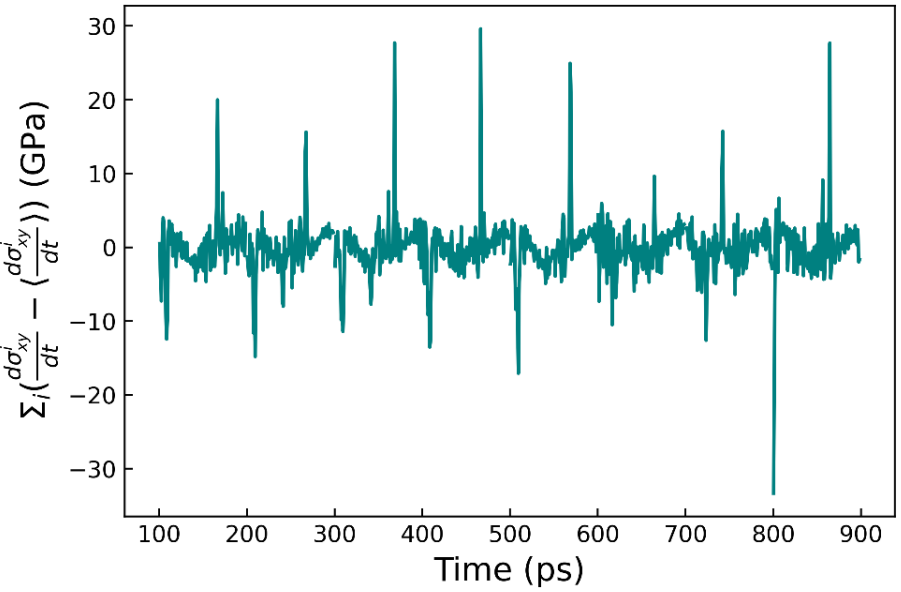

Fig. 5.2 The sum of the derivative of the deviation of the shear stress response for 50 lossy atoms identified each cycle. This is shown over 8 cycles.

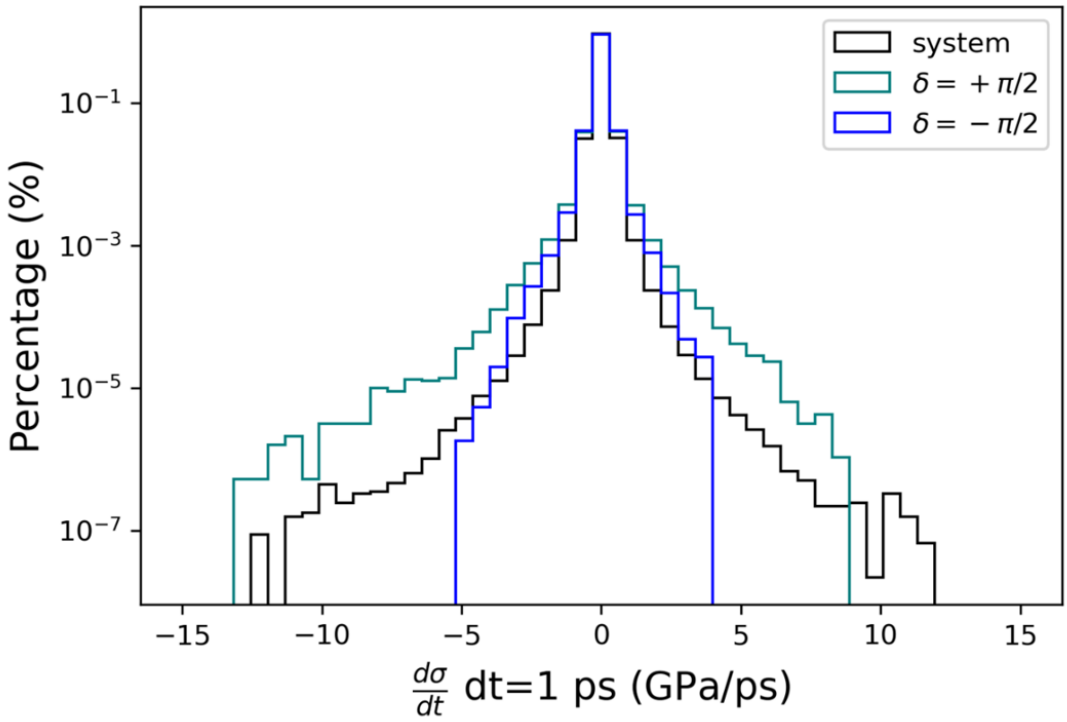

Fig. 5.3 The distribution of shear stress derivatives for lossy and energy gaining atoms.

Both the collective changes in the atomic-level shear stress seen in Fig. 5.2 and the distribution of the atomic-level shear stress derivative Fig. 5.3 suggests the importance of large shear stress jumps in the mechanism of mechanical loss. Consequently, we decided to investigate how large shear stress jumps may modify atomic-level mechanical loss. To do this we modify the atomic-level shear stress response of each atom by identifying the largest jump in shear stress response, $\frac{d\sigma_{xy}^{i}}{dt}$ is calculated over a time interval of Δt = 1 ps, giving us the largest jump at time t'. Then we subtract the effect of this shear stress jump at t' as follows:

$$\sigma_{xy}^{i}(t) = \begin{cases} \sigma_{xy}^{i}(t) & t < t' \\ \sigma_{\mathrm{xy}}^{i}(t) - \dfrac{d\sigma_{xy}^{i}(t')}{dt}\Delta\mathrm{t} & t \geq t' \end{cases}$$

An example of this process for a single lossy atom is shown in Fig. 5.5 whereby removing the largest jump in shear stress for a lossy atom we observe it changing its mechanical loss response going from having a mechanical loss of 19.5 GPa to -2.71 GPa. We repeat this process of removing the largest jumps in atomic-level shear stress for all lossy atoms across 30 cycles and plot this distribution in Fig. 5.4. This distribution shows a shift leftward indicating that by removing the largest jumps, the magnitude G''_{atom} as a group is reduced slightly. We also see that many atoms in the distribution now have a negative G''_{atom}. To further investigate the impact of the removal of jumps, we calculated the overall loss modulus reduction by excluding all jumps in atoms above a certain threshold as seen in Fig. 5.6. We find that until the magnitude of jumps is reduced to either 0.25 GPa or 0.10 GPa there is only a small reduction of perhaps 5% or less and the magnitude of smaller jumps is such that the atomic-level shear response of atoms is modified significantly. These results demonstrate that some jumps in the atomic-level shear stress response are important, but others are inconsequential. While we have characterized some of the temporal and coherent nature of loss at low temperature, we next moved to characterization of the spatial correlations at 300 K.

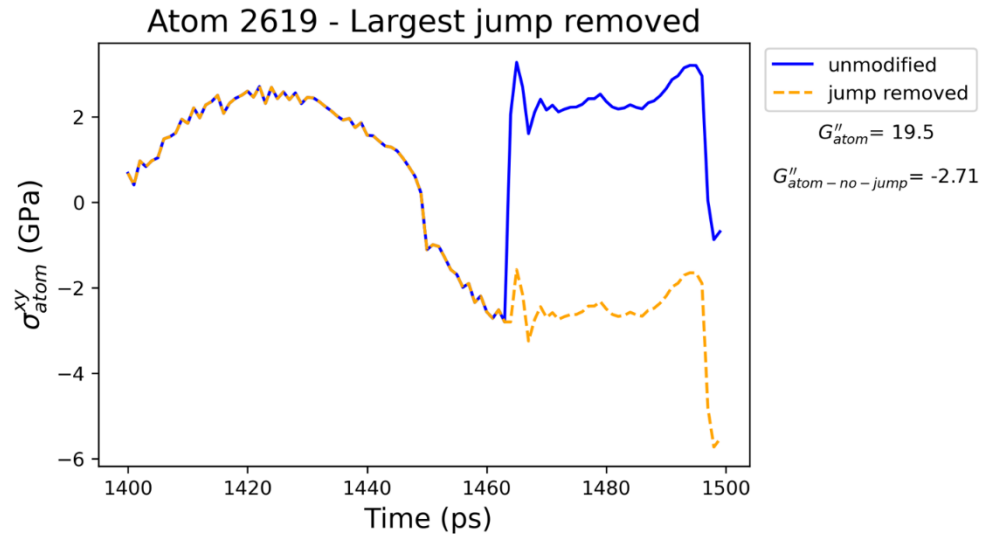

Fig. 5.4 Example of a modified shear stress response of a lossy atom, changing it from lossy to energy gaining just by removing the impact of one shear stress jump.

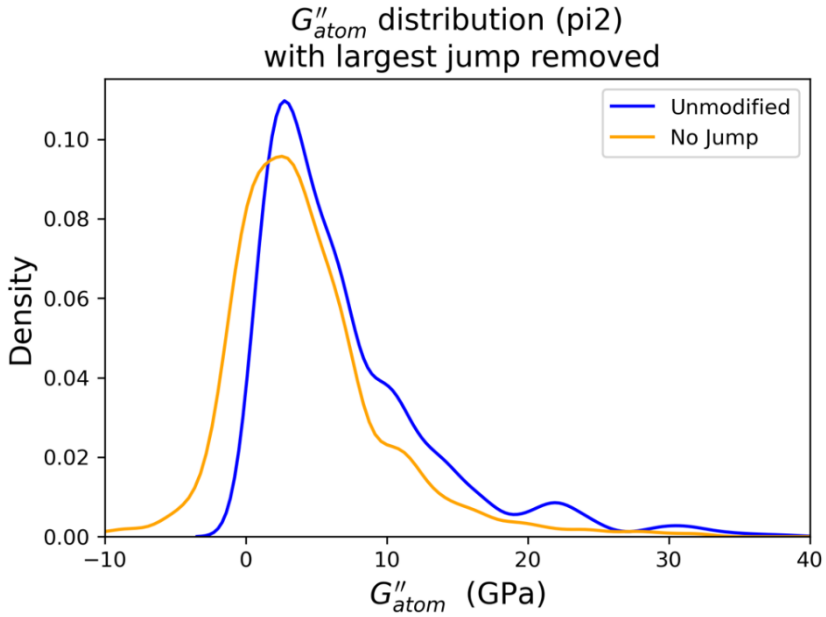

Fig. 5.5 Probability density of magnitude of atomic-level mechanical loss G''_{atom} for lossy atoms ($\delta_{atom} \approx \frac{\pi}{2}$) that were unmodified (in blue) and those with the largest shear stress jump removed (in orange).

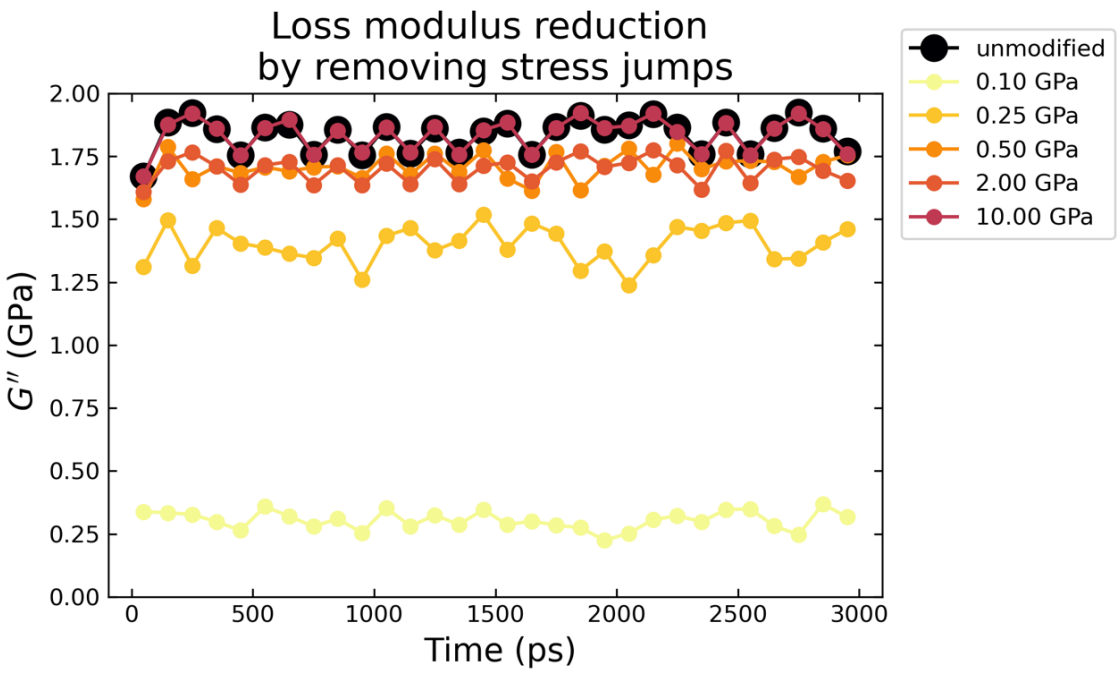

Fig. 5.6 Impact of removing all jumps in atomic-level shear stress from atoms above a threshold.

Spatial correlation of lossy atoms

As we demonstrated at low temperatures, there are correlated shear stress jumps for lossy atoms. As finite temperatures are more relevant to real mechanical loss, we examined the spatial correlations of these lossy atoms.

By calculating the partial radial-distribution function between lossy atoms and the rest of the atoms in the system, $g(r)_{lossy-system}$ and comparing this to the total radial-distribution function we can understand the pair-correlations of these lossy atoms. This calculation is shown in Fig. 5.7 where there is a slight increase in the spatial correlation of lossy atoms to other lossy atoms over the total radial distribution function. However, by examining the comparison of the total pair-distribution function $g(r)$ against $g(r)_{lossy-system}$ we see essentially no difference. This indicates that the local environment of lossy atoms is essentially indistinguishable based on the local density which is in line with the results of Chapter 3 regarding the atomic-level volumes of lossy atoms. By examining the correlation function between groups of lossy atoms as they evolve over subsequent cycles of mechanical straining and to the system, we can understand how these lossy atoms are correlated in both space and time. Through calculating $g(r)_{lossy-lossy}$ during cycle n when the lossy atoms are identified, then calculating how the lossy group is correlated in space some number of cycles *m* later, we are essentially calculating the distinct van Hove function [150]. This represents the correlation in space and time between an atom *i* at time *t* given the position at some time origin. This calculation is shown in Fig. 5.8 demonstrating a higher correlation for the cycle of identification, $n + 0$. After just one cycle of identifying lossy atoms, this correlation quickly decays and remains constant for the other 9 cycles later. If there was no spatial correlation at all for lossy atoms, we would expect that the $n + 0$ radial distribution function would be identical to later cycles. To confirm this result, we calculate the average coordination number, $\langle N_c \rangle$, of the lossy atoms to other lossy atoms in future cycles of loss up to 10 cycles later. This is shown in Fig. 5.9 which demonstrates that during the cycle which atoms are lossy they on average have ~1.5 other lossy neighbors which has a small drop to ~1.3 lossy atoms in subsequent cycles and remains constant. This is compared with the system average of ~1.2 (shown as the dashed line in Fig. 5.9), showing that there is tendency for lossy atoms to aggregate which essentially reduced to the system response after 1 cycle.

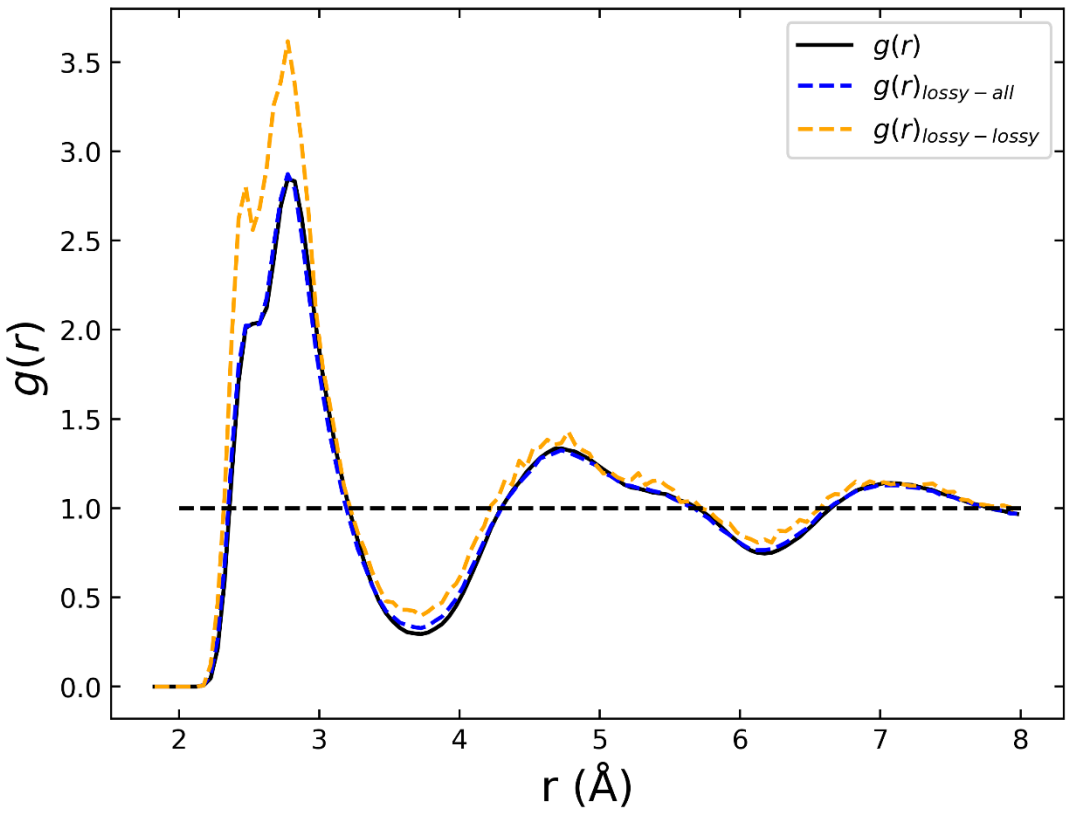

Fig. 5.7 Partial radial-distribution function between lossy atoms and other lossy atoms as well as lossy atoms with all other atoms in the system. There is shown to be a slight tendency of lossy atoms to aggregate together from the $g(r)_{lossy-lossy}$.

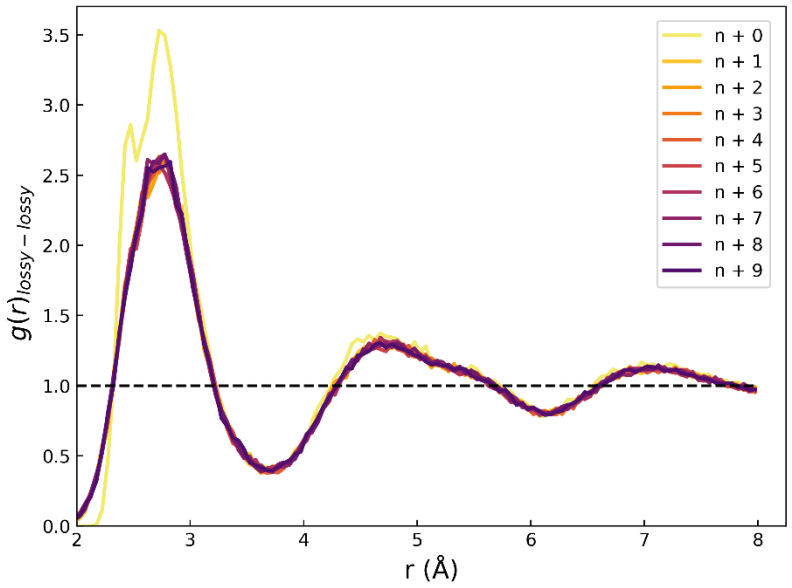

Fig. 5.8 Partial radial-distribution function between lossy atoms identified in some cycle n then calculated with lossy atoms identified up to 9 cycles later. A higher correlation between lossy atoms is found in the cycle of identification which quickly decays only one cycle later.

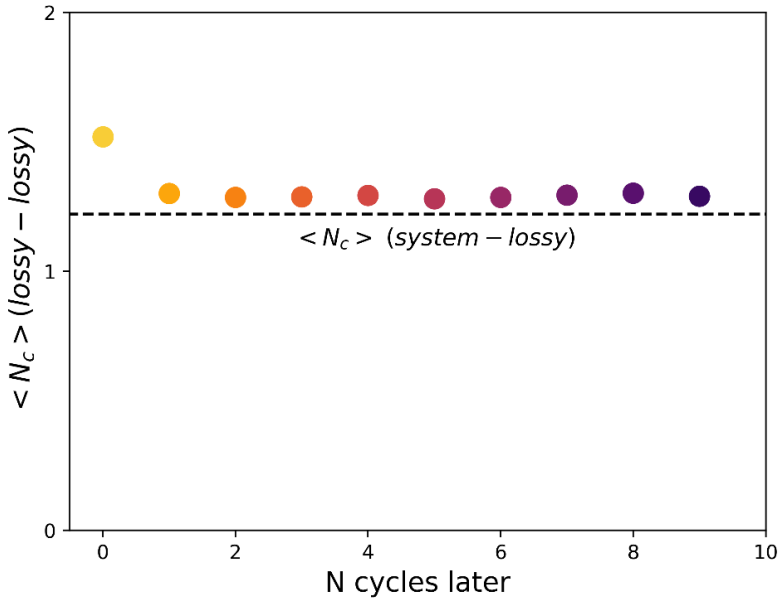

Fig. 5.9 Average coordination number, $\langle N_c \rangle$, for lossy atoms to lossy atoms identified in future cycles up to 10 cycles later. During cycle of loss there are ~1.5 other lossy neighbors which has a small drop to ~1.3 lossy atoms in subsequent cycles and remains constant. This is compared to system average as the dashed line.

This is in line with the $g(r)$ calculation for lossy atoms demonstrating a correlation with other lossy atoms during the cycle of identification which decays by the next cycle. To determine what the length of this spatial correlation was, we calculate the average atomic-level phase shift, $\langle \delta_{atom} \rangle$, around all atoms that are identified as lossy in a single cycle. This is calculated with the structure corresponding to the end of the cycle where the atoms were identified as lossy to avoid the complications of the non-affine displacements during straining. Using a variety of cutoff lengths for the inclusion of neighbors, as seen in Fig. 5.10a, we show a strong spatial correlation that extends all the way out to the second set of nearest neighbors in Fig. 5.10b. This correlation at the first cutoff of roughly has an average of nearly .1 rad larger than the ensemble average, this is quite a significant increase and to have an equivalent increase in phase shift of the system would require 300 – 400 K increase in temperature. Even out to the furthest cutoff of 8 Å there is still a small increase over the ensemble average. Based on the exponential decay we see in the average phase shift around lossy atoms, we fit $\langle \delta_{atom} \rangle \approx Ae^{-\frac{r}{\xi_s}} + B$ with ξ_s representing the correlation length. From this we calculate the correlation length to be $\xi_s \approx 2.34$ Å.

Discussion

The low temperature response at 0.1 K of lossy and energy gaining atoms suggests that the mechanical loss occurs through groups of atoms that coherently and collectively experience large atomic-level shear stress breaks. This is because the deviations in atomic-level shear stress occur collectively as a group, we also demonstrate that some stress breaks are quite important and can drastically change the magnitude of atomic-level mechanical loss. As atomic-level stresses are the first order local response to strain, it is not surprising that these lossy atoms demonstrate large stress breaks when they reach a local instability that results in mechanical loss [123]. In a previous work Egami et al. [80,81] demonstrated that a volume strain above 11% results in instability, so it is expected that if local shear stresses result in this volume strain there should subsequently be a relaxation. Additionally, local instability can come from the fraction of liquidlike sites that do not support the mechanical load which represent roughly 25% of the atoms as found by the anisotropic pair-density function measured by X-ray diffraction of a $Zr_{52.5}Cu_{17.9}Ni_{14.6}Al_{10}Ti_5$ metallic glass [107].

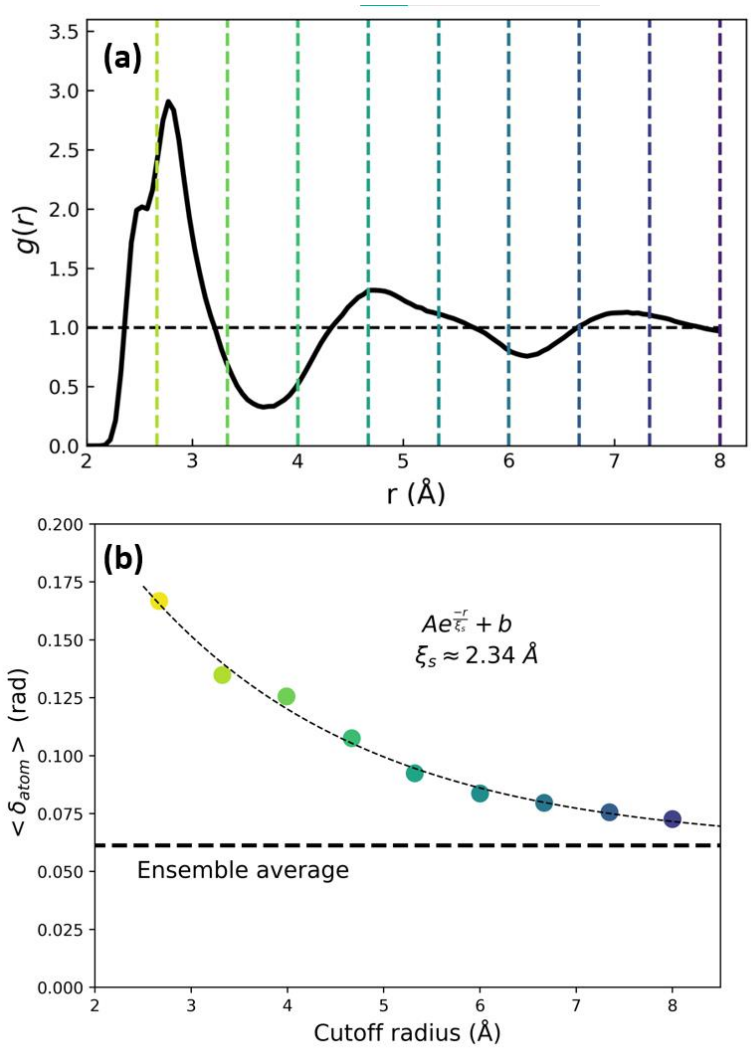

Fig. 5.10 Average phase of neighboring atoms to lossy atoms that are identified. This is calculated with an increased cutoff radius for the inclusion of additional neighbors. There is a significant spatial correlation that even goes to MRO. (a) Cutoff radius overlayed on $g(r)$ (b) The average phase of atoms around lossy atoms, $\langle \delta_{atom} \rangle$ including all atoms in the cutoff radius. The bold dashed line indicates the ensemble average of atomic-level phase shift for a comparison point.

Simulations of a-Si by Demkowicz and Argon [151] have shown that stress relaxations occurring during plastic flow occur via atomic-level changes in the stress tensor which characterize their liquidlike environment.

In terms of the response of lossy atoms as a group, it is clear from Fig. 5.1 and Fig. 5.2 that these deviations in shear stress are coherent in time. Similarly work by Mizuno et al. [152] calculated the low temperature rearrangements occurring from thermal fluctuations of a bidispersed model glass, which showed intermittent rearrangements that are also quite coherent in time and occur cooperatively.

As for the mechanism of how this mechanical loss might occur, the atomic-level shear stress at low temperature looks quite similar to elastic atoms except for large jumps in the shear stress response as seen in by comparing Fig. 2.6 and Fig. 2.7 from Chapter 2. Looking at the time scale of how long these jumps take gives a rough estimate of 1-2 ps for this jump to occur and this corresponds with results from Ding et al. [132] which show the melting time for activation of the β relaxation takes 1-2 ps. Based on the buildup seen of the shear stress of the group of lossy atoms in Fig. 5.1, it may be that lossy atoms as a group build up shear stress until they are at an instability and then coherently and cooperatively in time experience a break or jump in shear stress which would cause the mechanical loss observed in the system. Additionally, by subtracting the contribution of the largest atomic-level shear stress jumps, it was shown that some atoms have a large decrease in loss but not all jumps are created equal, and Fig. 5.6 showed that systematically removing jumps does not have a large decrease on $G"$. These results point to how atomic jumps and collective response may be involved in the mechanisms of mechanical loss. However, it is difficult to determine if at higher temperatures mechanical loss occurs by the same mechanism due to the magnitude of the thermal fluctuations as readily seen by comparing the atomic-level shear stress response of a lossy atom at low temperature in Fig. 2.7 and one at 300 K in Fig. 2.5. This is especially the case because we see that the transient nature of mechanical loss changes by measuring the lossy fraction at 0.1 K versus at 300 K which was discussed in the previous chapter.

To further understand nature of how this mechanical loss operates at finite temperature, we showed the spatial correlation that exists between lossy atoms in Fig. 5.6. From this it was evident that the spatial correlation that exists in the cycle during which lossy atoms are

identified, quickly decays after one cycle with no sign of further decay further supporting the transience identified in Chapter Three. Comparing the calculated correlation length ξ_s, of the average phase around lossy atoms we can compare this with the correlation length of the medium range order calculated by Ryu and Egami [153]. For a $Cu_{65}Zr_{35}$ glass the medium range order correlation length was found to be $\xi_s \approx 3.7$ Å which is larger than the correlation length we calculated at $\xi_s \approx 2.34$ Å. This is inline with the evidence that the medium range order freezes at the glass transition shown by another work by Ryu and Egami [129] in which the temperature dependence of the first, second and third peaks in $g(r)$ were calculated for a variety of metallic glasses and a clear change in slope was seen at T_g for the third peak corresponding to the medium-range. Because of this change in slope, it is implied that the medium-range ordering freezes at T_g and that the short-range ordering is not frozen. Calculations examining the fast relaxation mode in the form of rattling modes [98] did not explicitly discuss the length scale of these rattling regions, or their correlation length.

Conclusions

By utilizing both low temperature mechanical response and the calculation of spatial correlations at finite temperature using the pair-distribution function and the distinct van Hove function, we gain insight into the mechanical relaxation behavior of the fast relaxation processes in metallic glasses. We showed the cooperative nature of atomic-level shear stress jumps that lossy atoms have during the sinusoidal strain cycles and connected these with the atomic-level mechanical loss. By examining the derivative of the atomic-level shear stress response as a group, we observed the large spikes that represent the collective response of lossy atoms. These two features of collective response and the spikes in the shear stress response may be contributing to the mechanism of mechanical loss at low temperature. However, as shown in Chapter 4, the nature of this low temperature response would likely change due to the effective temperature of the quantum zero-point fluctuations. Therefore, while we do demonstrate several features of this response, it is not known if these features continue to exist at finite temperatures.

Our calculations demonstrating the correlation length were performed at 300 K which is within the regime known as nearly constant loss (NCL) and is a relaxation phenomenon found in many disordered systems. While the spatial correlations for the β relaxation have been

extensively studied, the fast relaxation phenomena in metallic glass have many remaining questions regarding the microscopic nature of the relaxation. The spatial correlation of lossy groups to other lossy atoms shows a weak tendency to aggregate from the partial radial-distribution function. We also calculate the correlation length of this loss and find it to be smaller than that of the corresponding MRO correlation length suggesting that this mechanical loss represents the short-range motions that are not frozen in at the glass transition. This presents a radically different picture of the nature of mechanical loss as opposed to the rattling groups of atoms seen in other simulation works or the string-like excitations that occur atom by atom that have been attributed to the β relaxation. With our low temperature simulations and results from 300 K we characterize both the mechanism of mechanical loss and the spatial correlations of this mechanical loss.

CHAPTER SIX CONCLUSIONS

Metallic glasses exhibit many of the fundamental relaxation processes that exist in other amorphous solids. This means they are excellent, simple, and real glassy systems to study relaxation behavior. These same relaxation mechanisms describe important phenomena of interest that exist in glass such as the glass transition, deformation, diffusion, and aging/rejuvenation. Through a deeper understanding of these relaxation phenomena, we further improve our understanding of the relationship between structure and property in disordered matter. The microscopic view of these relaxation mechanisms, including the fast relaxations in metallic glass, is lacking. Therefore, our aim was to utilize novel molecular dynamics simulation tools to uncover some of the characteristics of fast relaxation in metallic glass.

To study these relaxation phenomena, we utilize classical molecular dynamics simulations to sinusoidally shear a model metallic glass in a way that is analogous to the experimental technique of dynamic mechanical analysis. We further build off this technique in a unique fashion by decomposing the system stress into atomic-level stress components to systematically identify atoms involved in the mechanical relaxation on a cycle-by-cycle basis. This allowed for the characterization of these groups of lossy atoms as they evolve in time.

Through this cycle-by-cycle identification, we demonstrated that the fast relaxations in metallic glass have a transient nature during which nearly completely different groups of atoms are involved in the relaxation behavior. Additionally, there were no obvious signs of structural defects linked to these groups of lossy atoms. This transient behavior is in stark contrast to other simulation works where rattling like centers persistently are involved in the fast relaxation or works showing that fast moving atoms are predominantly contributing to mechanical loss.

We also characterize the bottom of the potential energy landscape (PEL) which is the statistical thermodynamic framework which captures the activation relaxation phenomena that are available. Through our calculations of the temperature dependence of the lossy fraction of atoms, we find a characteristic change in the relaxation behavior from mostly reversible to mostly transient and this transient behavior is accessible by the quantum mechanical zero-point motion. This activation phenomenon we characterize represents the small ripples in the PEL at the bottom of sub-basins.

Finally, we showed the low temperature atomic-level shear stress response that characterizes the mechanical loss and the collective breaks that are potentially responsible for the mechanical loss. At higher temperatures the spatial correlation was calculated and extends to the second group of nearest neighbors and shows a fast decay in time. Through our classical molecular dynamics simulations, we can gain further insight into the microscopic nature of relaxation behavior in metallic glass that would otherwise be difficult to extract using conventional experimental techniques.

The glassy state below the level of β relaxation is seen as 'frozen'; however, our results show this is not the case and subtle microscopic rearrangements are still present. Additionally, the glassy literature has continued to search for defects that are like those in crystalline systems and our results of transient relaxation show no evidence of defects suggesting that the concept of defects in metallic glass may not be that useful. We also show the small ripples in the potential energy landscape which further characterizes how the many glassy states are connected with each other at the bottom of the sub-basins. As these relaxation phenomena we studied are also present in other amorphous solids, the insights we have gained may be applicable to a wide range of disordered systems.

When our results are compared with the current views on the fast relaxation behavior of glass, we note significant differences in the structure-property relationship of the atomic-level structure to the short-range dynamics. The fact that we found no clear defining defects relating to underlying structure suggests that attempting to remove structural defects to modify the fast relaxation may be fruitless and other avenues of modifying glass properties should be pursued. Because we further described the underlying potential energy landscape, we expect our results will give further insight into how all relaxation phenomena are connected such as the basin to meta-basin picture of α and β relaxation. Additionally, because metallic glass exhibits many of the same fundamental relaxations in glasses these results may extend to other disordered systems like polymers, covalent glasses and molecular glasses.

Future works would focus on determining if the results found within this work apply to other disordered solids and how we might connect the fast relaxation studied to desirable properties of glasses. As we narrowly focused on one composition of metallic glass, studying other disordered systems, such as amorphous polymers or covalent glasses, would allow us to

determine whether our characterization of fast relaxation is specific to metallic glass or a more universal phenomenon of disordered solids. Another lingering question that we may follow up on is the impact of thermal history on the transient mechanical response and the small ~1 meV activation phenomena that we found. To study the impact of thermal history on the fast relaxation, a method such as swap Monte Carlo [154] may be used to study a glass deeper in the potential energy landscape. If we observe the same characteristic transient response in glasses prepared by swap Monte Carlo, this will add further evidence that our results are applicable to metallic glasses with realistic cooling rates. A more applied future work may involve characterizing how the magnitude of the fast relaxation modifies the magnitude of phenomena such as internal friction, microscopic deformation behavior and rejuvenation.

Amorphous solids are an important class of matter that shares many essential relaxations and dynamics. The precise control of these features and dynamics has yet been elusive due to the lack of fundamental understanding of the disordered state of matter. To solve important engineering problems, it is far more desirable to design from first principles than by trial and error. By further characterizing phenomena that are difficult to examine microscopically we aim to improve the existing understanding of the relaxation phenomena in disordered matter.

LIST OF REFERENCES

[1] Julian. Henderson, Ancient Glass : An Interdisciplinary Exploration., Cambridge University Press, New York, 2013.

[2] A.K. Varshneya, Fundamentals of inorganic glasses, Elsevier, 2013.

[3] P.G. Debenedetti, F.H. Stillinger, Supercooled liquids and the glass transition, Nature. 410 (2001) 259–267. https://doi.org/10.1038/35065704.

[4] M.D. Ediger, C.A. Angell, S.R. Nagel, Supercooled Liquids and Glasses, J. Phys. Chem. 100 (1996) 13200–13212. https://doi.org/10.1021/jp953538d.

[5] Y.Q. Cheng, E. Ma, Atomic-level structure and structure-property relationship in metallic glasses, Progress in Materials Science. 56 (2011) 379–473. https://doi.org/10.1016/j.pmatsci.2010.12.002.

[6] L. Berthier, R.L. Jack, Structure and dynamics of glass formers: Predictability at large length scales, Phys. Rev. E. 76 (2007) 041509. https://doi.org/10.1103/PhysRevE.76.041509.

[7] A.K. Varshneya, Chemical Strengthening of Glass: Lessons Learned and Yet To Be Learned, International Journal of Applied Glass Science. 1 (2010) 131–142. https://doi.org/10.1111/j.2041-1294.2010.00010.x.

[8] N.C. Keim, J.D. Paulsen, Z. Zeravcic, S. Sastry, S.R. Nagel, Memory formation in matter, Rev. Mod. Phys. 91 (2019) 035002. https://doi.org/10.1103/RevModPhys.91.035002.

[9] I. Regev, T. Lookman, C. Reichhardt, Onset of irreversibility and chaos in amorphous solids under periodic shear, Phys. Rev. E. 88 (2013) 062401. https://doi.org/10.1103/PhysRevE.88.062401.

[10] D. Fiocco, G. Foffi, S. Sastry, Encoding of Memory in Sheared Amorphous Solids, Phys. Rev. Lett. 112 (2014) 025702. https://doi.org/10.1103/PhysRevLett.112.025702.

[11] S. Slotterback, M. Mailman, K. Ronaszegi, M. Van Hecke, M. Girvan, W. Losert, Onset of irreversibility in cyclic shear of granular packings, Phys. Rev. E. 85 (2012) 021309. https://doi.org/10.1103/PhysRevE.85.021309.

[12] B. Shang, P. Guan, J.-L. Barrat, Elastic avalanches reveal marginal behavior in amorphous solids, Proc Natl Acad Sci U S A. 117 (2020) 86–92. https://doi.org/10.1073/pnas.1915070117.

[13] B. Riechers, K. Samwer, Nonlinear response and avalanche behavior in metallic glasses, Eur. Phys. J. Spec. Top. 226 (2017) 2997–3021. https://doi.org/10.1140/epjst/e2017-70087-9.

[14] H. Bhaumik, G. Foffi, S. Sastry, Avalanches, Clusters, and Structural Change in Cyclically Sheared Silica Glass, Phys. Rev. Lett. 128 (2022) 098001. https://doi.org/10.1103/PhysRevLett.128.098001.

[15] A. Alegria, E. Guerrica-Echevarria, L. Goitiandia, I. Telleria, J. Colmenero, .alpha.-Relaxation in the Glass Transition Range of Amorphous Polymers. 1. Temperature Behavior across the Glass transition, Macromolecules. 28 (1995) 1516–1527. https://doi.org/10.1021/ma00109a025.

[16] R.D. Priestley, C.J. Ellison, L.J. Broadbelt, J.M. Torkelson, Structural Relaxation of Polymer Glasses at Surfaces, Interfaces, and In Between, Science. 309 (2005) 456–459. https://doi.org/10.1126/science.1112217.

[17] G.P. Johari, M. Goldstein, Viscous Liquids and the Glass Transition. II. Secondary Relaxations in Glasses of Rigid Molecules, J. Chem. Phys. 53 (1970) 2372–2388. https://doi.org/10.1063/1.1674335.
[18] W. Klement, R.H. Willens, P. Duwez, Non-crystalline Structure in Solidified Gold–Silicon Alloys, Nature. 187 (1960) 869–870. https://doi.org/10.1038/187869b0.
[19] C.A. Schuh, T.C. Hufnagel, U. Ramamurty, Mechanical behavior of amorphous alloys, Acta Materialia. 55 (2007) 4067–4109. https://doi.org/10.1016/j.actamat.2007.01.052.
[20] T. Egami, T. Iwashita, W. Dmowski, Mechanical Properties of Metallic Glasses, Metals. 3 (2013) 77–113. https://doi.org/10.3390/met3010077.
[21] J. Schroers, Processing of Bulk Metallic Glass, Advanced Materials. 22 (2010) 1566–1597. https://doi.org/10.1002/adma.200902776.
[22] J.F. Löffler, Bulk metallic glasses, Intermetallics. 11 (2003) 529–540. https://doi.org/10.1016/S0966-9795(03)00046-3.
[23] H.J. Barlow, J.O. Cochran, S.M. Fielding, Ductile and Brittle Yielding in Thermal and Athermal Amorphous Materials, Phys. Rev. Lett. 125 (2020) 168003. https://doi.org/10.1103/PhysRevLett.125.168003.
[24] Q. Wang, J.J. Liu, Y.F. Ye, T.T. Liu, S. Wang, C.T. Liu, J. Lu, Y. Yang, Universal secondary relaxation and unusual brittle-to-ductile transition in metallic glasses, Materials Today. 20 (2017) 293–300. https://doi.org/10.1016/j.mattod.2017.05.007.
[25] A.L. Greer, Y.Q. Cheng, E. Ma, Shear bands in metallic glasses, Materials Science and Engineering: R: Reports. 74 (2013) 71–132. https://doi.org/10.1016/j.mser.2013.04.001.
[26] T.C. Hufnagel, C.A. Schuh, M.L. Falk, Deformation of metallic glasses: Recent developments in theory, simulations, and experiments, Acta Materialia. 109 (2016) 375–393. https://doi.org/10.1016/j.actamat.2016.01.049.
[27] H. Jia, G. Wang, S. Chen, Y. Gao, W. Li, P.K. Liaw, Fatigue and fracture behavior of bulk metallic glasses and their composites, Progress in Materials Science. 98 (2018) 168–248. https://doi.org/10.1016/j.pmatsci.2018.07.002.
[28] P. Lunkenheimer, U. Schneider, R. Brand, A. Loidl, Glassy dynamics, Contemporary Physics. 41 (2000) 15–36. https://doi.org/10.1080/001075100181259.
[29] M. Goldstein, Viscous Liquids and the Glass Transition: A Potential Energy Barrier Picture, The Journal of Chemical Physics. 51 (1969) 3728–3739. https://doi.org/10.1063/1.1672587.
[30] P.K. Gupta, W. Kob, Basis glass states: New insights from the potential energy landscape, Journal of Non-Crystalline Solids: X. 3 (2019) 100031. https://doi.org/10.1016/j.nocx.2019.100031.
[31] F.H. Stillinger, T.A. Weber, Dynamics of structural transitions in liquids, Physical Review A. 28 (1983) 2408–2416. https://doi.org/10.1103/PhysRevA.28.2408.
[32] F. Spaepen, A microscopic mechanism for steady state inhomogeneous flow in metallic glasses, Acta Metallurgica. 25 (1977) 407–415. https://doi.org/10.1016/0001-6160(77)90232-2.
[33] A.S. Argon, Plastic deformation in metallic glasses, Acta Metallurgica. 27 (1979) 47–58. https://doi.org/10.1016/0001-6160(79)90055-5.
[34] M.L. Falk, J.S. Langer, Dynamics of viscoplastic deformation in amorphous solids, Phys. Rev. E. 57 (1998) 7192–7205. https://doi.org/10.1103/PhysRevE.57.7192.

[35] D. Rodney, C. Schuh, Distribution of Thermally Activated Plastic Events in a Flowing Glass, Phys. Rev. Lett. 102 (2009) 235503. https://doi.org/10.1103/PhysRevLett.102.235503.
[36] S. Swayamjyoti, J.F. Löffler, P.M. Derlet, Local structural excitations in model glass systems under applied load, Phys. Rev. B. 93 (2016) 144202. https://doi.org/10.1103/PhysRevB.93.144202.
[37] H.Y. Jiang, P. Luo, P. Wen, H.Y. Bai, W.H. Wang, M.X. Pan, The near constant loss dynamic mode in metallic glass, Journal of Applied Physics. 120 (2016) 145106. https://doi.org/10.1063/1.4964809.
[38] K.P. Menard, N.R. Menard, Dynamic mechanical analysis, CRC press, 2020.
[39] F.H. Stillinger, A Topographic View of Supercooled Liquids and Glass Formation, Science. 267 (1995) 1935–1939.
[40] Y. Shinohara, T. Osaka, I. Inoue, T. Iwashita, W. Dmowski, C.W. Ryu, Y. Sarathchandran, T. Egami, Split-pulse X-ray photon correlation spectroscopy with seeded X-rays from X-ray laser to study atomic-level dynamics, Nature Communications. 11 (2020) 1–7. https://doi.org/10.1038/s41467-020-20036-z.
[41] V.M. Giordano, B. Ruta, Unveiling the structural arrangements responsible for the atomic dynamics in metallic glasses during physical aging, Nature Communications. 7 (2016). https://doi.org/10.1038/ncomms10344.
[42] H. Zhang, C. Zhong, J.F. Douglas, X. Wang, Q. Cao, D. Zhang, J.-Z. Jiang, Role of string-like collective atomic motion on diffusion and structural relaxation in glass forming Cu-Zr alloys, J. Chem. Phys. 142 (2015) 164506. https://doi.org/10.1063/1.4918807.
[43] J.D. Stevenson, P.G. Wolynes, A universal origin for secondary relaxations in supercooled liquids and structural glasses, Nature Phys. 6 (2010) 62–68. https://doi.org/10.1038/nphys1432.
[44] H.-B. Yu, R. Richert, K. Samwer, Structural rearrangements governing Johari-Goldstein relaxations in metallic glasses, Sci. Adv. 3 (2017) e1701577. https://doi.org/10.1126/sciadv.1701577.
[45] Y. Cohen, S. Karmakar, I. Procaccia, K. Samwer, The nature of the β-peak in the loss modulus of amorphous solids, Epl. 100 (2012). https://doi.org/10.1209/0295-5075/100/36003.
[46] H.-B. Yu, K. Samwer, Atomic mechanism of internal friction in a model metallic glass, Phys. Rev. B. 90 (2014) 144201. https://doi.org/10.1103/PhysRevB.90.144201.
[47] W.H. Wang, Dynamic relaxations and relaxation-property relationships in metallic glasses, Progress in Materials Science. 106 (2019) 100561. https://doi.org/10.1016/j.pmatsci.2019.03.006.
[48] Y.H. Liu, T. Fujita, D.P.B. Aji, M. Matsuura, M.W. Chen, Structural origins of Johari-Goldstein relaxation in a metallic glass, Nature Communications. 5 (2014) 1–7. https://doi.org/10.1038/ncomms4238.
[49] B. Guiselin, C. Scalliet, L. Berthier, Microscopic origin of excess wings in relaxation spectra of supercooled liquids, Nat. Phys. (2022). https://doi.org/10.1038/s41567-022-01508-z.
[50] H.B. Yu, W.H. Wang, K. Samwer, The β relaxation in metallic glasses: An overview, Materials Today. 16 (2013) 183–191. https://doi.org/10.1016/j.mattod.2013.05.002.

[51] G.T. Barkema, N. Mousseau, Event-Based Relaxation of Continuous Disordered Systems, Phys. Rev. Lett. 77 (1996) 4358–4361. https://doi.org/10.1103/PhysRevLett.77.4358.
[52] E. Cancès, F. Legoll, M.-C. Marinica, K. Minoukadeh, F. Willaime, Some improvements of the activation-relaxation technique method for finding transition pathways on potential energy surfaces, The Journal of Chemical Physics. 130 (2009) 114711. https://doi.org/10.1063/1.3088532.
[53] Y. Fan, T. Iwashita, T. Egami, How thermally activated deformation starts in metallic glass, Nature Communications. 5 (2014) 1–7. https://doi.org/10.1038/ncomms6083.
[54] L. Berthier, W. Kob, Static point-to-set correlations in glass-forming liquids, Physical Review E - Statistical, Nonlinear, and Soft Matter Physics. 85 (2012) 2–6. https://doi.org/10.1103/PhysRevE.85.011102.
[55] B. Wang, L.J. Wang, B.S. Shang, X.Q. Gao, Y. Yang, H.Y. Bai, M.X. Pan, W.H. Wang, P.F. Guan, Revealing the ultra-low-temperature relaxation peak in a model metallic glass, Acta Materialia. 195 (2020) 611–620. https://doi.org/10.1016/j.actamat.2020.05.067.
[56] B.J. Alder, T.E. Wainwright, Phase Transition for a Hard Sphere System, The Journal of Chemical Physics. 27 (1957) 1208–1209. https://doi.org/10.1063/1.1743957.
[57] J.B. Gibson, A.N. Goland, M. Milgram, G.H. Vineyard, Dynamics of Radiation Damage, Phys. Rev. 120 (1960) 1229–1253. https://doi.org/10.1103/PhysRev.120.1229.
[58] M.S. Daw, S.M. Foiles, M.I. Baskes, The embedded-atom method: a review of theory and applications, Materials Science Reports. 9 (1993) 251–310. https://doi.org/10.1016/0920-2307(93)90001-U.
[59] S. Plimpton, Fast Parallel Algorithms for Short-Range Molecular Dynamics, Journal of Computational Physics. 117 (1995) 1–19. https://doi.org/10.1006/jcph.1995.1039.
[60] J.C. Mauro, R.J. Loucks, P.K. Gupta, Metabasin Approach for Computing the Master Equation Dynamics of Systems with Broken Ergodicity, J. Phys. Chem. A. 111 (2007) 7957–7965. https://doi.org/10.1021/jp0731194.
[61] A. Ninarello, L. Berthier, D. Coslovich, Models and algorithms for the next generation of glass transition studies, Physical Review X. 7 (2017) 1–22. https://doi.org/10.1103/PhysRevX.7.021039.
[62] D. Srolovitz, K. Maeda, V. Vitek, T. Egami, Structural defects in amorphous solids Statistical analysis of a computer model, Philosophical Magazine A. 44 (1981) 847–866. https://doi.org/10.1080/01418618108239553.
[63] V.A. Levashov, T. Egami, R.S. Aga, J.R. Morris, Equipartition theorem and the dynamics of liquids, Physical Review B. 78 (2008) 064205. https://doi.org/10.1103/PhysRevB.78.064205.
[64] T. Egami, S.J.L. Billinge, Underneath the Bragg Peaks: Structural Analysis of Complex Materials, Elsevier, 2003.
[65] K.-W. Park, J. Jang, M. Wakeda, Y. Shibutani, J.-C. Lee, Atomic packing density and its influence on the properties of Cu–Zr amorphous alloys, Scripta Materialia. 57 (2007) 805–808. https://doi.org/10.1016/j.scriptamat.2007.07.019.
[66] O.J. Kwon, Y.C. Kim, K.B. Kim, Y.K. Lee, E. Fleury, Formation of amorphous phase in the binary Cu-Zr alloy system, Metals and Materials International. 12 (2006) 207–212. https://doi.org/10.1007/BF03027532.

[67] M.I. Mendelev, M.J. Kramer, R.T. Ott, D.J. Sordelet, D. Yagodin, P. Popel, Development of suitable interatomic potentials for simulation of liquid and amorphous Cu-Zr alloys, Philosophical Magazine. 89 (2009) 967–987. https://doi.org/10.1080/14786430902832773.
[68] J.C. Qiao, J.M. Pelletier, Dynamic Mechanical Relaxation in Bulk Metallic Glasses: A Review, Journal of Materials Science & Technology. 30 (2014) 523–545. https://doi.org/10.1016/j.jmst.2014.04.018.
[69] B. Wang, B.S. Shang, X.Q. Gao, W.H. Wang, H.Y. Bai, M.X. Pan, P.F. Guan, Understanding Atomic-Scale Features of Low Temperature-Relaxation Dynamics in Metallic Glasses, Journal of Physical Chemistry Letters. 7 (2016) 4945–4950. https://doi.org/10.1021/acs.jpclett.6b02466.
[70] Z. Lu, B.S. Shang, Y.T. Sun, Z.G. Zhu, P.F. Guan, W.H. Wang, H.Y. Bai, Revealing β-relaxation mechanism based on energy distribution of flow units in metallic glass, Journal of Chemical Physics. 144 (2016). https://doi.org/10.1063/1.4945279.
[71] H.-B. Yu, M.-H. Yang, Y. Sun, F. Zhang, J.-B. Liu, C.Z. Wang, K.M. Ho, R. Richert, K. Samwer, Fundamental Link between β Relaxation, Excess Wings, and Cage-Breaking in Metallic Glasses, J. Phys. Chem. Lett. 9 (2018) 5877–5883. https://doi.org/10.1021/acs.jpclett.8b02629.
[72] S. Ashtekar, G. Scott, J. Lyding, M. Gruebele, Direct Visualization of Two-State Dynamics on Metallic Glass Surfaces Well Below Tg, J. Phys. Chem. Lett. 1 (2010) 1941–1945. https://doi.org/10.1021/jz100633d.
[73] T. Dziuba, Y. Luo, K. Samwer, Local mechanical properties of an ultrastable metallic glass, Journal of Physics Condensed Matter. 32 (2020). https://doi.org/10.1088/1361-648X/ab8aa2.
[74] H. Wagner, D. Bedorf, S. Küchemann, M. Schwabe, B. Zhang, W. Arnold, K. Samwer, Local elastic properties of a metallic glass, Nature Materials. 10 (2011) 439–442. https://doi.org/10.1038/nmat3024.
[75] C. Cammarota, G. Birolia, Ideal glass transitions by random pinning, Proceedings of the National Academy of Sciences of the United States of America. 109 (2012) 8850–8855. https://doi.org/10.1073/pnas.1111582109.
[76] S. Karmakar, G. Parisi, Random pinning glass model, Proceedings of the National Academy of Sciences of the United States of America. 110 (2013) 2752–2757. https://doi.org/10.1073/pnas.1222848110.
[77] T. Egami, D. Srolovitz, Local structural fluctuations in amorphous and liquid metals: A simple theory of the glass transition, Journal of Physics F: Metal Physics. 12 (1982) 2141–2163. https://doi.org/10.1088/0305-4608/12/10/010.
[78] T. Egami, Atomic level stresses, Progress in Materials Science. 56 (2011) 637–653. https://doi.org/10.1016/j.pmatsci.2011.01.004.
[79] C.H. Rycroft, VORO++ : A three-dimensional Voronoi cell library in C++, Chaos: An Interdisciplinary Journal of Nonlinear Science. 19 (2009) 041111. https://doi.org/10.1063/1.3215722.
[80] T. Egami, Universal criterion for metallic glass formation, Materials Science and Engineering: A. 226–228 (1997) 261–267. https://doi.org/10.1016/S0921-5093(97)80041-X.

[81] T. Egami, S.J. Poon, Z. Zhang, V. Keppens, Glass transition in metallic glasses: A microscopic model of topological fluctuations in the bonding network, Physical Review B - Condensed Matter and Materials Physics. 76 (2007) 1–6. https://doi.org/10.1103/PhysRevB.76.024203.
[82] L. Zella, J. Moon, D. Keffer, T. Egami, Transient nature of fast relaxation in metallic glass, Acta Materialia. 239 (2022) 118254. https://doi.org/10.1016/j.actamat.2022.118254.
[83] W.H. Wang, Dynamic relaxations and relaxation-property relationships in metallic glasses, Progress in Materials Science. 106 (2019) 100561. https://doi.org/10.1016/j.pmatsci.2019.03.006.
[84] J.C. Qiao, Q. Wang, D. Crespo, Y. Yang, J.M. Pelletier, Amorphous physics and materials: Secondary relaxation and dynamic heterogeneity in metallic glasses: A brief review, Chinese Phys. B. 26 (2017) 016402. https://doi.org/10.1088/1674-1056/26/1/016402.
[85] J. Zhao, S.L. Simon, G.B. McKenna, Using 20-million-year-old amber to test the super-Arrhenius behaviour of glass-forming systems, Nature Communications. 4 (2013) 1–6. https://doi.org/10.1038/ncomms2809.
[86] B. Zhang, D.Q. Zhao, M.X. Pan, W.H. Wang, A.L. Greer, Amorphous metallic plastic, Physical Review Letters. 94 (2005) 1–4. https://doi.org/10.1103/PhysRevLett.94.205502.
[87] Y. Fan, T. Iwashita, T. Egami, Evolution of elastic heterogeneity during aging in metallic glasses, Physical Review E - Statistical, Nonlinear, and Soft Matter Physics. 89 (2014) 1–7. https://doi.org/10.1103/PhysRevE.89.062313.
[88] P.K. Dixon, L. Wu, S.R. Nagel, B.D. Williams, J.P. Carini, Scaling in the Relaxation of Supercooled Liquids,PRL, Dixon , Nagel, 65 (1990) 1108–1111.
[89] X.D. Wang, J. Zhang, T.D. Xu, Q. Yu, Q.P. Cao, D.X. Zhang, J.Z. Jiang, Structural Signature of β-Relaxation in La-Based Metallic Glasses, Journal of Physical Chemistry Letters. 9 (2018) 4308–4313. https://doi.org/10.1021/acs.jpclett.8b02013.
[90] Q. Wang, S.T. Zhang, Y. Yang, Y.D. Dong, C.T. Liu, J. Lu, Unusual fast secondary relaxation in metallic glass, Nature Communications. 6 (2015). https://doi.org/10.1038/ncomms8876.
[91] L.Z. Zhao, R.J. Xue, Z.G. Zhu, K.L. Ngai, W.H. Wang, H.Y. Bai, A fast dynamic mode in rare earth based glasses, The Journal of Chemical Physics. 144 (2016) 204507. https://doi.org/10.1063/1.4952421.
[92] N. Jakse, A. Nassour, A. Pasturel, Structural and dynamic origin of the boson peak in a Cu-Zr metallic glass, Physical Review B - Condensed Matter and Materials Physics. 85 (2012) 1–6. https://doi.org/10.1103/PhysRevB.85.174201.
[93] B. Wang, L.J. Wang, B.S. Shang, X.Q. Gao, Y. Yang, H.Y. Bai, M.X. Pan, W.H. Wang, P.F. Guan, Revealing the ultra-low-temperature relaxation peak in a model metallic glass, Acta Materialia. 195 (2020) 611–620. https://doi.org/10.1016/j.actamat.2020.05.067.
[94] C. Léon, A. Rivera, A. Várez, J. Sanz, J. Santamaria, K.L. Ngai, Origin of constant loss in ionic conductors, Physical Review Letters. 86 (2001) 1279–1282. https://doi.org/10.1103/PhysRevLett.86.1279.
[95] C.M. Roland, M.J. Schroeder, J.J. Fontanella, K.L. Ngai, Evolution of the Dynamics in 1,4-Polyisoprene from a Nearly Constant Loss to a Johari-Goldstein β-Relaxation to the α-Relaxation, Macromolecules. 37 (2004) 2630–2635. https://doi.org/10.1021/ma0358071.

[96] Z. Wang, K.L. Ngai, W.H. Wang, S. Capaccioli, Coupling of caged molecule dynamics to Johari-Goldstein β-relaxation in metallic glasses, Journal of Applied Physics. 119 (2016). https://doi.org/10.1063/1.4939676.
[97] W. Götze, Recent tests of the mode-coupling theory for glassy dynamics, Journal of Physics: Condensed Matter. 11 (1999) A1–A45. https://doi.org/10.1088/0953-8984/11/10A/002.
[98] P. Palomino Rico, D.G. Papageorgiou, A.L. Greer, G.A. Evangelakis, The atomistic mechanism of fast relaxation processes in Cu65Zr35 glass, Acta Materialia. 135 (2017) 290–296. https://doi.org/10.1016/j.actamat.2017.06.028.
[99] S. Plimpton, Fast Parallel Algorithms for Short-Range Molecular Dynamics, Journal of Computational Physics. 117 (1995) 1–19. https://doi.org/10.1006/jcph.1995.1039.
[100] Y.Q. Cheng, E. Ma, Atomic-level structure and structure-property relationship in metallic glasses, Progress in Materials Science. 56 (2011) 379–473. https://doi.org/10.1016/j.pmatsci.2010.12.002.
[101] Y. Cohen, S. Karmakar, I. Procaccia, K. Samwer, The nature of the β-peak in the loss modulus of amorphous solids, Epl. 100 (2012). https://doi.org/10.1209/0295-5075/100/36003.
[102] A.P. Thompson, S.J. Plimpton, W. Mattson, General formulation of pressure and stress tensor for arbitrary many-body interaction potentials under periodic boundary conditions, Journal of Chemical Physics. 131 (2009). https://doi.org/10.1063/1.3245303.
[103] C.H. Rycroft, VORO++ : A three-dimensional Voronoi cell library in C++, Chaos: An Interdisciplinary Journal of Nonlinear Science. 19 (2009) 041111. https://doi.org/10.1063/1.3215722.
[104] S. Shanbhag, Extraction of self-diffusivity in systems with nondiffusive short-time behavior, Physical Review E - Statistical, Nonlinear, and Soft Matter Physics. 88 (2013) 1–7. https://doi.org/10.1103/PhysRevE.88.042816.
[105] Y. Sun, S.X. Peng, Q. Yang, F. Zhang, M.H. Yang, C.Z. Wang, K.M. Ho, H. Bin Yu, Predicting complex relaxation processes in metallic glass, Physical Review Letters. 123 (2019) 105701. https://doi.org/10.1103/PhysRevLett.123.105701.
[106] H. Bin Yu, K. Samwer, Atomic mechanism of internal friction in a model metallic glass, Physical Review B - Condensed Matter and Materials Physics. 90 (2014). https://doi.org/10.1103/PhysRevB.90.144201.
[107] W. Dmowski, T. Iwashita, C.P. Chuang, J. Almer, T. Egami, Elastic heterogeneity in metallic glasses, Physical Review Letters. 105 (2010) 2–5. https://doi.org/10.1103/PhysRevLett.105.205502.
[108] M.H. Cohen, D. Turnbull, Molecular Transport in Liquids and Glasses, The Journal of Chemical Physics. 31 (1959) 1164–1169. https://doi.org/10.1063/1.1730566.
[109] J. Ding, L. Li, N. Wang, L. Tian, M. Asta, R.O. Ritchie, T. Egami, Universal nature of the saddle states of structural excitations in metallic glasses, Materials Today Physics. 17 (2021) 100359. https://doi.org/10.1016/j.mtphys.2021.100359.
[110] D.J. Wales, Energy landscapes, Cambridge University Press, Cambridge, UK ; New York, 2003.

[111] P. Cao, M.P. Short, S. Yip, Potential energy landscape activations governing plastic flows in glass rheology, Proc. Natl. Acad. Sci. U.S.A. 116 (2019) 18790–18797. https://doi.org/10.1073/pnas.1907317116.
[112] C. Liu, Y. Fan, Emergent Fractal Energy Landscape as the Origin of Stress-Accelerated Dynamics in Amorphous Solids, Phys. Rev. Lett. 127 (2021) 215502. https://doi.org/10.1103/PhysRevLett.127.215502.
[113] P. Charbonneau, J. Kurchan, G. Parisi, P. Urbani, F. Zamponi, Fractal free energy landscapes in structural glasses, Nat Commun. 5 (2014) 3725. https://doi.org/10.1038/ncomms4725.
[114] H.B. Yu, W.H. Wang, H.Y. Bai, K. Samwer, The β-relaxation in metallic glasses, National Science Review. 1 (2014) 429–461. https://doi.org/10.1093/nsr/nwu018.
[115] Y. Suzuki, T. Egami, Shear deformation of glassy metals: Breakdown of cauchy relationship and anelasticity, Journal of Non-Crystalline Solids. 75 (1985) 361–366. https://doi.org/10.1016/0022-3093(85)90242-X.
[116] J.C. Ye, J. Lu, C.T. Liu, Q. Wang, Y. Yang, Atomistic free-volume zones and inelastic deformation of metallic glasses, Nature Mater. 9 (2010) 619–623. https://doi.org/10.1038/nmat2802.
[117] M. Samavatian, R. Gholamipour, A.A. Amadeh, S. Mirdamadi, Role of tensile elastostatic loading on atomic structure and mechanical properties of Zr55Cu30Ni5Al10 bulk metallic glass, Materials Science and Engineering: A. 753 (2019) 218–223. https://doi.org/10.1016/j.msea.2019.03.058.
[118] P.M. Derlet, R. Maaß, Micro-plasticity in a fragile model binary glass, Acta Materialia. 209 (2021) 116771. https://doi.org/10.1016/j.actamat.2021.116771.
[119] R. Maaß, P.M. Derlet, Micro-plasticity and recent insights from intermittent and small-scale plasticity, Acta Materialia. 143 (2018) 338–363. https://doi.org/10.1016/j.actamat.2017.06.023.
[120] D. Weaire, M.F. Ashby, J. Logan, M.J. Weins, On the use of pair potentials to calculate the properties of amorphous metals, Acta Metallurgica. 19 (1971) 779–788. https://doi.org/10.1016/0001-6160(71)90134-9.
[121] R. Hilfer, Excess wing physics and nearly constant loss in glasses, Journal of Statistical Mechanics: Theory and Experiment. 2019 (2019). https://doi.org/10.1088/1742-5468/ab38bc.
[122] T. Egami, D. Srolovitz, Local structural fluctuations in amorphous and liquid metals: A simple theory of the glass transition, Journal of Physics F: Metal Physics. 12 (1982) 2141–2163. https://doi.org/10.1088/0305-4608/12/10/010.
[123] T. Egami, Atomic level stresses, Progress in Materials Science. 56 (2011) 637–653. https://doi.org/10.1016/j.pmatsci.2011.01.004.
[124] J.W. Cooley, J.W. Tukey, An Algorithm for the Machine Calculation of Complex Fourier Series, Mathematics of Computation. 19 (1965) 297–301. https://doi.org/10.2307/2003354.
[125] J. Moon, A. J. Minnich, Sub-amorphous thermal conductivity in amorphous heterogeneous nanocomposites, RSC Advances. 6 (2016) 105154–105160. https://doi.org/10.1039/C6RA24053D.
[126] J.M. Dickey, A. Paskin, Computer Simulation of the Lattice Dynamics of Solids, Phys. Rev. 188 (1969) 1407–1418. https://doi.org/10.1103/PhysRev.188.1407.

[127] J. Moon, S. Thébaud, L. Lindsay, T. Egami, Microscopic view of heat capacity of matter: solid, liquid, and gas, (2022). https://doi.org/10.48550/ARXIV.2210.06218.
[128] G. Parisi, Order Parameter for Spin-Glasses, Phys. Rev. Lett. 50 (1983) 1946–1948. https://doi.org/10.1103/PhysRevLett.50.1946.
[129] C.W. Ryu, T. Egami, Medium-range atomic correlation in simple liquids. I. Distinction from short-range order, Phys. Rev. E. 104 (2021) 064109. https://doi.org/10.1103/PhysRevE.104.064109.
[130] H.R. Schober, Collectivity of motion in undercooled liquids and amorphous solids, Journal of Non-Crystalline Solids. 307–310 (2002) 40–49. https://doi.org/10.1016/S0022-3093(02)01438-2.
[131] T. Iwashita, D.M. Nicholson, T. Egami, Elementary Excitations and Crossover Phenomenon in Liquids, Phys. Rev. Lett. 110 (2013) 205504. https://doi.org/10.1103/PhysRevLett.110.205504.
[132] J. Ding, L. Li, N. Wang, L. Tian, M. Asta, R.O. Ritchie, T. Egami, Universal nature of the saddle states of structural excitations in metallic glasses, Materials Today Physics. 17 (2021) 100359. https://doi.org/10.1016/j.mtphys.2021.100359.
[133] Y. Fan, T. Iwashita, T. Egami, Energy landscape-driven non-equilibrium evolution of inherent structure in disordered material, Nature Communications. 8 (2017) 1–7. https://doi.org/10.1038/ncomms15417.
[134] C.E. Maloney, A. Lemaître, Amorphous systems in athermal, quasistatic shear, Phys. Rev. E. 74 (2006) 016118. https://doi.org/10.1103/PhysRevE.74.016118.
[135] C. Maloney, A. Lemaître, Subextensive Scaling in the Athermal, Quasistatic Limit of Amorphous Matter in Plastic Shear Flow, Phys. Rev. Lett. 93 (2004) 016001. https://doi.org/10.1103/PhysRevLett.93.016001.
[136] D. Richard, M. Ozawa, S. Patinet, E. Stanifer, B. Shang, S.A. Ridout, B. Xu, G. Zhang, P.K. Morse, J.-L. Barrat, L. Berthier, M.L. Falk, P. Guan, A.J. Liu, K. Martens, S. Sastry, D. Vandembroucq, E. Lerner, M.L. Manning, Predicting plasticity in disordered solids from structural indicators, Phys. Rev. Materials. 4 (2020) 113609. https://doi.org/10.1103/PhysRevMaterials.4.113609.
[137] E.D. Cubuk, S.S. Schoenholz, J.M. Rieser, B.D. Malone, J. Rottler, D.J. Durian, E. Kaxiras, A.J. Liu, Identifying Structural Flow Defects in Disordered Solids Using Machine-Learning Methods, Phys. Rev. Lett. 114 (2015) 108001. https://doi.org/10.1103/PhysRevLett.114.108001.
[138] H. Liu, M.M. Smedskjaer, M. Bauchy, Deciphering a structural signature of glass dynamics by machine learning, Phys. Rev. B. 106 (2022) 214206. https://doi.org/10.1103/PhysRevB.106.214206.
[139] P.M. Anderson, J.P. Hirth, J. Lothe, Theory of Dislocations, Cambridge University Press, 2017.
[140] B. Xu, M.L. Falk, J.F. Li, L.T. Kong, Predicting Shear Transformation Events in Metallic Glasses, Phys. Rev. Lett. 120 (2018) 125503. https://doi.org/10.1103/PhysRevLett.120.125503.
[141] Y. Jin, P. Urbani, F. Zamponi, H. Yoshino, A stability-reversibility map unifies elasticity, plasticity, yielding, and jamming in hard sphere glasses, Science Advances. 4 (2018) eaat6387. https://doi.org/10.1126/sciadv.aat6387.

[142] N.V. Priezjev, Accelerated relaxation in disordered solids under cyclic loading with alternating shear orientation, Journal of Non-Crystalline Solids. 525 (2019) 119683. https://doi.org/10.1016/j.jnoncrysol.2019.119683.
[143] D. Fiocco, G. Foffi, S. Sastry, Oscillatory athermal quasistatic deformation of a model glass, Phys. Rev. E. 88 (2013) 020301. https://doi.org/10.1103/PhysRevE.88.020301.
[144] P. Das, A.D.S. Parmar, S. Sastry, Annealing glasses by cyclic shear deformation, J. Chem. Phys. 157 (2022) 044501. https://doi.org/10.1063/5.0100523.
[145] L. Berthier, G. Biroli, Theoretical perspective on the glass transition and amorphous materials, Rev. Mod. Phys. 83 (2011) 587–645. https://doi.org/10.1103/RevModPhys.83.587.
[146] H. Zhang, X. Wang, H.-B. Yu, J.F. Douglas, Dynamic heterogeneity, cooperative motion, and Johari–Goldstein $$\beta $$-relaxation in a metallic glass-forming material exhibiting a fragile-to-strong transition, Eur. Phys. J. E. 44 (2021) 56. https://doi.org/10.1140/epje/s10189-021-00060-7.
[147] G.P. Johari, Localized molecular motions of β-relaxation and its energy landscape, Journal of Non-Crystalline Solids. 307–310 (2002) 317–325. https://doi.org/10.1016/S0022-3093(02)01491-6.
[148] U. Bengtzelius, W. Gotze, A. Sjolander, Dynamics of supercooled liquids and the glass transition, J. Phys. C: Solid State Phys. 17 (1984) 5915. https://doi.org/10.1088/0022-3719/17/33/005.
[149] W. Gotze, L. Sjogren, Relaxation processes in supercooled liquids, Rep. Prog. Phys. 55 (1992) 241. https://doi.org/10.1088/0034-4885/55/3/001.
[150] L. Van Hove, Correlations in Space and Time and Born Approximation Scattering in Systems of Interacting Particles, Phys. Rev. 95 (1954) 249–262. https://doi.org/10.1103/PhysRev.95.249.
[151] M.J. Demkowicz, A.S. Argon, Autocatalytic avalanches of unit inelastic shearing events are the mechanism of plastic deformation in amorphous silicon, Phys. Rev. B. 72 (2005) 245206. https://doi.org/10.1103/PhysRevB.72.245206.
[152] H. Mizuno, H. Tong, A. Ikeda, S. Mossa, Intermittent rearrangements accompanying thermal fluctuations distinguish glasses from crystals, Journal of Chemical Physics. 153 (2020). https://doi.org/10.1063/5.0021228.
[153] C.W. Ryu, T. Egami, Origin of liquid fragility, Phys. Rev. E. 102 (2020) 042615. https://doi.org/10.1103/PhysRevE.102.042615.
[154] L. Berthier, E. Flenner, C.J. Fullerton, C. Scalliet, M. Singh, Efficient swap algorithms for molecular dynamics simulations of equilibrium supercooled liquids, J. Stat. Mech. 2019 (2019) 064004. https://doi.org/10.1088/1742-5468/ab1910.

VITA

Leo Zella is currently a PhD candidate at the University of Knoxville Tennessee in Materials Science and Engineering. His research under the supervision of Prof. Takeshi Egami focuses on using simulation tools to understand the microscopic mechanisms of relaxation in metallic glasses. During his graduate studies he spent time as a visiting scholar at Forschungszentrum Jülich in Germany studying polymer dynamics. Prior to coming to University of Tennessee Knoxville he earned a master's degree in physics at Ohio University.